High productivity hollow fiber membranes for CO2 capture

Etxeberria Benavides, M.

DOI
10.4233/uuid:c5f9cdd2-fc2b-433b-bffe-2e68cb3799c7

Publication date
2021

Document Version
Final published version

Citation (APA)
Etxeberria Benavides, M. (2021). *High productivity hollow fiber membranes for CO2 capture*. [Dissertation (TU Delft), Delft University of Technology]. https://doi.org/10.4233/uuid:c5f9cdd2-fc2b-433b-bffe-2e68cb3799c7

High productivity hollow fiber membranes for CO_2 capture

Author: Miren Etxeberria Benavides

Cover design: Sara Miguel and Miren Etxeberria Benavides

PhD Thesis, Delft University of Technology

The Netherlands, January 2021

High productivity hollow fiber membranes for CO_2 capture

Dissertation

for the purpose of obtaining the degree of doctor

at Delft University of Technology

by the authority of the Rector Magnificus Prof.dr.ir. T.H.J.J. van der Hagen

chair of the Board for Doctorates

to be defended publicly on

Thursday 14 January 2021 at 10:00 o'clock

by

Miren ETXEBERRIA BENAVIDES

Master of Science in Applied Chemistry and Polymeric Materials, University of the Basque Country, Spain

born in Donostia-San Sebastian, Spain

This dissertation has been approved by the promotors:
Prof. dr. F. Kapteijn and Prof. dr. J. Gascón Sabaté

Composition of the doctoral committee:

Rector Magnificus	Chairman
Prof. dr. F. Kapteijn	Delft University of Technology, promotor
Prof. dr. J. Gascón Sabaté	Delft University of Technology and King Abdullah University of Science and Technology, promotor
Independent members:	
Prof.dr. M Eddaoudi	KAUST, Saudi Arabia
Prof.dr. A. Urtiaga	University of Cantabria, Spain
Prof.dr. A. Urakawa	Delft University of Technology
Prof.dr. J.J.C. Geerlings	Delft University of Technology
Other members:	
Dr. Oana David	TECNALIA, Basque Research and Technology Alliance (BRTA), Spain

The research reported in this thesis was carried out in the Catalysis Engineering section, Department of Chemical Engineering, Faculty of Applied Sciences (TNW), Delft University of Technology, and in the Membrane Technology and Process Intensification group, within the Energy and Environmental Division of Tecnalia, Basque Research and Technology Alliance (BRTA), Donostia-San Sebastian.

This research has received funding from the European Union's Seventh Framework Programme (FP/2007-2013) under grant agreement number 608490 and Horizon 2020 research and innovation programme (H2020) under grant agreement n° 760944.

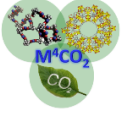

ISBN: 978-94-6421-145-0

Printed by: Ipskamp Printing, Enschede

An electronic version of this dissertation is available at:
http://repository.tudelft.nl/

Index

Chapter 1

Introduction

1.1. CO_2 capture and membrane technology

Carbon dioxide concentration in the atmosphere has been increasing significantly over the past century. Nowadays, almost 80% of global primary energy use is fossil fuels based. About one-third of the generated global energy was consumed by industry and responsible for almost a third part of global greenhouse gas emissions in 2019 [1] The Intergovernmental Panel on Climate Change (IPCC) estimates that, in order to limit global warming, both direct and indirect emissions must fall by 75-90 % by 2050 [2]. The aforementioned overwhelming contribution of industry suggests that, in addition to the development of energy generation processes based on renewable resources, carbon capture and storage (CCS) should be implemented in current running energy generation plants [3–5]. CCS will play an important role on the industrial decarbonisation and net-zero emissions target [6].

Apart from increasing energy efficiency and consumption reduction, three major ways are considered to reduce CO_2 emissions in combustion processes: pre-combustion CO_2 capture, post-combustion CO_2 capture from power plant flue gas, and oxyfuel combustion [7]. A scheme of the three CO_2 capture processes is presented in Figure 1.1. In pre-combustion CO_2 capture, a fuel gas is reacted with steam and oxygen at high temperature and pressure [8]. The result is a gaseous mixture consisting mainly of CO_2 and H_2 (15-50% CO_2). The H_2 is separated from the mixture and the H_2 enriched stream is used in a combustion process to produce electricity. The CO_2 from the enriched stream is captured for further storage. In post-combustion CO_2 capture, the fuel (fossil fuel, coal or biomass) is mixed with air and burned. A turbine is fed with the steam generated by the heat released from the combustion process. The exhaust gas of the boiler consists mainly of N_2 and low concentration of water vapour and CO_2 (4-30 %, depending on the fuel used). Finally, CO_2 is removed from the combustion process stream before emission to the atmosphere. In oxyfuel CO_2 capture, combustion is performed using oxygen, obtaining a flue gas containing mainly water vapor and CO_2. An almost pure CO_2 stream is obtained after condensation of water.

Conventional technologies used in industry for gas separation include cryogenic distillation, condensation, and physical and chemical (amine) absorption. However, membrane based gas separation has gained a lot of interest both in industry and academia due to several major benefits over conventional separation technologies [9]:

1) lower energy cost, there is no gas-liquid phase change of the gas mixture to be separated

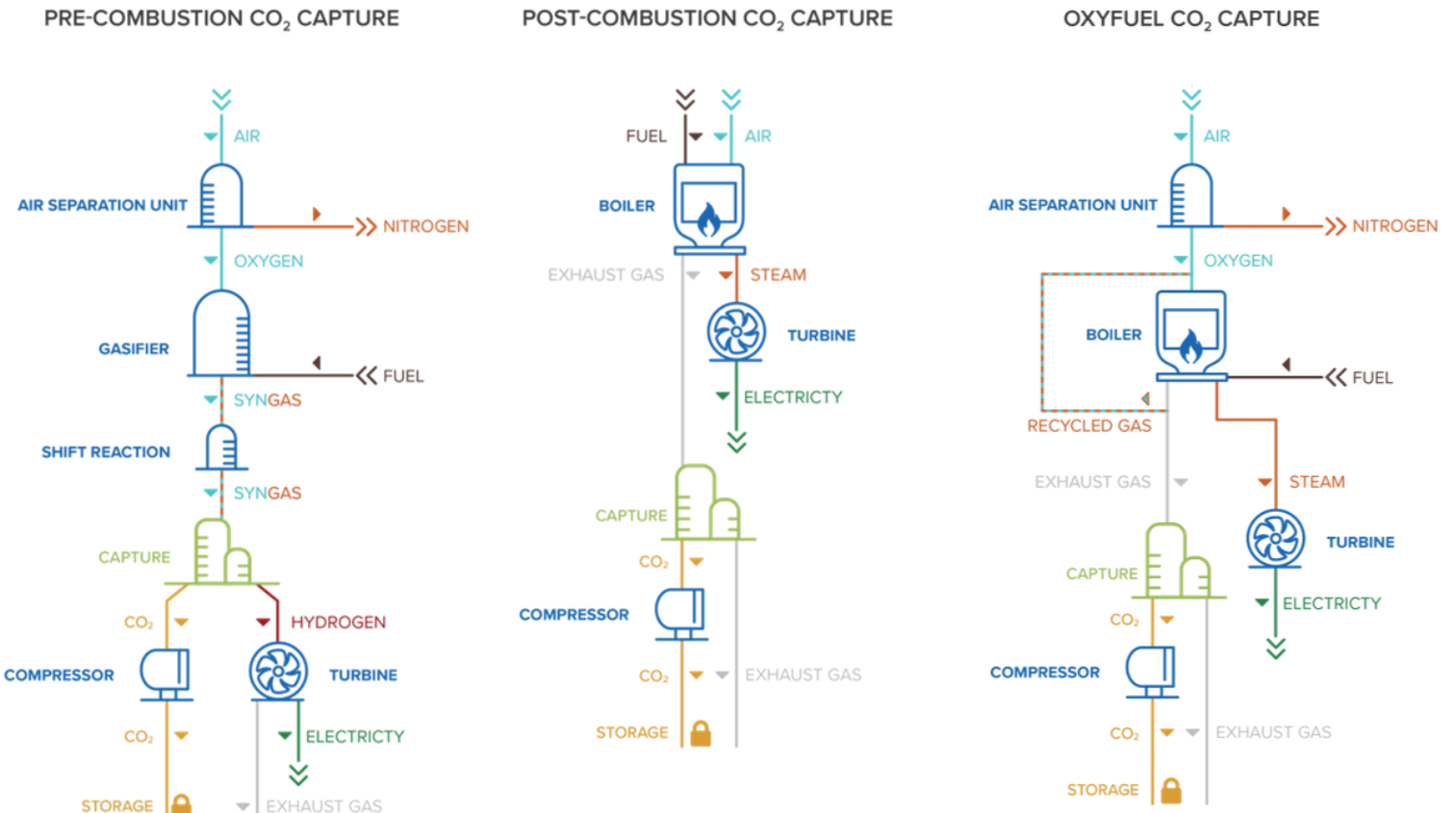

Figure 1.1. Scheme of pre-combustion, post-combustion and oxyfuel CO_2 capture process. Image provided by Global CCS Institute [10]

2) relatively small physical footprint - gas separation membrane units are smaller than other types of plants, like amine stripping plants
3) low mechanical complexity – no moving parts
4) operation under continuous, steady-state conditions

The use of membranes offers additional advantages in case of pre-combustion CO_2 capture. On the one hand, the H_2 and CO_2 mixture is already at high pressure. On the other hand, as H_2 selective membranes are used, CO_2 remains in the pressurized retentate stream and CO_2 is delivered already at high pressure, significantly reducing the compression energy cost.

1.2. Polymeric membranes for gas separation

Gas separation membrane performance is measured in terms of permeability and selectivity. The permeability is an intrinsic property of the material and is defined by the following expression:

$$P_i = \frac{J_i \cdot l}{\Delta p_i} \quad \text{(Eq. 1.1)}$$

where J_i is the flux of component i (cm^3 (STP)/cm^2·s) through a membrane of thickness l (cm) normalized by Δp_i the partial pressure difference across the membrane (cmHg). Permeability is commonly given in Barrer.

$$1\ Barrer = 1 \cdot 10^{-10}\ \frac{cm^3(STP) \cdot cm}{cm^2 \cdot s \cdot cmHg} \quad \text{(Eq. 1.2)}$$

The solution-diffusion model is used to describe gas permeation through a nonporous dense polymeric membrane, where the permeability (P_i) is the product of diffusivity (D_i) and the solubility coefficient (S_i):

$$P_i = S_i \cdot D_i \quad \text{(Eq. 1.3)}$$

In the solution-diffusion model, gas molecules at the high-pressure side of the membranes dissolve in the polymer, diffuse through the membrane driven by a pressure or concentration gradient and finally desorb. The solubility coefficient is a thermodynamic term and reflects the number of gas molecules dissolved in the polymer. The solubility coefficient depends on gas condensability and increases with increasing the molecular size of the penetrant, since large molecules are usually more condensable than smaller ones. The diffusivity is a kinetic term and reflects the mobility

of gas molecules in the membrane material. The diffusivity decreases with increasing molecular size of the gas.

The selectivity (α_{ij}) measures the ability of a membrane to separate two gases and is defined as the ratio of the permeability of more permeable compound *i* to the permeability of the less permeable compound *j*:

$$\alpha_{ij} = \frac{P_i}{P_j} = \frac{S_i}{S_j} \cdot \frac{D_i}{D_j} \quad \text{(Eq. 1.4)}$$

where S_i/S_j is the solubility selectivity and D_i/D_j the diffusivity selectivity. The solubility selectivity favours the permeation of larger molecules and is the dominant term in rubbery polymers. On the contrary, the diffusivity selectivity is the dominant term in glassy polymers, where the permeation of small molecules is favoured [11].

Membranes are used in several gas separation applications, being the more stablish processes the hydrogen recovery (H_2/N_2, H_2/CH_4 and H_2/CO separation), nitrogen production (O_2/N_2 separation), natural gas treatment (CO_2/CH_4, H_2S/CH_4 and He/CH_4 separation) and vapor recovery. However, membranes used in these applications are based on a small number of polymers, such as polysulfone, polyimides, cellulose acetate polyphenylene oxide and silicone rubber. There are several potential new applications, such as olefin/paraffin separation, CO_2 capture (CO_2/N_2 and H_2/CO_2 separation) and vapor/vapor separation, were new membrane materials with improved separation properties are required [12].

The ideal membrane for gas separation should have a high permeability and high selectivity. Polymeric membranes have been widely used in industry due to their low cost, easy processing and mechanical strength [13]. However, a limit in the trade-off between permeability and selectivity, known as Robeson upper bound limit, is among the main disadvantages of polymeric membranes. This upper bound correlation represented by Robeson for H_2/CO_2 and CO_2/N_2 separation is presented in Figure 1.2. In addition, low chemical and thermal stability and plasticization at high pressures in the presence of strong adsorbing penetrants such as CO_2 are other disadvantages of polymeric membranes.

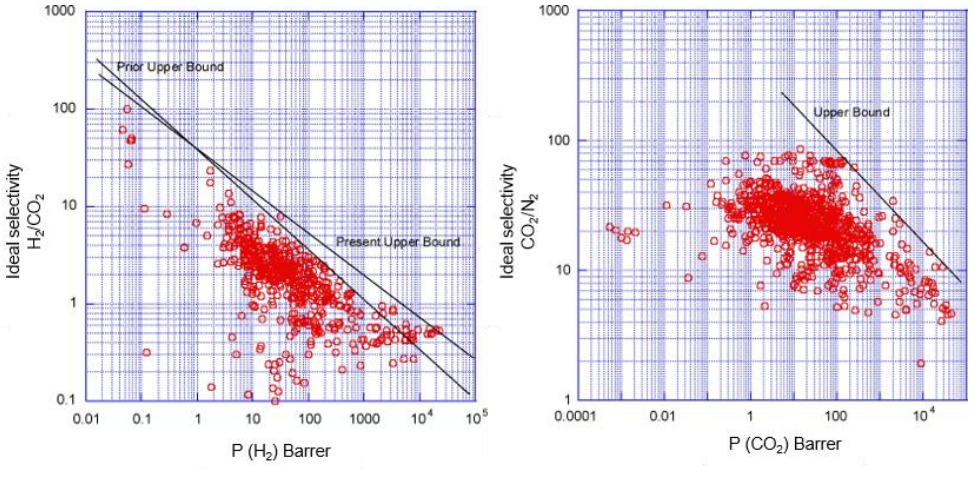

Figure 1.2. Upper bound correlation at 35 ºC for H_2/CO_2 (*left*) and CO_2/N_2 (*right*) separation. Reproduced from reference [14]

1.3. MOF based Mixed Matrix Membranes

Inorganic membranes based on ceramics [15], carbon [16], zeolite [17], oxides [18], metal organic frameworks (MOF) [19] or metals [20] present an excellent thermal and chemical stability, good erosion resistance and high gas flux and selectivity for gas separation, showing the potential to go beyond the upper bound limit of polymeric membranes. However, their implementation at industrial scale has been hindered due to their low mechanical resistance, modest reproducibility, scale-up problems and the high fabrication cost [19,21].

Mixed matrix membranes (MMMs) were presented as an alternative to overcome the limitations of both polymeric and inorganic membranes. In a MMM, filler particles are dispersed in a polymer matrix that should improve the properties of the composite relative to the pure polymer [13,22]. A good adhesion between the polymer and filler particles is crucial to prevent the formation of non-selective voids in MMMs [23]. In that sense, MOFs have been identified as promising filler materials for the preparation of MMMs [24]. MOFs are a class of porous materials consisting of metal ions or clusters connected by organic ligands to form one-, two- or three-dimensional porous structures. They have high surface area and pore volume and their porosity is in general higher than that of their earlier considered inorganic counterpart, zeolites. Due to their partially organic nature, MOFs usually display better polymer-filler compatibility than other inorganic fillers used for MMM preparation. Therefore, formation of the

aforementioned non-selective voids at the polymer-filler interface is prevented [25]. Gas separation in MOFs is accomplished by one or several mechanisms [26], the two main ones being:

- The size exclusion, where some components of a gas mixture are allowed to enter the pores of the MOF and subsequently adsorbed while other gas molecules are not. It is also known as molecular sieving effect
- The adsorbate-surface interaction, where certain components of the gas mixture are preferentially adsorbed over other components. This mechanism is governed by the thermodynamic equilibrium, which is determined by the surface characteristics of the absorbent material and the properties of gas molecules such as polarity, quadrupole moment, permanent dipole moment…

Gas transport through MMMs is governed by the combination of solution-diffusion mechanism in the continuous polymer matrix and size exclusion and/or adsorbate-surface interaction mechanism in the dispersed MOF phase. The addition of filler particles into the polymeric matrix introduces fast and/or selective transport routes through MOF, and therefore an increase in gas permeability and/or selectivity with respect to the bare polymer is induced. Using high aspect ratio thin sheet like fillers can further improve the size exclusion. A perpendicular pore orientation may be induced, shortening the diffusion path for the desired component while a more tortuous pathway will be created for the other components [27–29]. Ideal mixed matrix membrane permeability can be predicted by the Maxwell model [30]. The model was originally developed for estimating dielectric properties of composite materials and then adapted to predict effective permeability of mixed matrix membranes:

$$P_{eff} = P_c \left[\frac{P_d+2P_c-2\Phi(P_c-P_d)}{P_d+2P_c+\Phi(P_c-P_d)}\right] \quad \text{(Eq. 1.5)}$$

where P_{eff} is the permeability of the mixed matrix membrane, Φ the volume fraction of dispersed filler particles, P_c the permeability of the continuous polymer phase and P_d the permeability of the dispersed filler phase. This model is effective for low spherical filler loadings ($\Phi < 0.2$) and morphological parameters of the filler (particle size, shape and distribution) are not considered. An ideal filler-polymer interface morphology is considered on this model, i.e. the interfacial layer contains no defects and no distortion. Other models have been also applied for predicting the effective permeability of ideal MMMs, such as Bruggeman and Lewis−Nielsen models. However, in some cases it is difficult to obtain this ideal morphology since defects are created at the filler-polymer interface. Three types of defects can be formed: non-selective interface voids or sieves-in-a-cage, rigidification of polymer chains around the filler and particle pore blockage

caused by the penetration of polymer chains. Generally, polymer chain rigidification causes a decrease in gas permeability and increase in selectivity. Pore blockage always decreases the permeability, while the effect on selectivity may depend on the pore dimension of the filler [31,32]. Several models have been developed to predict the permeability of non-ideal MMM morphology, where the interfacial defects are considered: the modified Maxwell, modified Lewis−Nielsen, Felske and modified Felske, modified Pal, and Hashemifard−Ismail−Matsuura models [22].

An extensive review on MOF based mixed matrix membranes for CO_2 separation separation was published by Seoane *et al.* [33]. In most of the reviewed works improvements of permeability at constant selectivity were reported and only in circa 10% of the cases improvements in both permeability and selectivity were achieved. They have also noticed that plasticization of the polymeric membrane at high CO_2 pressures was partially suppressed by the addition of MOF particles.

1.4. Gas separation hollow fiber membranes

A membrane material presenting a proper selectivity and permeability should also have the ability to be processed into an asymmetric membrane with a meaningful productivity. The importance of asymmetric membranes was not appreciated until Loeb and Sourirajan developed a process to prepare defect-free high flux asymmetric reverse osmosis membranes in the early 1960s [34]. These membranes consist of an ultrathin selective layer over an open porous support. The work of Loeb and Sourirajan together with the funding of US Department of interior resulted in the commercialization of the first reverse osmosis membrane modules [11]. Commercialization of membrane modules was then extended to other separation processes. In 1980 Monsanto commercialized hydrogen separation Prism membranes for the first time. Since then, only polymeric membranes have been implemented for gas separation on a large scale in industry. The commercial implementation of polymeric gas separation membrane was achieved mainly due to their easy processing and mechanical strength [13]. Gas separation membrane module commercialization was followed in the next decades by other companies such as: Separex, Cyrana and Grace Membrane Systems (CO_2/CH_4 separation); Dow, DuPont and Ube (O_2/N_2, H_2/N_2 and H_2/CH_4 separation) and MTR, GKSS and MTR (vapor separation plants) [11].

High-flux asymmetric membranes can be formed in flat sheets, tubular and hollow fiber geometries. Membranes must be efficiently packed in a module to satisfy large membrane area required for an industrial application. Membranes packed in membrane modules are classified based on membrane geometry as follows: plate and frame, spiral-wound, tubular modules and hollow fiber modules. Plate and frame and tubular modules were used at the beginning and they are still used nowadays. However, due to their relatively high cost, in most applications they have been replaced by the spiral-wound and hollow fiber modules. Hollow fiber membrane offer several advantages compared to plate and frame modules [35–37]:

1) High packing density (over 10000 m^2/m^3), about ten times higher than for plate and frame modules
2) Hollow fibers can handle very high transmembrane pressure differences (up to 70 bar)
3) 5 to 20 times lower fabrication costs

Figure 1.3. shows the cross-section SEM image of typical hollow fiber membrane for gas separation. It consists of a thin selective layer on the outer side of the fiber (< 1 μm) supported by an open porous sponge like sub-structure. The outer skin layer is the selective part of the membrane while the inner porous layer acts as support layer with minimum resistance to gas transport. The most common fabrication method for asymmetric hollow fibers is the phase inversion process (also called dry jet-wet quench spinning or wet spinning) [36,37]. Other methods have been also used for asymmetric membrane fabrication, such as interfacial polymerization and solution-coating or dip coating. In these fabrication methods a porous support is coated with a thin dense layer to form a composite membrane.

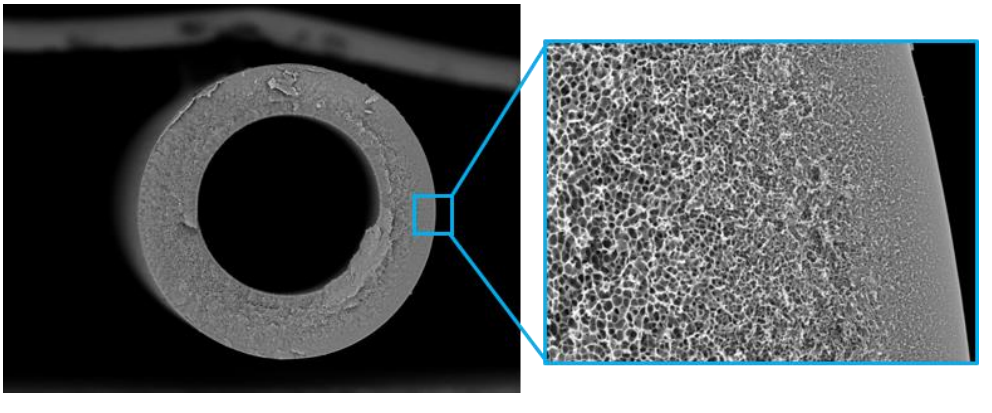

Figure 1.3. SEM image of typical hollow fiber membrane for gas separation

For asymmetric membranes, since the selective layer thickness is very difficult or impossible to measure [38], the pressure normalized flux or permeance is often used instead of permeability. Permeance is measured in gas permeation units (GPU).

$$1\ GPU = 1 \cdot 10^{-6}\ \frac{cm^3(STP)}{cm^2 \cdot s \cdot cmHg} \qquad \text{(Eq. 1.6)}$$

1.4.1. Formation of asymmetric gas separation hollow fiber membranes by dry followed by wet phase inversion

In the spinning process, the polymer solution (dope solution) and a bore fluid are co-extruded through a nozzle (spinneret) into a coagulation bath. During the spinning process, the fiber is continuously collected on a drum after precipitation in the coagulation bath (Figure 1.4). There are several parameters involved in the spinning process, listed below:

- Dope composition
- Bore fluid composition
- Dope/bore fluid flow rate
- Spinneret temperature
- Air gap height
- Coagulation bath composition and temperatures.
- Take-up rate

Optimization of polymer dope composition is a key to success on the formation of defect-free gas separation hollow fiber membranes. The dope usually has a complex composition as it contains polymer, solvents and additives (non-solvents) that are miscible with the solvent but not with the polymer. Xu *et al.* presented the qualitative dope composition trajectories in the ternary phase diagram during a dry-jet/wet-quench spinning process [39], represented in Figure 1.5. The corners of the ternary diagram represent the three pure components (polymer, solvent and non-solvent), whereas the points within the diagram represent mixtures of the three components [11]. The diagram is separated in two main regions by the phase boundary or the binodal line: the one-phase region, where all components are miscible, and the two-phase region, where the system separates into a solid phase and a liquid phase. The potentially useful dope composition should be in the one-phase region and close to the binodal line. The evaporation of volatile components in the air gap causes an increase in polymer concentration in the outermost region of the fiber, so a dense skin is

formed. The porous substructure is formed when the fiber enters the coagulation bath and the dope composition beneath the dense skin enters into the two-phase region. Therefore, the choice of a proper dope component is highly important.

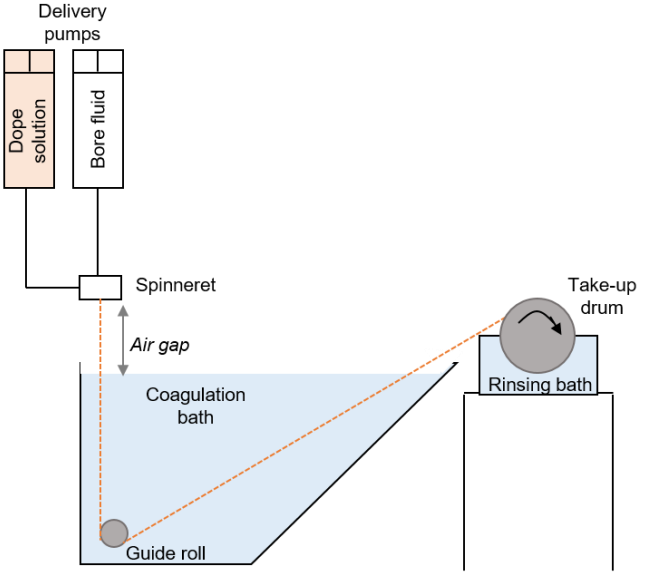

Figure 1.4. Dry-wet phase inversion process for asymmetric hollow fiber membrane formation

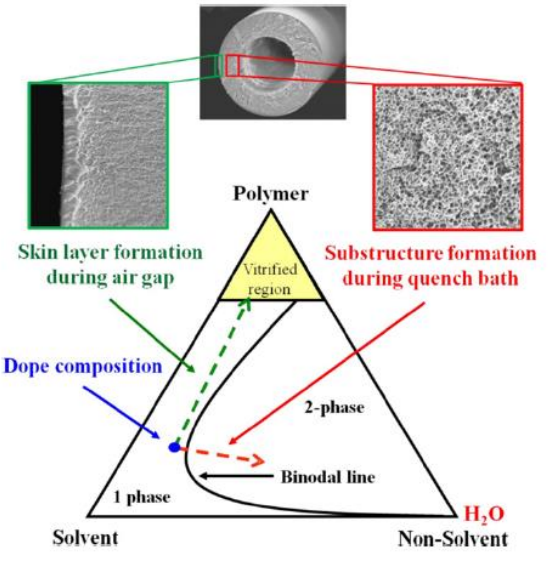

Figure 1.5. Gas separation asymmetric hollow fiber formation process represented in a ternary phase diagram. Reproduced from reference [39].

On the other hand, the polymer dope concentration is of great importance. One requirement to produce hollow fibers with minimum defects is a high polymer concentration in order to create significant chain entanglement during skin formation. Nevertheless, a too high polymer concentration is not desired because it creates a support layer with lower porosity and higher resistance to gas transport. Therefore, the optimum value is met when the dope has sufficient viscosity to allow extrusion of the polymer dope and take-up at a relevant speed without breaking (*i.e.* a spinnable dope). In a polymer solution, the viscosity increases slightly with polymer concentration, up to a point from where it begins to increase exponentially, as illustrated in Figure 1.6. The critical polymer concentration (c.p.c.) is extrapolated from the typical viscosity versus polymer concentration curve, more specifically from the back interpolation of the linear part. The optimum polymer concentration in the dope is equal to or slightly above the c.p.c. Nevertheless, all the spinning parameters described above have a direct influence on the final structure and therefore the separation performance of the fiber. The acquisition of the optimal hollow fiber structure implies the simultaneous fine tuning of all the spinning parameters.

Regardless of the method used for asymmetric membrane fabrication, the selective layer must be as thin as possible and defect-free since permeance and selectivity of the membrane will be determined by the quality of the selective layer. Asymmetric membranes are defined to be "defect-free" if the ideal selectivity is greater than 80% of the intrinsic selectivity of dense films [40]. The formation of ultrathin and defect-free asymmetric membranes is quite challenging, since the probability for the creation of defect will increase as the selective layer thickness decreases [41–43]. Henis and Tripodi reported that defects in asymmetric membranes could be repaired with a thin coating layer of a highly permeable polymer such as silicone rubber [44]. Since then, healing techniques have been widely used to seal the defects. In a recent publication, Nunes *et al.* presented a perspective for advanced and new membrane materials and manufacturing processes. Developing membranes with zero defect has been identified as one of the main challenges to be address for gas and vapour separation membranes [45]. In that sense, significant efforts have been made during the last decades in the development of defect-free as-spun hollow fiber membranes. Several approaches have been followed in order to overcome the formation of defects during asymmetric hollow fiber membrane preparation, such as by the addition a highly volatile additive in the dope to facilitate the skin formation [46–49] or by controlling the shear-induced and elongation-induced polymer chain orientation during the spinning process [17].

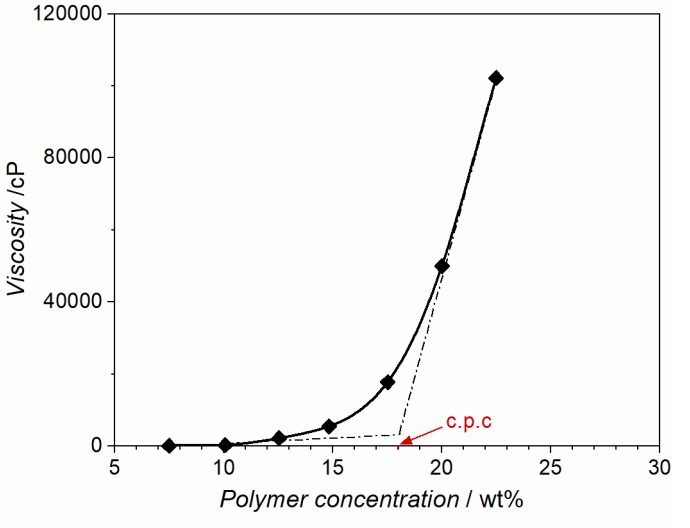

Figure 1.6. Typical viscosity versus polymer concentration curve and the determination of the critical polymer concentration, c.p.c.

1.4.2. MOF based hollow fiber MMMs

Fabrication of mixed matrix hollow fiber membranes presents additional issues to deal with, such as the compatibility of the polymer and filler particles and a proper distribution of filler particles within the fiber wall. Compatibility issues are overcome using MOFs since polymer-filler compatibility is improved due to the partially organic nature of this type of filler. According to Zhang *et al.* [50], the main challenge is to form an asymmetric structure with a very thin selective layer populated with the filler particles (see Figure 1.7). In an asymmetric structure a minimized skin layer thickness is desired to ensure a high permeance, commonly < 500 nm. In that sense, the particle size cannot be larger than the selective layer thickness, thus nano-sized filler particles are preferred over micrometer sized ones. Furthermore, filler particles must be homogeneously dispersed without causing major defects in the skin layer. Therefore, preparation of homogeneous particle dispersion in the spinning dope is highly important.

A large number of polymer/MOF pairs have been studied in literature in dense film configuration. However, few of them have been transferred into practical asymmetric hollow fiber geometry. $Cu_3(BTC)_2$/polyimide-mixed matrix hollow fibers were successfully fabricated by Hu *et al.* [51]. 6 wt% Loaded membranes showed a H_2 permeance increase by 45% with a H_2/CO_2 selectivity increase of 2.7 times compared to pure PI (polyimide). Asymmetric ZIF-8-PBI/Matrimid dual layer mixed matrix

hollow fibers were fabricated by Yang *et al.* [37] for H_2/CO_2 separation. Two types of hollow fibers were developed, 10 wt% ZIF-8 loaded fibers with a medium H_2 permeance and high H_2/CO_2 selectivity and 33 wt% loaded fibers with a high permeance and a medium selectivity. Regarding post-combustion CO_2 capture, asymmetric ZIF-8/Ultem ® 100 polyetherimide dual layer hollow fibers were prepared by Dai *et al.* [52]. Both permeance and permselectivity were increased by the addition of 17 vol% ZIF-8 filler. ZIF-8/6FDA–DAM:DABA polyimide mixed matrix hollow fiber membranes were also prepared by Lively *et al.* for CO_2/N_2 separation [53]. Mixed matrix hollow fibers were prepared by Zhu *et al.* by the incorporation of post-functionalized S-MIL-53 into Ultem ®1000 polyetherimide [54]. Compared to the pure polymer, 15 wt% S-MIL-53 loaded hollow fiber membranes showed a CO_2 permeance increase of 157% with an increase in CO_2/N_2 selectivity of 40%.Dual layer ZIF-8/6FDA-DAM mixed-matrix hollow fiber membranes with ZIF-8 loading up to 30 wt % were fabricated by Zhang *et al.* for hydrocarbon separation [50], showing a significantly enhanced C_3H_6/C_3H_8 selectivity compared to the neat polymer.

As mentioned above, there is a limited number of publications related to hollow fiber mixed matrix membrane fabrication compared to dense film preparation. There may be several possible reasons for this, such as the complexity of the hollow fiber fabrication process compared to dense film preparation method and the challenge of creating thin and defect free asymmetric hollow fiber membranes. Furthermore, the required amount of material to perform a spinning process is much greater than for dense film preparation. Many polymers and fillers used for dense film permeation studies are synthetized in small batches at lab-scale, and therefore an intermediate material scaling up step is required before the hollow fiber spinning preparation step. Nevertheless, a dense film permeation study is just the first step in the membrane product development process and effort should also be put on thin and defect free asymmetric hollow fiber membrane development [55].

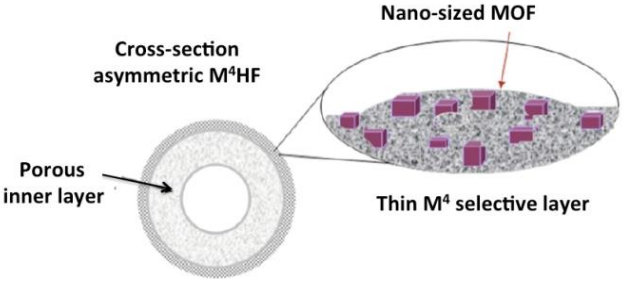

Figure 1.7. Cross section morphology of a mixed matrix hollow fiber membrane. Reproduced from reference [37].

1.5. From material to product development

Figure 1.8 shows how to proceed when asymmetric hollow fiber membranes are being developed. The first step consists on material development and/or selection based on defined target performance (Permeability and Selectivity) and separation process requirements (*e.g.* temperature, pressure…). Then, dense films are prepared and characterized in order to obtain the intrinsic separation properties of the selected material (permeability and selectivity). If the target properties are not met, material development and/or selection steps will be performed again. Rather than optimal separation properties, a membrane material should have a meaningful productivity. Therefore, the next step consists of asymmetric membrane (usually hollow fiber) preparation and characterization. During this step it is determined if the material can be processed into an asymmetric configuration. If this ability is demonstrated, the analysis of possible scaling up and prototyping is the last step of the hollow fiber membranes development process. Several steps of this process will be addressed along the different chapters of this thesis.

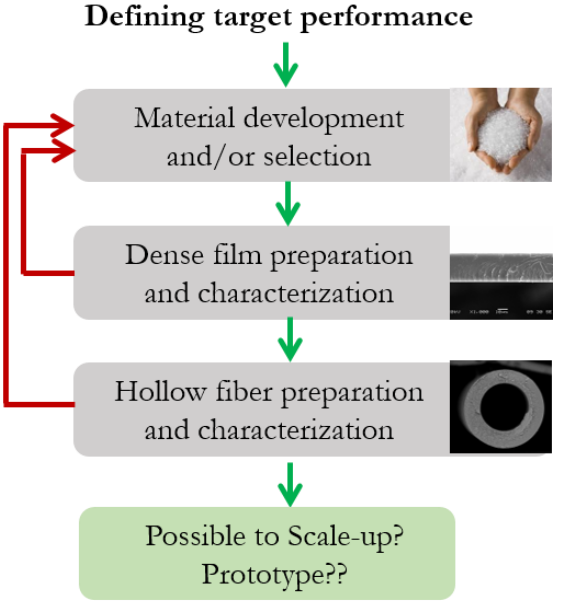

Figure 1.8. Scheme of hollow fiber membranes development process

1.6. Thesis outline

The main objective of this thesis is to develop high productivity membranes for pre- and post-combustion CO_2 capture. High productivity membranes imply thin selective separation layers. Also, among different membrane configurations, hollow fiber membranes are the most desired ones due to high packing density, *i.e.* membrane area per module volume. Therefore, development of asymmetric hollow fiber membranes consisting of a very thin and dense separating skin layer and a highly porous support layer with low resistance to gas flow is highly attractive and is the core concept of this work.

This thesis consists of two main parts. Part I focuses on the development mixed matrix membranes based on MOFs for post-combustion separation (Chapter 2) and for pre-combustion separation (Chapter 3). In **Chapter 2** ZIF-94 metal organic framework particles have been synthesized and incorporated into 6FDA-DAM polyimide up to 40 wt% loading to form dense MMMs. Intrinsic gas separation properties of the dense membranes have been tested under process conditions relevant for CO_2 capture in post-combustion applications. In **Chapter 3** commercially attractive mixed-matrix membranes were developed for H_2/CO_2 separation via a scalable hollow fiber spinning process. Neat PBI and ZIF-8/PBI mixed matrix hollow fibers were prepared and the influence of ZIF-8 filler over H_2/CO_2 separation performance at high temperature and pressure was studied.

Part II focuses (Chapter 4 and 5) on the fabrication of defect-free asymmetric hollow fiber membranes by phase inversion. In **Chapter 4**, the dope composition has been optimized using volatile additive tetrahydrofuran as key parameters, resulting in defect-free ultra-thin P84® asymmetric hollow fiber membranes with no need for a defect healing post treatment. In **Chapter 5**, additive was used as PVP to improve the scalability in the production of PBI hollow fiber membranes for H_2/CO_2 separation in pre-combustion CO_2 capture processes. The addition of PVP significantly increases the as-spun fiber elasticity and therefore increased the take up rate during the spinning process, resulting in a significant reduction of fiber dimensions.

Note that all chapters have been written as individual publications and can be read independently. Therefore, some overlap may be present.

References

[1] U.S. Energy Information Administration, Monthly Energy Review. April 2020, 2020.

[2] Intergovernmental Panel on Climate Change, Special report on global Warming of 1.5 °C, 2018. https://www.ipcc.ch/sr15/.

[3] 2011 Technology Map of the European Strategic Energy Technology Plan (SET-Plan), 2011.

[4] Technology Roadmap. Carbon Capture and Storage, 2013.

[5] D.S. Sholl, R.P. Lively, Seven chemical separations to change the world, Nature. 532 (2016) 435–437. doi:10.1038/532435a.

[6] Global CCS Institute, The Global Status of CCS: 2019, Melbourne, 2019.

[7] J.D. Figueroa, T. Fout, S. Plasynski, H. McIlvried, R.D. Srivastava, Advances in CO2 capture technology—The U.S. Department of Energy's Carbon Sequestration Program, Int. J. Greenh. Gas Control. 2 (2008) 9–20. doi:http://dx.doi.org/10.1016/S1750-5836(07)00094-1.

[8] B. Seoane, J. Coronas, I. Gascon, M.E. Benavides, O. Karvan, J. Caro, F. Kapteijn, J. Gascon, Metal-organic framework based mixed matrix membranes: A solution for highly efficient CO2 capture?, Chem. Soc. Rev. 44 (2015). doi:10.1039/c4cs00437j.

[9] P. Bernardo, E. Drioli, G. Golemme, Membrane Gas Separation: A Review/State of the Art, Ind. Eng. Chem. Res. 48 (2009) 4638–4663. doi:10.1021/ie8019032.

[10] Global CCS Institute, CCS Image Library, (2020). https://www.globalccsinstitute.com/resources/ccs-image-library/ (accessed March 23, 2020).

[11] R.W. Baker, Membrane Technology and Applications, 2nd Editio, Wiley, 2004.

[12] M. Galizia, W.S. Chi, Z.P. Smith, T.C. Merkel, R.W. Baker, B.D. Freeman, 50th Anniversary Perspective: Polymers and Mixed Matrix Membranes for Gas and Vapor Separation: A Review and Prospective Opportunities, Macromolecules. 50 (2017) 7809–7843. doi:10.1021/acs.macromol.7b01718.

[13] M.A. Aroon, A.F. Ismail, T. Matsuura, M.M. Montazer-Rahmati, Performance studies of mixed matrix membranes for gas separation: A review, Sep. Purif. Technol. 75 (2010) 229–242. doi:10.1016/j.seppur.2010.08.023.

[14] L.M. Robeson, The upper bound revisited, J. Memb. Sci. 320 (2008) 390–400. doi:10.1016/j.memsci.2008.04.030.

[15] S. Smart, C.X.C. Lin, L. Ding, K. Thambimuthu, J.C. Diniz da Costa, Ceramic membranes for gas processing in coal gasification, Energy Environ. Sci. 3 (2010) 268–278. doi:10.1039/B924327E.

[16] A. Ismail, L. David, A review on the latest development of carbon membranes for gas separation, J. Memb. Sci. 193 (2001) 1–18. doi:10.1016/S0376-7388(01)00510-5.

[17] N. Kosinov, J. Gascon, F. Kapteijn, E.J.M. Hensen, Recent developments in zeolite membranes for gas separation, J. Memb. Sci. 499 (2016) 65–79. doi:http://dx.doi.org/10.1016/j.memsci.2015.10.049.

[18] S. Basu, A.L. Khan, A. Cano-Odena, C. Liu, I.F.J. Vankelecom, Membrane-based technologies for biogas separations., Chem. Soc. Rev. 39 (2010) 750–768. doi:10.1039/b817050a.

[19] J. Gascon, F. Kapteijn, B. Zornoza, V. Sebastián, C. Casado, J. Coronas, Practical Approach to Zeolitic Membranes and Coatings: State of the Art, Opportunities, Barriers, and Future Perspectives, Chem. Mater. 24 (2012) 2829–2844. doi:10.1021/cm301435j.

[20] E. Fernandez, K. Coenen, A. Helmi, J. Melendez, J. Zuñiga, D.A. Pacheco Tanaka, M. van Sint Annaland, F. Gallucci, Preparation and characterization of thin-film Pd–Ag supported membranes for high-temperature applications, Int. J. Hydrogen Energy. 40 (2015) 13463–13478. doi:http://dx.doi.org/10.1016/j.ijhydene.2015.08.050.

[21] J. Coronas, Present and future synthesis challenges for zeolites, Chem. Eng. J. 156 (2010) 236–242. doi:10.1016/j.cej.2009.11.006.

[22] H. Vinh-Thang, S. Kaliaguine, Predictive Models for Mixed-Matrix Membrane Performance: A Review, Chem. Rev. 113 (2013) 4980–5028. doi:10.1021/cr3003888.

[23] S. Hwang, R. Semino, B. Seoane, M. Zahan, C. Chmelik, R. Valiullin, M. Bertmer, J. Haase, F. Kapteijn, J. Gascon, G. Maurin, J. Kärger, Revealing the Transient Concentration of CO2 in a Mixed-Matrix Membrane by IR Microimaging and Molecular Modeling, Angew. Chemie Int. Ed. 57 (2018) 5156–5160. doi:10.1002/anie.201713160.

[24] P.S. Goh, A.F. Ismail, S.M. Sanip, B.C. Ng, M. Aziz, Recent advances of inorganic fillers in mixed matrix membrane for gas separation, Sep. Purif. Technol. 81 (2011) 243–264. doi:10.1016/j.seppur.2011.07.042.

[25] T. Rodenas, M. van Dalen, E. García-Pérez, P. Serra-Crespo, B. Zornoza, F. Kapteijn, J. Gascon, Visualizing MOF Mixed Matrix Membranes at the Nanoscale: Towards Structure-Performance Relationships in CO2/CH4 Separation Over NH2-MIL-53(Al)@PI, Adv. Funct. Mater. 24 (2014) 268. doi:10.1002/adfm.201470014.

[26] J.-R. Li, R.J. Kuppler, H.-C. Zhou, Selective gas adsorption and separation in metal–organic frameworks, Chem. Soc. Rev. 38 (2009) 1477–1504. doi:10.1039/B802426J.

[27] T. Rodenas, I. Luz, G. Prieto, B. Seoane, H. Miro, A. Corma, F. Kapteijn, F.X. Llabrés I Xamena, J. Gascon, Metal-organic framework nanosheets in polymer composite materials for gas separation, Nat. Mater. 14 (2015) 48–55. doi:10.1038/nmat4113.

[28] A. Pustovarenko, M.G. Goesten, S. Sachdeva, M. Shan, Z. Amghouz, Y. Belmabkhout, A. Dikhtiarenko, T. Rodenas, D. Keskin, I.K. Voets, B.M. Weckhuysen, M. Eddaoudi, L.C.P.M. de Smet, E.J.R. Sudhölter, F. Kapteijn, B. Seoane, J. Gascon, Nanosheets of Nonlayered Aluminum Metal–Organic Frameworks through a Surfactant-Assisted Method, Adv. Mater. 30 (2018) 1–8. doi:10.1002/adma.201707234.

[29] A. Sabetghadam, X. Liu, S. Gottmer, L. Chu, J. Gascon, F. Kapteijn, Thin mixed matrix and dual layer membranes containing metal-organic framework nanosheets and Polyactive™ for CO2 capture, J. Memb. Sci. 570–571 (2019) 226–235. doi:10.1016/j.memsci.2018.10.047.

[30] J.C. Maxwell, Treatise on Electricity and Magnetism, Oxford University Press, London, 1873.

[31] R. Lin, B. Villacorta Hernandez, L. Ge, Z. Zhu, Metal organic framework based mixed matrix membranes: an overview on filler/polymer interfaces, J. Mater. Chem. A. 6 (2018) 293–312. doi:10.1039/C7TA07294E.

[32] T.-S. Chung, L.Y. Jiang, Y. Li, S. Kulprathipanja, Mixed matrix membranes (MMMs) comprising organic polymers with dispersed inorganic fillers for gas separation, Prog. Polym. Sci. 32 (2007) 483–507. doi:10.1016/j.progpolymsci.2007.01.008.

[33] B. Seoane, J. Coronas, I. Gascon, M.E. Benavides, O. Karvan, J. Caro, F. Kapteijn, J. Gascon, Metal–organic framework based mixed matrix membranes: a solution for highly efficient CO2 capture?, Chem. Soc. Rev. 44 (2015) 2421–2454. doi:10.1039/C4CS00437J.

[34] S. LOEB, S. SOURIRAJAN, Sea Water Demineralization by Means of an Osmotic Membrane, in: Saline Water Conversion—II, AMERICAN CHEMICAL SOCIETY, 1963: pp. 117-132 SE–9. doi:doi:10.1021/ba-1963-0038.ch009.

[35] M.F.A. Wahab, A.F. Ismail, S.J. Shilton, Studies on gas permeation performance of asymmetric polysulfone hollow fiber mixed matrix membranes using nanosized fumed silica as fillers, Sep. Purif. Technol. 86 (2012) 41–48. doi:10.1016/j.seppur.2011.10.018.

[36] S. Husain, W.J. Koros, Mixed matrix hollow fiber membranes made with

modified HSSZ-13 zeolite in polyetherimide polymer matrix for gas separation, J. Memb. Sci. 288 (2007) 195–207. doi:10.1016/j.memsci.2006.11.016.

[37] N. Peng, N. Widjojo, P. Sukitpaneenit, M.M. Teoh, G.G. Lipscomb, T.-S. Chung, J.-Y. Lai, Evolution of polymeric hollow fibers as sustainable technologies: Past, present, and future, Prog. Polym. Sci. 37 (2012) 1401–1424. doi:10.1016/j.progpolymsci.2012.01.001.

[38] B.F. Yuri Yampolskii, Ingo Pinnau, Materials Science of Membranes for Gas and Vapor Separation, 2006.

[39] L. Xu, C. Zhang, M. Rungta, W. Qiu, J. Liu, W.J. Koros, Formation of defect-free 6FDA-DAM asymmetric hollow fiber membranes for gas separations, J. Memb. Sci. 459 (2014) 223–232. doi:10.1016/j.memsci.2014.02.023.

[40] S.C. Pesek, W.J. Koros, Aqueous quenched asymmetric polysulfone membranes prepared by dry/wet phase separation, J. Memb. Sci. 81 (1993) 71–88. doi:10.1016/0376-7388(93)85032-R.

[41] Y. Yampolskii, Polymeric Gas Separation Membranes, Macromolecules. 45 (2012) 3298–3311. doi:10.1021/ma300213b.

[42] N. Peng, T.-S. Chung, J.-Y. Lai, The rheology of Torlon® solutions and its role in the formation of ultra-thin defect-free Torlon® hollow fiber membranes for gas separation, J. Memb. Sci. 326 (2009) 608–617. doi:https://doi.org/10.1016/j.memsci.2008.10.038.

[43] I. Pinnau, W.J. Koros, Gas-permeation properties of asymmetric polycarbonate, polyestercarbonate, and fluorinated polyimide membranes prepared by the generalized dry–wet phase inversion process, J. Appl. Polym. Sci. 46 (1992) 1195–1204. doi:10.1002/app.1992.070460709.

[44] J.M.S. Henis, M.K. Tripodi, Composite hollow fiber membranes for gas separation: the resistance model approach, J. Memb. Sci. 8 (1981) 233–246. doi:https://doi.org/10.1016/S0376-7388(00)82312-1.

[45] S.P. Nunes, P.Z. Culfaz-Emecen, G.Z. Ramon, T. Visser, G.H. Koops, W. Jin, M. Ulbricht, Thinking the future of membranes: Perspectives for advanced and new membrane materials and manufacturing processes, J. Memb. Sci. 598 (2020) 117761. doi:https://doi.org/10.1016/j.memsci.2019.117761.

[46] D.T. Clausi, W.J. Koros, Formation of defect-free polyimide hollow fiber membranes for gas separations, J. Memb. Sci. 167 (2000) 79–89. doi:10.1016/S0376-7388(99)00276-8.

[47] J.J. Krol, M. Boerrigter, G.H. Koops, Polyimide hollow fiber gas separation membranes: preparation and the suppression of plasticization in propane/propylene environments, J. Memb. Sci. 184 (2001) 275–286. doi:https://doi.org/10.1016/S0376-7388(00)00640-2.

[48] T. Visser, Mixed gas plasticization phenomena in asymmetric membranes, University of Twente, Enschede, The Netherlands, 2006.

[49] M.R. Kosuri, W.J. Koros, Defect-free asymmetric hollow fiber membranes from Torlon®, a polyamide–imide polymer, for high-pressure CO2 separations, J. Memb. Sci. 320 (2008) 65–72. doi:10.1016/j.memsci.2008.03.062.

[50] C. Zhang, K. Zhang, L. Xu, Y. Labreche, B. Kraftschik, W.J. Koros, Highly scalable ZIF-based mixed-matrix hollow fiber membranes for advanced hydrocarbon separations, AIChE J. 60 (2014) 2625–2635. doi:10.1002/aic.14496.

[51] J. Hu, H. Cai, H. Ren, Y. Wei, Z. Xu, H. Liu, Y. Hu, Mixed-Matrix Membrane Hollow Fibers of Cu3(BTC)2 MOF and Polyimide for Gas Separation and Adsorption, Ind. Eng. Chem. Res. 49 (2010) 12605–12612. doi:10.1021/ie1014958.

[52] Y. Dai, J.R. Johnson, O. Karvan, D.S. Sholl, W.J. Koros, Ultem®/ZIF-8 mixed matrix hollow fiber membranes for CO2/N2 separations, J. Memb. Sci. 401–402 (2012) 76–82. doi:10.1016/j.memsci.2012.01.044.

[53] R.P. Lively, M.E. Dose, L. Xu, J.T. Vaughn, J.R. Johnson, J.A. Thompson, K. Zhang, M.E. Lydon, J.-S. Lee, L. Liu, Z. Hu, O. Karvan, M.J. Realff, W.J. Koros, A high-flux polyimide hollow fiber membrane to minimize footprint and energy penalty for CO2 recovery from flue gas, J. Memb. Sci. 423–424 (2012) 302–313. doi:10.1016/j.memsci.2012.08.026.

[54] H. Zhu, X. Jie, L. Wang, G. Kang, D. Liu, Y. Cao, Enhanced gas separation performance of mixed matrix hollow fiber membranes containing post-functionalized S-MIL-53, J. Energy Chem. 27 (2018) 781–790. doi:https://doi.org/10.1016/j.jechem.2017.04.016.

[55] A. Livingston, R. Baker, Membranes from academia to industry, Nat. Mater. 16 (2017) 280–282. doi:10.1038/nmat4861.

Chapter 2

High Performance Mixed Matrix Membranes (MMMs) Composed of ZIF-94 Filler and 6FDA-DAM Polymer

In this chapter the development of high-performance mixed matrix membranes (MMMs) composed of ZIF-94 filler and 6FDA-DAM polymer matrix is presented. The CO_2/N_2 separation performance was evaluated by mixed gas tests ($15CO_2$:$85N_2$) at 25ºC and 1 to 4 bar transmembrane pressure difference. The CO_2 membrane permeability was increased by the addition of the ZIF-94 particles, maintaining a constant CO_2/N_2 selectivity of ~22. The largest increase in CO_2 permeability of ~200% was observed for 40 wt% ZIF-94 loading, reaching the highest permeability (2310 Barrer) at similar selectivity among 6FDA-DAM MMMs reported in literature. For the first time, the ZIF-94 metal organic framework crystals with particle size smaller than 500 nm were synthesized using nonhazardous solvent (tetrahydrofuran and methanol) instead of dimethylformamide (DMF) in a scalable process. Membranes were characterized by three non-invasive image techniques, *viz.* SEM, AFM and nanoscale infrared imaging by scattering-type scanning near-field optical microscopy (s-SNOM). The combination of these techniques demonstrates a very good dispersion and interaction of the filler in the polymer layer, even at very high loadings.

This chapter is based on the following publication:

M. Etxeberria-Benavides, O. David, T. Johnson, M. M. Łozińska, A. Orsi, P. A. Wright, S. Mastel, R. Hillenbrand, F. Kapteijn, J. Gascon, High Performance Mixed Matrix Membranes (MMMs) Composed of ZIF-94 Filler and 6FDA-DAM Polymer, J. Membr. Sci, 550 (2018) 198-207

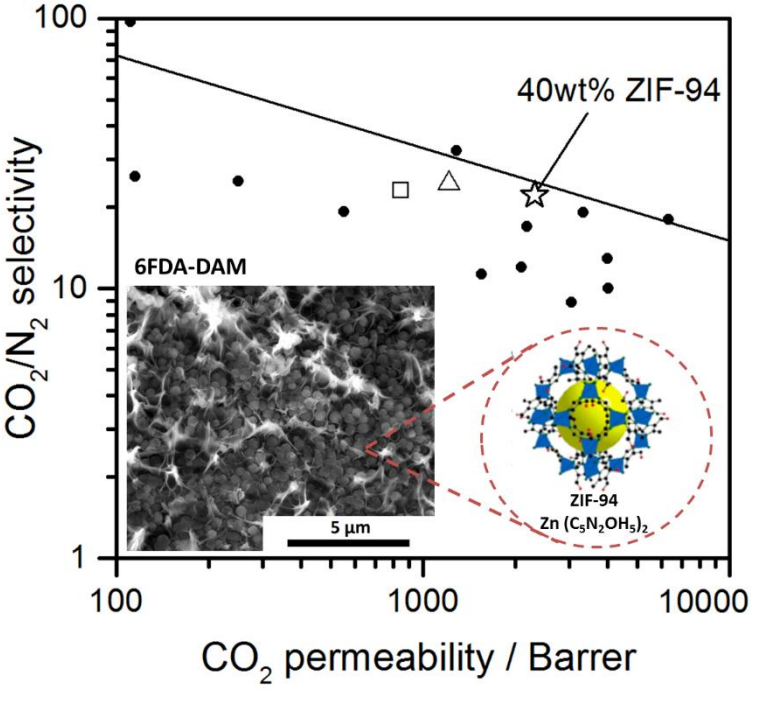
100
10
1
100
1000
10000
CO_2/N_2 selectivity
CO_2 permeability / Barrer
40wt% ZIF-94
6FDA-DAM
5 µm
ZIF-94
Zn $(C_5N_2OH_5)_2$

2.1. Introduction

Carbon dioxide concentration in the atmosphere has been increasing significantly over the past century. Fuel combustion for electricity and heat generation represented by far the largest source in 2014, more than 40% of global CO_2 emissions [1]. These overwhelming contribution suggests that, in addition to the development of energy generation processes that rely on renewable resources, carbon capture and storage (CCS) should be implemented in currently running energy generation plants [2,3]. Three major ways have been considered to reduce CO_2 emissions in combustion processes: pre-combustion CO_2 capture (after coal gasification), post-combustion CO_2 capture from power plant flue gas, and oxyfuel combustion [4].

Since the serial production of commercial polymeric membranes was implemented in 1980 by Henis and Tripodi, membrane gas separation has rapidly become a competitive separation technology. Membrane gas separation offers several benefits over conventional gas separation technologies [5]: lower energy cost, a relatively small footprint, low mechanical complexity and operation under continuous, steady-state conditions.

To date mainly polymeric membranes have been implemented for gas separation on a large scale in industry, mainly due to their easy processing and mechanical strength [6]. However, their performance is limited by the trade-off relationship between permeability and selectivity, represented by the 'Robeson upper bound' [7,8]. Low chemical and thermal stability and plasticization at high pressures in the presence of strongly adsorbing penetrants such as CO_2 are among the main disadvantages of this type of membranes. On the other hand, although inorganic membranes based on ceramics [9], carbon [10], zeolites [11], oxides [12], metal organic frameworks (MOF) [13] or metals [14] present an excellent thermal and chemical stability, good erosion resistance and high gas flux and selectivity for gas separation, their implementation at industrial scale has been hampered due to the low mechanical resistance, modest reproducibility, scale-up problems and the high fabrication cost of this type of membranes [13,15].

Mixed matrix membranes (MMMs) were presented as an alternative to overcome limitations of both polymeric and inorganic membranes. In a MMM, filler particles are dispersed in a polymer matrix that should improve the properties of the composite relative to the pure polymer [6,16]. Recently metal organic frameworks (MOFs) have been identified as promising filler materials for the preparation of MMMs [17]. They have a high specific surface area and pore volume and their porosity is in general higher

than that of their earlier considered inorganic counterpart, zeolites. Moreover, in contrast with zeolites, due to their partial organic nature, MOFs usually display better polymer-filler compatibility. This prevents formation of non-selective voids at the polymer-filler interface and consequently defect-free membranes can be made [18]. One of the first reports of a MOF used in a MMM concerned the additions of copper biphenyl dicarboxylate-triethylene diamine to poly(3-acetoxyethylthiophene (PAET) [19]. Since then quite a few MOF/polymer pairs have been studied in literature [20,21]. Zeolitic imidazolate frameworks (ZIFs) are a subclass of MOFs whit a similar structure of zeolites. Several ZIF/polymer pairs have been studied in literature as MMMs for CO_2/N_2 separation. ZIF-8 was used to improve the permeability of 6FDA–DAM:DABA(4:1) films by Lively *et al.* [22]. At 20 wt% loading, the membrane permeability increased by 2.5 times over the neat polymer membrane, with only a modest 9.4% loss in CO_2/N_2 selectivity. ZIF-8 was also used as filler by Nafisi *et al.* [23] and Wijenayake *et al.* [24] for the preparation of 6FDA-durene MMMs. In both cases an increased CO_2 permeability was observed due to polymer chain interruption and an increase in fractional free volume caused by the filler, 1.5 times higher CO_2 permeability for 30 wt% ZIF-8 loaded membrane and 3.3 times higher for 33.3 wt% loading, respectively. However, a slight decrease in CO_2/N_2 selectivity was observed in both cases, attributed to the relatively large increase in N_2 permeability. ZIF-71 nanoparticles were incorporated to the same polymer by Japip *et al.* [25]. With a 20 wt% ZIF-71 addition, the single component CO_2 permeability of the MMM was increased by 3-fold, while the ideal CO_2/N_2 selectivity was reduced from 14.7 to 12.9.

Different ZIF fillers have been added to different Pebax polymers. ZIF-8 filler and Pebax 2533 polymer matrix was used by Nafisi *et al.* [26] to prepare self-supported dual layer mixed matrix membranes. CO_2 permeability was increased by 3.6 times by the addition of 35 wt% ZIF-8, while a slight decrease in CO_2/N_2 selectivity was observed. In another study, an asymmetric membrane was prepared by Li *et al.* [27] by depositing a thin mixed matrix layer of <1 mm of Pebax 1657 and ZIF-7 on a porous polyacrylonitrile support. An intermediate gutter layer of PTMSP was applied to serve as a flat and smooth surface for coating to avoid polymer penetration into the porous support. The CO_2 permeability was increased by 1.5 times and the CO_2/N_2 selectivity was tripled by the addition of 22 wt% ZIF-7 filler. The enhanced performance was attributed to the combination of a molecular sieving effect from the ZIF-7 filler and the high solubility of CO_2 in Pebax.

In the present work ZIF-94 particles have been prepared and incorporated into 6FDA-DAM to form MMMs with the aim of achieving membrane properties similar to those recommended by Merkel *et al.* for the post-combustion CO_2 capture (the focus of this

chapter). 6FDA-based polyimides possess impressive gas separation performance, pairing high permeability with a good permselectivity. Their rigid primary structure contains bulky CF_3 groups through which the efficient packing of polymeric chains is inhibited and local segment mobility is reduced [28]. Many other desirable properties such as spinnability, thermal and chemical stability and mechanical strength as compared with non-fluoropolyimides make this polymer family suitable for gas separation applications [29–33]. In our case, a commercially available high-flux 6FDA-DAM polyimide was selected for membrane preparation. The preparation of 6FDA-DAM MMMs by the addition of several fillers such us NH_2-MIL-53(Al) [34], ZIF-11 [35], CPO-27(Mg) [36], ZIF-90 [37] and ZIF-8 [38] has been reported in literature. Membrane properties for gas separation are shown and compared with our MMM in the results and discussion section of this chapter (Table 2.1). The selection of the MOF filler was first based on CO_2 adsorption capacity and selectivity over N_2. ZIF-94 (also known as SIM-1, Substituted Imidazolate Material-1) has the **sod** topology and it is constructed by Zn atoms and 4-methyl-5 imidazole-carboxaldehyde (aImeIm) linkers. It has a high CO_2 uptake of 2.4 mmol g^{-1} at 1 bar, higher than its topological counterpart ZIF-93 with the **rho** topology (1.7 mmol g^{-1}, 17.9 Å pore diameter) or other MOFs such as ZIF-7 (1.6 mmol g^{-1}, 7.5 Å pore diameter) and ZIF-11 (0.8 mmol g^{-1}, 14.9 Å pore diameter). The higher CO_2 uptake is attributed to the smaller pore diameter of ZIF-94 (9.1 Å) compared to other ZIFs. Small pores are advantageous when considering CO_2 adsorption in the low-pressure regime [39]. ZIF-94/SIM-1 has already been used as membrane material in some publications. Marti *et al.* [40] reported the fabrication of SIM-1 membranes by post-synthetic modification of ZIF 8 particles for the separation of water from water/ethanol mixtures. The membrane fabricated using nano SIM-1 crystals separated water completely from the mixture. SIM-1 membrane for CO_2/N_2 separation has been crystallized in situ on a tubular asymmetric alumina support by Aguado *et al.* [41]. In a recent study, layered ZIF/polymer hollow fiber membranes for H_2/CH_4 and CO_2/CH_4 separation were prepared by Cacho-Bailo *et al.* growing a continuous ZIF-94 layer on the bore side of a porous P84 polyimide hollow fiber [42].

ZIF-94 also meets several highly important requirements for product development: (i) Preparation as nanoparticles for inclusion in thin membranes (<1 μm as target), (ii) scale up production *via* green synthesis, using non- or less toxic solvents such as water, THF or DMSO, (iii) low cost of metals and linkers and (iv) stability in water vapor. Prior to up scaling, the synthesis of the ZIF-94 MOF was optimized at the lab scale to yield particles in accordance with membrane fillers requirements.

In this chapter the preparation, characterization and performance of unique mixed matrix membranes made of highly engineered materials ZIF-94 and 6FDA-DAM is reported. The membranes have remarkable gas separation properties under process conditions relevant for CO_2 capture in post-combustion applications.

2.2 Experimental Section

2.2.1 Materials

6FDA-DAM (M_n = 170177 Dalton, T_g = 395 ºC) was purchased from Akron Polymer Systems (USA). ZIF-94 particles were synthesized solvothermally. For lab scale synthesis zinc acetate dehydrate was purchased from Sigma-Aldrich and 4-methyl-5-imidazolecarboxaldehyde from Maybridge. For scale-up, zinc acetate dihydrate and 4-methyl-5-imidazolecarboxaldehyde were purchased from Acros Chemicals (98 % and 99% purity, respectively). Methanol (99.8 %) and anhydrous tetrahydrofuran (≥99.9%) were supplied by Sigma-Aldrich.

2.2.2 Synthesis of ZIF-94 crystals

The synthesis of the ZIF-94 particles was first optimized at the lab scale and then scaled up. Lab scale synthesis of ZIF-94 involved dissolving 0.4392 g $Zn(CH_3COO)_2{\cdot}2H_2O$ (2 mmol) in 20 mL methanol and 0.4404 g 4-methyl-5-imidazolecarboxaldehyde (aImeIm, 4 mmol) in 50 mL THF. For scale-up, 3.52 g Zn(CH3COO)2·2H2O (160 mmol) were dissolved in 160 mL methanol and 3.52 g 4-methyl-5-imidazole-carboxaldehyde (aImeIm, 31 mmol) in 400 mL THF. After the solids were completely dissolved, the $Zn(CH_3COO)_2{\cdot}2H_2O$-methanol solution was poured slowly into the aImeIm-THF solution. The mixture was continuously stirred for 60 min at room temperature (30 min for scale-up). The product was collected by centrifugation and washed with methanol three times before drying at room temperature (at 105ºC for scale-up).

2.2.3 ZIF-94 characterization

Scanning electron micrographs were obtained from a JEOL JSM-6700F FE-SEM. Samples were sputter coated three times with gold in a Quorum Q150R ES (10 mA, 30 s and 2.3 tooling factor).

Powder X-ray diffraction (PXRD) data of lab scale sample was collected in Debye-Scherrer (capillary) geometry from STOE STAD i/p diffractometers with primary

monochromation (Cu *K*α1, λ = 1.54056 Å). Prior to analysis, samples were ground to a fine powder and introduced to a 0.7 mm glass capillary. PXRD pattern of up scaled sample was collected using a Bruker AXS D8 diffractometer using Cu *Ka* radiation (λ = 1.5406 and 1.54439 Å) over the 2θ range of 3-130° in 0.02° steps. Powder was places on a PTFE sample holder and analyzed in Bragg-Brentano reflection geometry. Le Bail refinement was performed using Topas with reflection profiles modelled using a fundamental parameters approach [43] with reference data collected from NIST660 LaB_6.

N_2 (-196 °C) adsorption isotherms were measured on a Micromeritics 2020 volumetric instrument (lab scale sample) and Quantachrome Autosorb iQ instrument (scaled up sample). CO_2 (25 °C, 1 bar) adsorption isotherm was measured on a Hiden IGA porosimeter. Lab scale sample was activated at 120 °C for 6 h under vacuum and scaled up sample at 200ºC for 12 h prior to adsorption measurements.

Thermogravimetric analysis (TGA) data were acquired for lab scale samples (~3 mg) in the temperature range 15 - 800 °C at a heating rate of 5 °C min^{-1} in flowing air. The scaled-up sample was analysed on a Netzsch TGA 760 between room temperature and 1000 ºC heating at 3 ºC min^{-1} in 80:20 Ar:O_2.

2.2.4 Membrane preparation

6FDA-DAM/ZIF-94 MMMs were prepared at different MOF loadings (10, 20, 30 and 40 wt%). Scaled-up ZIF-94 was used for membrane preparation. For comparison purposes, the pure polymer membrane was also prepared. Membranes were prepared by a casting method. Polymer and MOF were dried in a vacuum oven at 100 ºC overnight before casting solution preparation. A polymeric pre-dope composed of 13 wt% 6FDA-DAM in THF was prepared. ZIF-94 was dispersed in tetrahydrofuran in an ultrasonic bath for 1 h. The polymeric pre-dope was added to the ZIF-94/THF suspension and was stirred overnight at room temperature. The solvent/filler-polymer mass ratio of the final solution was of 91/9. In a doctor blade technique the solution was cast over a glass plate (casting thickness of 80 μm) and the solvent was evaporated at room temperature for 24 h in a solvent rich environment. Membranes were heat treated in a vacuum oven at 160 ºC overnight to eliminate residual solvent. Membrane thickness was measured with a digital micrometer (Mitutoyo) at different locations of the membrane. The average thickness value of ten measurements was used for permeability calculations.

2.2.5 Membrane characterization

The surface and cross-section morphology of the dense MMMs were characterized by scanning electron microscopy (SEM) (Quanta 250 ESEM) equipped with energy dispersive X-ray spectroscopy (EDX). The samples for cross-section SEM characterization were prepared by freeze-fracturing in liquid nitrogen. The low voltage high contrast backscatter electron detector (vCD) and the large field detector (LFD) were used for the analysis of the membranes.

Fourier transform infrared spectroscopy (FTIR) of pure components was performed on a Vertex 70 instrument (Bruker). Infrared chemical mapping of the MMMs with nanoscale spatial resolution was performed with a scattering-type scanning near-field optical microscope (IR s-SNOM) [44] (neaSNOM, Neaspec GmbH, Germany). It is based on an atomic force microscope (AFM), where the tip is illuminated with monochromatic infrared radiation of frequency ω. Recording of the tip-scattered infrared field with a pseutoheterodyne interferometer yields infrared amplitude and phase images simultaneously with topography [45]. Strong phase contrast reveals areas of strong molecular vibrational absorption [46,47]. We used standard Pt-coated AFM tips for both topography and infrared imaging, and a frequency-tunable quantum cascade laser (QCL) (MIRcat, Daylight Solutions Inc., USA) for tip illumination.

Permeation experiments were performed for pure gases and CO_2/N_2 gas mixtures in the gas permeation setup described elsewhere [48]. Circular samples of 3.14 cm^2 were cut and placed in the permeation cell over a macroporous stainless steel SS 316L support with 20μm nominal pore size. Gas was fed at 25 ºC and different pressures (1-4 bar transmembrane pressure difference). Transmembrane pressure was adjusted using a back-pressure regulator at the retentate side while permeate side of the membrane was kept at atmospheric pressure. A CO_2/N_2 gas mixture (15:85) was used as feed gas for mixed gas experiments (20 ml min^{-1} CO_2 and 113 ml min^{-1} N_2) and helium (3 ml min^{-1}) as sweep gas at the permeate side. An online gas chromatograph (Interscience Compact GC) equipped with a packed Carboxen 1010 PLOT (30 m x 0.32 mm) column and thermal conductivity detector (TCD) and flame ionization detector (FID) was used to analyze permeate stream composition over time. Permeability was calculated once the steady state was reached in the permeate stream of the membrane. Two samples of each membrane were tested and average values of two membranes are reported.

The permeability for gas *i* was calculated by the following equation:

$$P_i = \frac{F_i \cdot l}{\Delta p_i \cdot A}$$

where P_i is the gas permeability in Barrer (1 Barrer = 10^{-10} cm^3 (STP) cm cm^{-2} s^{-1} $cmHg^{-1}$), F_i is the volumetric flow rate of component *i* (cm^3 (STP) s^{-1}), *l* is the thickness of the membrane (cm), Δp_i is the partial pressure difference of component *i* across the membrane (cmHg) and *A* is the effective membrane area (cm^2).

The separation factor or mixed gas selectivity *a* was calculated as the ratio of the permeability of more permeable compound *i* to the permeability of the less permeable compound *j*:

$$\alpha_{i/j} = \frac{P_i}{P_j}$$

2.3. Results and discussion

2.3.1. MOF characterization

ZIF-94 crystals were synthesized in this work by replacing dimethylformamide (DMF), previously used for synthesis of ZIF-94 [39], with a 2:5 ratio mixture of methanol:THF. A reaction yield of 82 % for lab scale synthesis and 99 % for up scaling, with respect to zinc were achieved. Higher reaction yield might be due to the use of a high-speed centrifuge for up-scale synthesis, not available for lab scale synthesis. The SEM image shown in Figure 2.1 indicates that spherical particles of ZIF-94 were produced with a diameter of 100-500 nm. The PXRD pattern of this material (Figure 2.2) was consistent with that reported by Aguado *et al.* [49] and with the sodalite topology.

TGA analysis of the as-prepared ZIF-94 in air showed a thermal stability up to ~225 ºC with ~20% weight loss due to THF and methanol removal (Figure 2.3). CO_2 adsorption capacities at 25 ºC were 0.85 mmol g^{-1} at 0.10 bar and 2.3 mmol g^{-1} at 0.9 bar for lab scale synthesis and 1.25 mmol g^{-1} at 0.10 bar and 2.75 mmol g^{-1} at 0.9 bar for up scaling (Figure 2.4). The BET surface area derived from the N_2 isotherm were 424 m^2 g^{-1} and 506 m^2 g^{-1} respectively, which is close to what has previously been reported (471 and 480 m^2 g^{-1}) [39,50].

The scale-up of the synthesis from the laboratory small scale to the laboratory pilot scale was achieved for ZIF-94. The characteristics of the resulting up-scaled sample match on the whole those of the solid produced at smaller scale, both in terms of crystallinity, purity and particle size and shape.

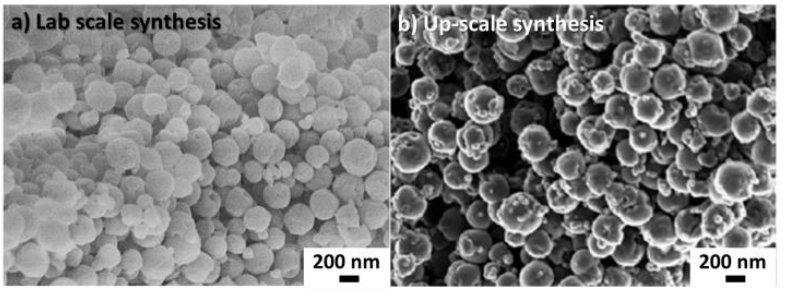

Figure 2.1. SEM image of (a) lab scale and (b) up-scale synthesized ZIF-94 particles.

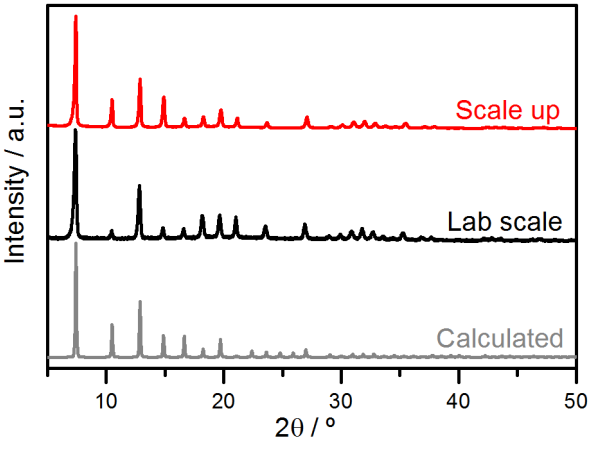

Figure 2.2. Simulated XRD diffraction pattern of ZIF-94 sodalite topology and PXRD patterns of lab scale and scaled up batches of ZIF-94 particles.

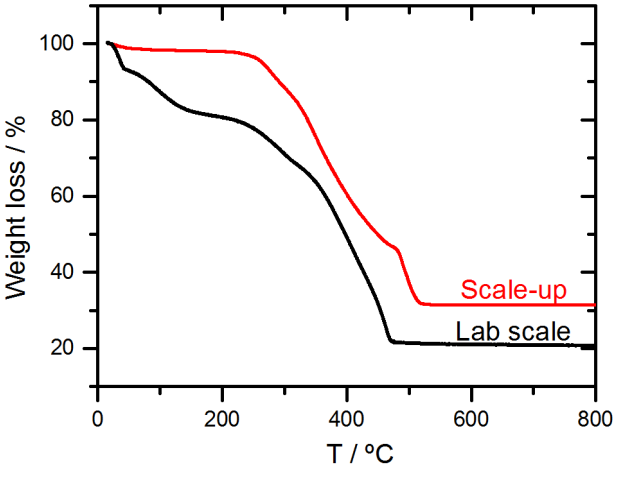

Figure 2.3. TGA of lab scale and scaled up samples of ZIF-94 particles.

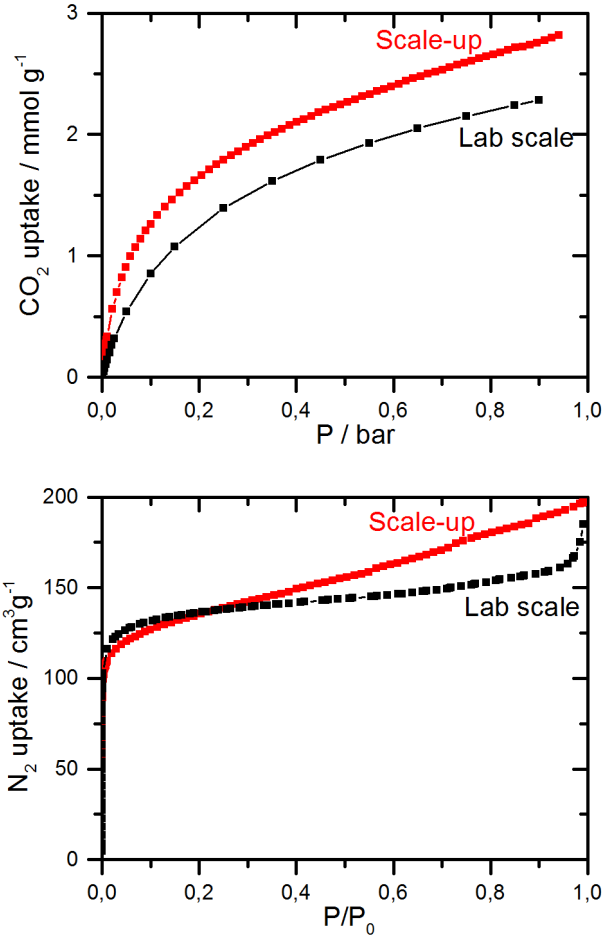

Figure 2.4. CO_2 Adsorption isotherms on lab scale and scaled up samples ZIF-94 at 25ºC (*top*) and N_2 at -196ºC (*bottom*). The N_2-BET areas were 424 $m^2\ g^{-1}$ and 506 $m^2\ g^{-1}$ respectively.

2.3.2. MMMs morphology

6FDA-DAM MMMs were prepared at 10, 20, 30 and 40 wt% ZIF-94 loadings. SEM images of the cross-section of a 10 wt% and 40 wt% ZIF-94 MMM are shown in Figure 2.5. A good dispersion of ZIF-94 particles in the polymer matrix without agglomeration was obtained even at high loadings. SEM images of the surface of the ZIF-94 MMMs analyzed using LFD and vCD detectors are shown in Figure 2.6. The use of the LFD detector allows analyzing the topography of the surface whereas the compositional contrast provided by the vCD detector allows observing the MOF distribution just beneath the surface of the membrane. The images taken by the LFD detector show a defect-free surface, while the presence of MOF particles is visible through the thin transparent polymer surface layer. The presence of the MOF particles under this polymer surface layer is better demonstrated by the vCD detector, since heavier elements such as metal atom of the MOF are brighter in vCD images. For an organic polymer at 20 kV the beam could go up to 5 μm depth into the sample. At the voltage used for SEM analysis (10 kV) it is estimated that the beam might go up to 2 or 3 μm deep. ZIF-94 particles appear with bright contrast in the vCD image. The good filler distribution might be due to a good compatibility between the polymer phase and ZIF-94 particles expected from interaction of the -CHO pending group of the MOF linker with the $-NH_2$ end group of the polymer.

XRD patterns of ZIF-94 powder, 6FDA-DAM polymer and MMMs with ZIF-94 loadings of 10 to 40 wt% are shown in Figure 2.7. Pure 6FDA-DAM polymer shows a typical broad spectrum of an amorphous polymer with no crystalline reflections. The diffraction pattern observed for the MMMs confirms the presence of the ZIF-94 phase. The ZIF-94 crystalline structure remained unchanged in the MMMs, suggesting that the membrane preparation procedure does not affect the crystallinity of MOF particles.

The infrared characterization of the 40 wt% ZIF-94 MMM is shown in Figure 2.8. From FTIR spectroscopy of the pure membrane and pure ZIF-94 reference samples (Figure 2.8a), the infrared frequencies for s-SNOM imaging (indicated by dashed lines) were determined. At 1665 cm^{-1}, the ZIF-94 exhibits a strong absorption of the -N-H bond vibration, where the polymer absorption is weak. Consequently, the infrared s-SNOM phase image at 1665 cm^{-1} (Figure 2.8d) exhibits a strong phase contrast revealing the individual ZIF-94 particles (bright disk-shaped objects), which are collocated with the surface protrusions seen in the AFM topography image of exactly the same sample area (Figure 2.8c). Furthermore, the contrast of the individual particles strongly varies, which we attribute to their vertical position in the membrane: In s-SNOM, a decreasing contrast of objects of the same size and chemical compositions

indicates an increasing depth below the surface [51]. To verify that molecular chemical contrast is observed, another infrared image was recorded at 1600 cm^{-1} (indicated by the dashed line in Figure 2.8a), where the absorption of both 6FDA-DAM and ZIF-94 is weak. Indeed, the infrared phase image at 1600 cm^{-1} does not show a significant contrast. In the future, s-SNOM could be applied for more detailed nanoscale studies, for example of inhomogeneities, and chemical interaction, particularly at the interfaces between individual membrane components [52].

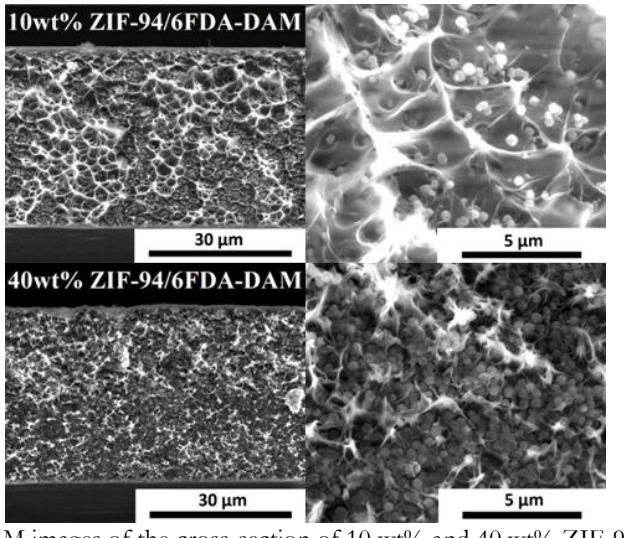

Figure 2.5. SEM images of the cross-section of 10 wt% and 40 wt% ZIF-94/6FDA-DAM MMMs obtained by the LFD detector at different magnifications.

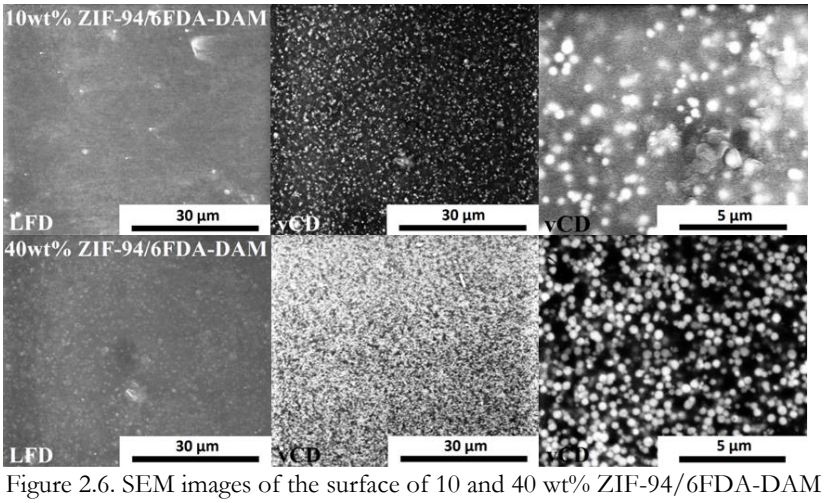

Figure 2.6. SEM images of the surface of 10 and 40 wt% ZIF-94/6FDA-DAM MMMs obtained by LFD detector and vCD detector at different magnifications.

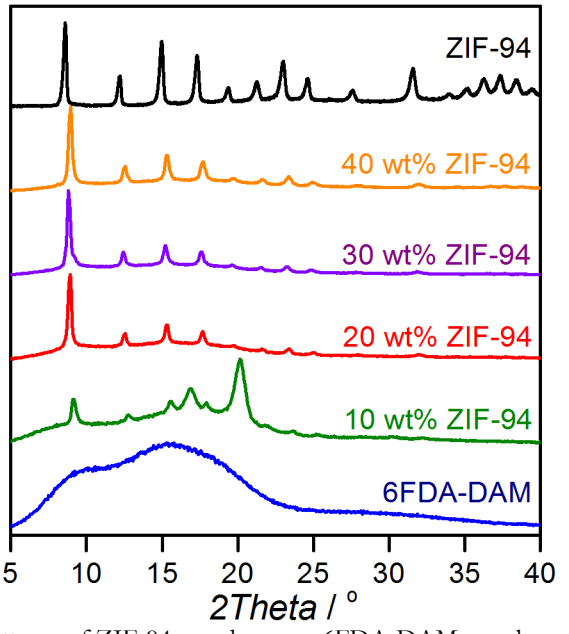

Figure 2.7. XRD patterns of ZIF-94 powder, pure 6FDA-DAM membrane and MMMs with different ZIF-94 loadings.

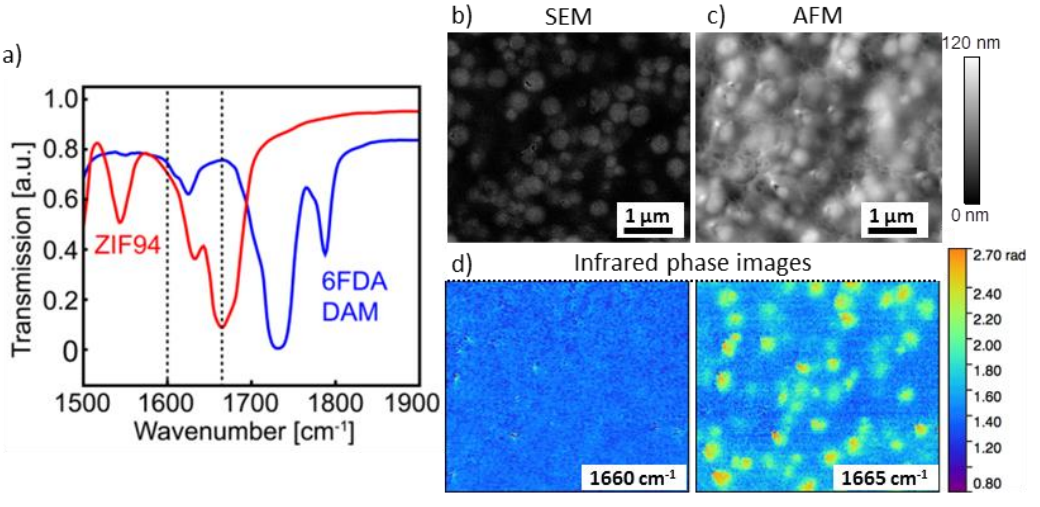

Figure 2.8. Infrared characterization of the 40 wt% ZIF-94 MMM surface. (a) Far-field transmission FTIR spectra of pure 6FDA-DAM and ZIF94, (b) SEM surface image obtained by LFD detector, (c) AFM surface topography and (d) infrared images of the membrane surface.

2.3.3. MMMs gas permeation

2.3.3.1. Pure polymer: pure gases *versus* mixed gases for 6FDA-DAM membrane

To date, most of the permeation data reported in literature is for pure gases. In most cases transport behavior of gas mixtures through membranes is different from that of pure gases [53,54]. This leads to differences in pure gas and mixed gas permeabilities and selectivities. Hence, in order to assess membrane properties under real process conditions, it is essential to determine mixed gas permeation performance.

The bare 6FDA-DAM membrane was tested both for pure gases (CO_2 and N_2) and CO_2/N_2 gas mixtures (15:85) at transmembrane pressure differences of 1 to 4 bar. Single and mixed gas permeabilities (CO_2 and N_2) and CO_2/N_2 selectivities are presented as a function of transmembrane pressure in Figure 2.9. For pure CO_2, permeability decreased with increasing feed pressure (from 540 to 450 Barrer at 1 and 4 bar, respectively), a behavior predicted by the dual-mode sorption and mobility models for gas permeation of condensable gases such as carbon dioxide in glassy polymers [55]. Meanwhile the permeability of the low adsorbing penetrant N_2 exhibited little or no dependency on pressure [55]. As a result, a slight decrease in the ideal CO_2/N_2 selectivity was observed with increasing feed pressure for pure gases. It is worth mentioning that another phenomenon that can influence gas permeation through membranes is plasticization, *i.e.* sorption induced swelling of the polymer matrix, causing an increased polymer chain mobility and consequently increased gas permeability. For the 6FDA-DAM polymer, plasticization with CO_2 takes place at pressures higher than 10 bar [56]. Therefore, plasticization is excluded to interfere under the studied conditions.

As expected, significant differences between pure and mixed gas permeation are observed. The mixed gas permeability for N_2 is lower than the pure gas permeability. In the case of CO_2, at first sight the mixed gas permeability seems higher than the pure gas permeability but, if instead of the total feed pressure, one takes into account the partial CO_2 transmembrane pressure difference (from 0.15 to 0.60 bar) then the values for CO_2 permeability fit the trend of higher permeability at lower pressures. The dual-mode sorption model for gas permeation estimates lower permeability for all mixture components due to competitive sorption between the gases for the polymer matrix sorption sites. Nevertheless, CO_2 has a much higher affinity constant and solubility in glassy polymers than N_2. Therefore, polymer matrix sorption sites are saturated with CO_2, and N_2 permeability is decreased. Similar to pure gases, a decrease in CO_2 permeability was also observed as the transmembrane pressure increased in the mixed gas test (from 768 to 670 Barrer at 1 and 4 bar, respectively). Furthermore, also a small

increase in N_2 permeability with increasing pressure was observed, resulting in an unchanged CO_2/N_2 separation factor.

An ideal CO_2/N_2 selectivity of around 14 was obtained based on pure gas permeation, whereas the CO_2/N_2 separation factor for the mixed gas test was 24 over the whole total transmembrane pressure difference range from 1 to 4 bar. This emphasizes the importance of performing mixed gas experiments in order to know membrane performance under relevant conditions for commercial applications. Hence only mixed gas performance is reported below for the MMMs prepared in this work.

2.3.3.2. MMMs: Effect of ZIF-94 loading on mixed gas separation performance

6FDA-DAM / ZIF-94 MMM were prepared at different MOF loadings (10-40 wt%). Mixed gas separation performance of the pure polymer membrane and MMMs with various loadings of ZIF-94 is shown in Figure 2.9. Both CO_2 and N_2 permeability gradually increased when ZIF-94 loading was increased from 0 to 30 wt%, from 770 to 1225 Barrer of CO_2, respectively. A further strong increase in permeability was observed at 40 wt% ZIF-94 loading. The CO_2 permeability nearly doubled up to 2310 Barrer at 1 bar transmembrane pressure difference, while the CO_2/N_2 selectivity remained unchanged by the addition of the ZIF-94 at an average value of 22.7 ± 1.5 (results slightly deviate for 30 wt% loading). The increased CO_2 permeability with filler loading might be related to (1) disruption of the chain packing of the polymer, (2) porosity introduced by MOF particles [34] and (3) increase in the polymer free volume [57–59]. The characterization of the MMM shows that in our case the MOF distribution is quite even throughout the membrane with good adhesion between the MOF filler and the polymer. Therefore, the permeability of MMMs is evaluated by the Maxwell equation [6]. First, the unknown parameter of the Maxwell equation P_d (disperse phase permeability) was determined from the experimental 10 wt% membrane permeability, whereas P_c (continuous phase permeability) was determined from the pure polymer permeation. P_d could in principle be determined experimentally from films made of pure MOF. Preparing such films is extremely challenging if not impossible because they should be self-supporting with the MOF phase densely packed, with no sub-nanometer defects between the particles. A MOF phase with such morphology was achieved only by *in-situ* synthesis on top of porous supports [60] and was not the subject of this study. ZIF-94 (SIM-1) membrane has been crystallized *in-situ* on a tubular asymmetric alumina support with pore size of 200 nm by Aguado *et al.* [41]. They demonstrated that the gas transport obeys the Knudsen diffusion mechanism such as found for microporous membranes. This translated in a higher gas

permeability than in polymers and a low (Knudsen) gas selectivity. At 35 ºC they have achieved overall single gas CO_2 permeance of 104 GPU. Considering the reported MOF layer thickness was of approximately 25 μm and no resistance to the overall transport by the support, we estimate the pure ZIF-94 phase permeability by multiplying permeance with layer thickness to a value of 2613 Barrer. This value is related to pure gas permeation. Our estimated P_d from the 10 wt.% experiment represents the mixed gas permeability and was equal to 4735 Barrer.

Then theoretical MMM permeabilities have further been predicted for other loadings. The experimental and predicted permeability are presented in Figure 2.10. Experimental permeability values of 10-30 wt% loaded membranes follow the trend predicted by the Maxwell relation. However, a higher experimental permeability than predicted is obtained for the 40 wt% loaded membrane. The lack of significant change in selectivity with MOF loading relative to the bare polymer demonstrates that the prepared MMMs are 'defect-free' and suggests that the polymer determines the selectivity, while the MOF introduces faster transport pathways. The larger permeability than predicted according to the Maxwell model indicates that at high loadings the ZIF-94 influence is not captured by this model, which is approximately only valid up to volume fractions of 20%.

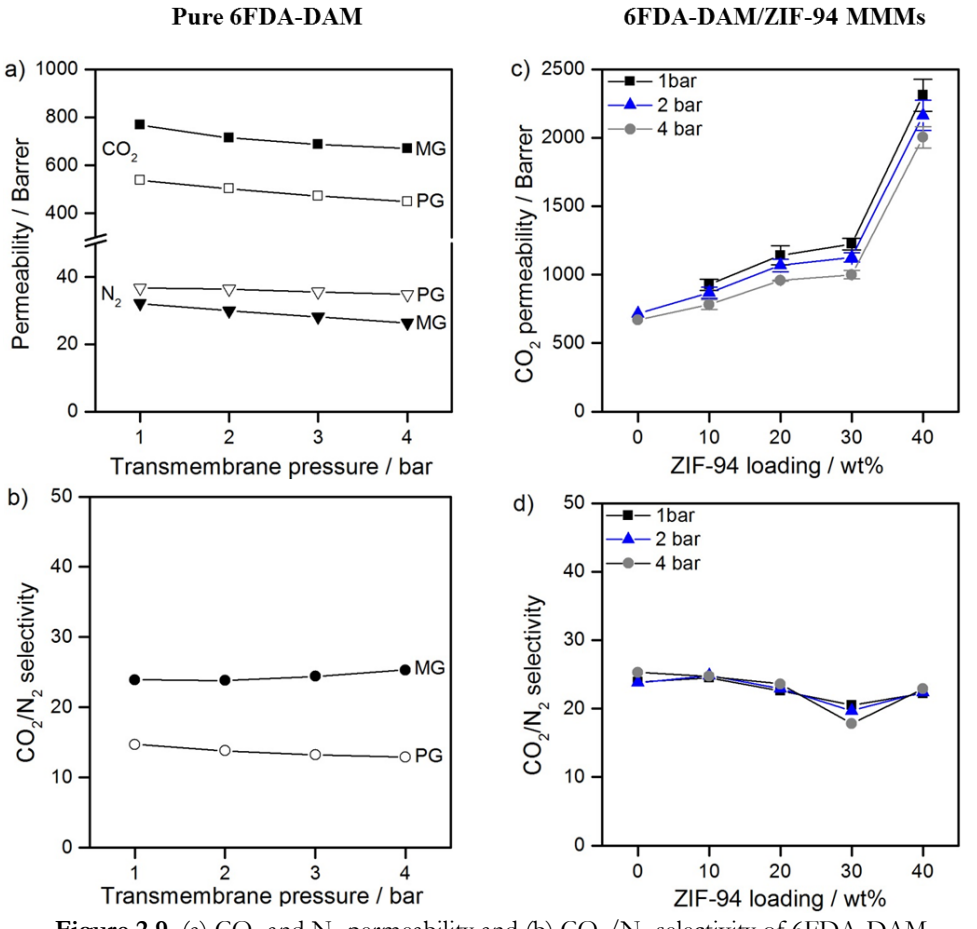

Figure 2.9. (a) CO_2 and N_2 permeability and (b) CO_2/N_2 selectivity of 6FDA-DAM membrane for pure gas (PG) and mixed gas (MG) experiments as a function of transmembrane pressure. Experimental results of mixed gas (c) CO_2 permeability and (d) CO_2/N_2 selectivity of prepared MMMs at as a function of ZIF-94 loading and 1-4 bar transmembrane pressure. The data are average values of two samples and error bars correspond to standard deviation. Experiments were performed at 25ºC. The lines are to guide the eye.

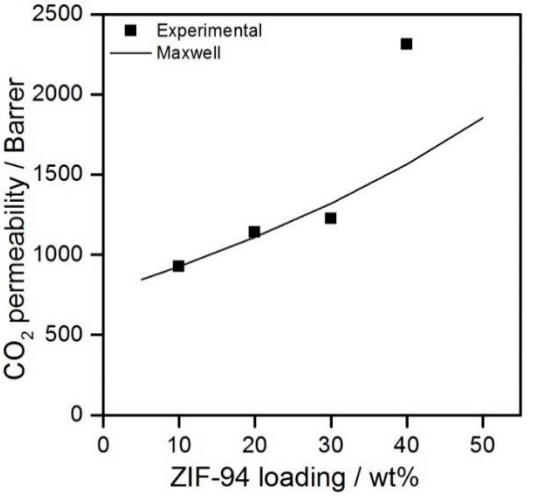

Figure 2.10. Experimental mixed gas CO_2 permeability results (square symbols) and permeability predicted by Maxwell equation (line) as a function of ZIF-94 loading at 25 ºC and 1 bar transmembrane pressure.

The results obtained in this work follow the general trend reported in a recent review about MOF based MMMs published by Seoane *et al.* [21]. In most studies, improvements in flux at constant selectivity with respect to the bare polymer have been reported. Only in circa 10% of cases improvements in both flux and selectivity were achieved. In order to benchmark our results with literature, separation performance of 6FDA-DAM based dense MMMs reported in literature are shown in Table 2.1. In terms of CO_2 permeation through pure polymer we can observe different results. Polymers used in literature were synthesized in the laboratory and different molecular weight could lead to differences in gas separation performance. Also, as 6FDA-DAM has a high free volume, the solvent used for the fabrication of the membrane and the membrane history might influence final separation performance of the membrane. Also, it is worth to mention that we compare single with mixed gas results. Nevertheless, the common feature is a significant increase in CO_2 permeability observed by the addition of the filler particles in the 6FDA-DAM polymer matrix. In some cases, there is a selectivity increase due to either molecular sieving [37] or to solubility increase [36]. Zhang *et al.* went a step further and prepared ZIF-8/6FDA-DAM mixed-matrix hollow fiber membranes with ZIF-8 nanoparticle loading up to 30 wt% [61]. The mixed-matrix hollow fibers showed significantly enhanced propylene/propane selectivity that was consistent with dense mixed-matrix films.

Table 2.1. Literature review: Gas separation performance of 6FDA-DAM based dense MMMs reported in literature. Pure polymer and mixed matrix membrane separation performance is reported at the same column separated by an arrow (pure polymer → MMM).

Filler	Filler loading (wt%)	CO_2 Permeability (Barrer)	Selectivity			Test	Ref.
			CO_2/N_2	CO_2/CH_4	Propylene /propane		
ZIF-94	40	770 → 2310	24 → 22	-	-	MG[a]	This work
NH_2-MIL-53(Al)	20	360 → 660	-	31 → 28	-	MG[b]	[34]
ZIF-11	20	20.6 → 257	-	33 → 31	-	SG	[35]
Mg-MMS	8	653 → 1214	19 → 24	-	-	MG	[62]
CPO-27(Mg)	10	650 → 850	14 → 23	-	-	SG	[36]
ZIF-90	15	390 → 720	-	24 → 37	-	MG	[37]
ZIF-8	48	Propylene 16 → 56	-	-	12 → 31	MG	[38]

[a]MG corresponds to mixed gas experiment

[b]SG to single gas experiment

We extend the benchmarking of our best membrane via a Robeson plot in Figure 2.11 (☆), including more relevant results reported in literature for other MOF based MMMs for the separation of CO_2 from N_2 [21] for pure gas permeation (●).The separation performance of the 40 wt% ZIF-94 loaded membrane developed in this work is situated on the Robeson limit and presents the highest permeability at similar selectivity among 6FDA-DAM MMMs reported in literature. Other membranes situated on the Robeson limit are (a) 30 wt% ZIF-8 loaded 6FDA-durene MMM (2185 Barrer CO_2, ideal CO_2/N_2 selectivity 17, point *i* in Figure 2.11), (b) 30 wt% Zn_2(1,4-bdc)$_2$dabco loaded 6FDA-4MPD MMM (3300 Barrer CO_2, ideal CO_2/N_2 selectivity 19.1, point *k* in Figure 2.11) and (c) 30 wt% loaded PIM-1 membrane (6300 Barrer CO_2, ideal CO_2/N_2 selectivity 18, point *n* in Figure 2.11). Their performance has been only tested for pure gases (ideal selectivity) while our membranes have been tested under relevant process conditions (mixed gas 15/85 CO_2/N_2).

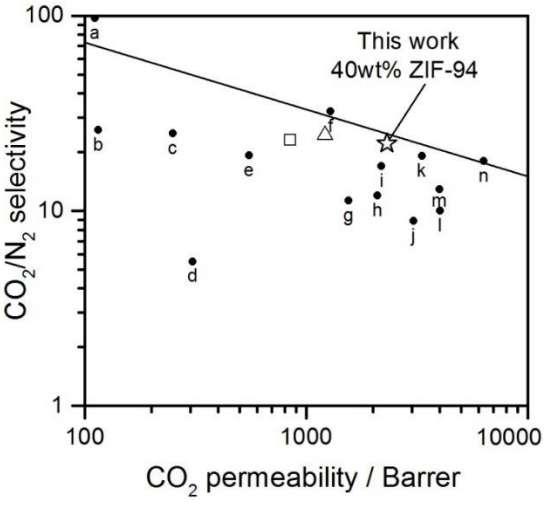

Figure 2.11. Robeson plot for the separation of CO_2 from N_2. The graph contains the most relevant results reported in literature for MOF based MMMs (●): (a) Pebax®/ZIF-7 [27], (b) PPO/HKUST-1 [63], (c) XLPEO/CPO-27(Mg) [36], (d) PMDA-ODA/HKUST-1 [64], (e) 6FDA-DAM:DABA 4:1 /ZIF-8 [22], (f) Pebax®/ZIF-8 [26], (g) 6FDA-durene/ZIF-8 [24], (h) PDMS/CPO-27(Mg) [36], (i) 6FDA-durene/ZIF-8 [23], (j) PDMS/HKUST-1 [65], (k) 6FDA-4MPD/$[Zn_2(bdc)_2(dabco)]\cdot 4DMF\cdot 0.5H_2O$ [66], (l) PDMS/$[Zn_2(bdc)_2(dabco)]\cdot 4DMF\cdot 0.5H_2O$ [66], (m) 6FDA-durene/ZIF-71 [25] and (n) PIM-1/ZIF-8 [67]. Separation performance of 6FDA-DAM MMMs reported in literature is represented by △ [62] and □ [36]. Separation performance of ZIF-94/6FDA-DAM MMM prepared in this work is represented by ☆. 1 Barrer = 1 GPU for 1 μm thick membrane.

This work focused on determining the intrinsic (mixed matrix) material properties for gas separation. In the future we will transfer the membrane preparation into applied hollow fiber configuration. Hollow fibers are highly productive because have thin selective layer and can be densely packed into membrane modules with high membrane area. Bare 6FDA-DAM polymer was already shown to be spinnable into a hollow fiber structure [68]. Merkel *et al.* assessed the competitiveness of membrane separation technology for post-combustion CO_2 capture application [69]. They identified an optimum region of membrane properties (in terms of selectivity and permeance): the minimum CO_2/N_2 selectivity and CO_2 permeance required are 20 and 800 GPU (gas permeation unit), respectively. Lively *et al.* [22] have assessed the potential of 6FDA-based hollow fiber membranes for post-combustion CO_2 capture for the same process configuration proposed by Merkel *et al.* They concluded that if hollow fibers can be produced with a CO_2 permeance higher than 1000 GPU and CO_2/N_2 selectivity of 20, CO_2 capture cost could be reduced to less than 23 $/ton of CO_2. Extrapolating MMM results of our work, at an estimated selective layer thickness of 500 nm, gives mixed

matrix hollow fiber with CO_2 permeability of 4620 GPU and CO_2/N_2 selectivity of 22. This is within the region of optimum membrane properties identified by Merkel *et al.* [69] for the separation of CO_2 from flue gas. Moreover, not only the 40 wt% ZIF-94 loaded membrane, but all the MMMs prepared in this work would be within this optimum region if they are transferred to a hollow fiber configuration (1850, 2280 and 2450 GPU of CO_2 for 10, 20 and 30 wt% ZIF-94 loaded MM HF, respectively). Furthermore, the increase in CO_2 permeance at higher ZIF-94 loading would lead to a significant reduction in total membrane area required, and hence in the reduction of investment cost for CO_2 capture, as reported by Lively *et al.* [22].

2.4. Conclusions

MMMs of ZIF-94 and glassy polyimide 6FDA-DAM have been successfully prepared up to high loadings of 40 wt%, using filler produced in up scaled and environmentally more benign process. Membranes are homogeneous and defect free with unaltered filler crystalline structure. Addition of filler increases gas membrane permeability is in accordance to the Maxwell model. An additional increase is observed at 40 wt% loading, attributed to the disruption of the chain packing of the polymer and increase in the polymer free volume. The separation performance of the 40 wt% ZIF-94 loaded membrane developed in this work shows the highest permeability at similar selectivity among 6FDA-DAM MMMs reported in literature. For the first time membranes were characterized by non-invasive infrared scattering type scanning near field optical microscopy, which provides nanoscale-resolved chemical information that complements standard analysis methods. In the future, s-SNOM could be applied for more detailed nanoscale studies, for example of inhomogeneities, and chemical interaction, particularly at the interfaces between individual membrane components [52].

The developed MMM has great potential to be spun into a hollow fiber membrane configuration since the bare polymer is spinnable and the ZIF-94 filler has a smaller size than the selective layer (< 500 nm). Therefore, the region of optimal membrane properties for the separation of CO_2 from flue gas identified by Merkel *et al.* [69] can be amply reached with any of the MMMs prepared in this work (10 to 40 wt% ZIF-94 loading).

Bibliography

[1] CO2 emissions from fuel combustion. Highlights (2016 edition), 2016.

[2] 2011 Technology Map of the European Strategic Energy Technology Plan (SET-Plan), 2011.

[3] Technology Roadmap. Carbon Capture and Storage, 2013.

[4] J.D. Figueroa, T. Fout, S. Plasynski, H. McIlvried, R.D. Srivastava, Advances in CO2 capture technology—The U.S. Department of Energy's Carbon Sequestration Program, Int. J. Greenh. Gas Control. 2 (2008) 9–20. doi:10.1016/S1750-5836(07)00094-1.

[5] P. Bernardo, E. Drioli, G. Golemme, Membrane Gas Separation: A Review/State of the Art, Ind. Eng. Chem. Res. 48 (2009) 4638–4663. doi:10.1021/ie8019032.

[6] M.A. Aroon, A.F. Ismail, T. Matsuura, M.M. Montazer-Rahmati, Performance studies of mixed matrix membranes for gas separation: A review, Sep. Purif. Technol. 75 (2010) 229–242. doi:10.1016/j.seppur.2010.08.023.

[7] L.M. Robeson, Correlation of separation factor versus permeability for polymeric membranes, J. Memb. Sci. 62 (1991) 165–185. doi:10.1016/0376-7388(91)80060-J.

[8] L.M. Robeson, The upper bound revisited, J. Memb. Sci. 320 (2008) 390–400. doi:10.1016/j.memsci.2008.04.030.

[9] S. Smart, C.X.C. Lin, L. Ding, K. Thambimuthu, J.C. Diniz da Costa, Ceramic membranes for gas processing in coal gasification, Energy Environ. Sci. 3 (2010) 268–278. doi:10.1039/B924327E.

[10] A. Ismail, L. David, A review on the latest development of carbon membranes for gas separation, J. Memb. Sci. 193 (2001) 1–18. doi:10.1016/S0376-7388(01)00510-5.

[11] N. Kosinov, J. Gascon, F. Kapteijn, E.J.M. Hensen, Recent developments in zeolite membranes for gas separation, J. Memb. Sci. 499 (2016) 65–79. doi:10.1016/j.memsci.2015.10.049.

[12] S. Basu, A.L. Khan, A. Cano-Odena, C. Liu, I.F.J. Vankelecom, Membrane-based technologies for biogas separations., Chem. Soc. Rev. 39 (2010) 750–768. doi:10.1039/b817050a.

[13] J. Gascon, F. Kapteijn, B. Zornoza, V. Sebastián, C. Casado, J. Coronas, Practical Approach to Zeolitic Membranes and Coatings: State of the Art, Opportunities, Barriers, and Future Perspectives, Chem. Mater. 24 (2012) 2829–2844. doi:10.1021/cm301435j.

[14] E. Fernandez, K. Coenen, A. Helmi, J. Melendez, J. Zuñiga, D.A. Pacheco Tanaka, M. van Sint Annaland, F. Gallucci, Preparation and characterization of thin-film Pd–Ag supported membranes for high-temperature applications, Int. J. Hydrogen Energy. 40 (2015) 13463–13478. doi:10.1016/j.ijhydene.2015.08.050.

[15] J. Coronas, Present and future synthesis challenges for zeolites, Chem. Eng. J. 156 (2010) 236–242. doi:10.1016/j.cej.2009.11.006.

[16] H. Vinh-Thang, S. Kaliaguine, Predictive Models for Mixed-Matrix Membrane Performance: A Review, Chem. Rev. 113 (2013) 4980–5028. doi:10.1021/cr3003888.

[17] P.S. Goh, A.F. Ismail, S.M. Sanip, B.C. Ng, M. Aziz, Recent advances of inorganic fillers in mixed matrix membrane for gas separation, Sep. Purif. Technol. 81 (2011) 243–264. doi:10.1016/j.seppur.2011.07.042.

[18] T. Rodenas, M. van Dalen, E. García-Pérez, P. Serra-Crespo, B. Zornoza, F. Kapteijn, J. Gascon, Visualizing MOF Mixed Matrix Membranes at the Nanoscale: Towards Structure-Performance Relationships in CO2/CH4 Separation Over NH2-MIL-53(Al)@PI, Adv. Funct. Mater. 24 (2014) 268. doi:10.1002/adfm.201470014.

[19] H. Yehia, T.J. Pisklak, J.P. Ferraris, K.J. Balkus, I.H. Musselman, Methane Facilitated Transport Using Copper(II) Biphenyl Dicarboxylate-Triethylenediamine/Poly (3-Acetoxyethylthiophene) Mixed Matrix Membranes, Polym. Prepr. Am. Chem. Soc. 45 (2004) 35–36.

[20] M. Rezakazemi, A. Ebadi, State-of-the-art membrane based CO2 separation using mixed matrix membranes (MMMs): An overview on current status and future directions, Prog. Polym. Sci. 39 (2014) 817–861. doi:10.1016/j.progpolymsci.2014.01.003.

[21] B. Seoane, J. Coronas, I. Gascon, M.E. Benavides, O. Karvan, J. Caro, F. Kapteijn, J. Gascon, Metal–organic framework based mixed matrix membranes: a solution for highly efficient CO2 capture?, Chem. Soc. Rev. 44 (2015) 2421–2454. doi:10.1039/C4CS00437J.

[22] R.P. Lively, M.E. Dose, L. Xu, J.T. Vaughn, J.R. Johnson, J.A. Thompson, K. Zhang, M.E. Lydon, J.-S. Lee, L. Liu, Z. Hu, O. Karvan, M.J. Realff, W.J. Koros, A high-flux polyimide hollow fiber membrane to minimize footprint and energy penalty for CO2 recovery from flue gas, J. Memb. Sci. 423–424 (2012) 302–313. doi:10.1016/j.memsci.2012.08.026.

[23] V. Nafisi, M.-B. Hägg, Gas separation properties of ZIF-8/6FDA-durene diamine mixed matrix membrane, Sep. Purif. Technol. 128 (2014) 31–38. doi:https://doi.org/10.1016/j.seppur.2014.03.006.

[24] S.N. Wijenayake, N.P. Panapitiya, S.H. Versteeg, C.N. Nguyen, S. Goel, K.J.

Balkus, I.H. Musselman, J.P. Ferraris, Surface Cross-Linking of ZIF-8/Polyimide Mixed Matrix Membranes (MMMs) for Gas Separation, Ind. Eng. Chem. Res. 52 (2013) 6991–7001. doi:10.1021/ie400149e.

[25] S. Japip, H. Wang, Y. Xiao, T. Shung Chung, Highly permeable zeolitic imidazolate framework (ZIF)-71 nano-particles enhanced polyimide membranes for gas separation, J. Memb. Sci. 467 (2014) 162–174. doi:10.1016/j.memsci.2014.05.025.

[26] V. Nafisi, M.-B. Hägg, Development of dual layer of ZIF-8/PEBAX-2533 mixed matrix membrane for CO2 capture, J. Memb. Sci. 459 (2014) 244–255. doi:10.1016/j.memsci.2014.02.002.

[27] T. Li, Y. Pan, K.-V. Peinemann, Z. Lai, Carbon dioxide selective mixed matrix composite membrane containing ZIF-7 nano-fillers, J. Memb. Sci. 425–426 (2013) 235–242. doi:10.1016/j.memsci.2012.09.006.

[28] C. Cao, The study of 6FDA-polyimide gas separation membranes, National University of Singapore, 2003.

[29] M.R. Coleman, R. Kohn, W.J. Koros, Gas-separation applications of miscible blends of isomeric polyimides, J. Appl. Polym. Sci. 50 (1993) 1059–1064. doi:10.1002/app.1993.070500614.

[30] M.R. Coleman, W.J. Koros, The transport properties of polyimide isomers containing hexafluoroisopropylidene in the diamine residue, J. Polym. Sci. Part B Polym. Phys. 32 (1994) 1915–1926. doi:10.1002/polb.1994.090321109.

[31] L.M. Costello, W.J. Koros, Thermally stable polyimide isomers for membrane-based gas separations at elevated temperatures, J. Polym. Sci. Part B Polym. Phys. 33 (1995) 135–146. doi:10.1002/polb.1995.090330114.

[32] H. Kawakami, M. Mikawa, S. Nagaoka, Formation of surface skin layer of asymmetric polyimide membranes and their gas transport properties, J. Memb. Sci. 137 (1997) 241–250. doi:10.1016/S0376-7388(97)00198-1.

[33] D.W. Wallace, C. Staudt-Bickel, W.J. Koros, Efficient development of effective hollow fiber membranes for gas separations from novel polymers, J. Memb. Sci. 278 (2006) 92–104. doi:10.1016/j.memsci.2005.11.001.

[34] A. Sabetghadam, B. Seoane, D. Keskin, N. Duim, T. Rodenas, S. Shahid, S. Sorribas, C. Le Guillouzer, G. Clet, C. Tellez, M. Daturi, J. Coronas, F. Kapteijn, J. Gascon, Metal Organic Framework Crystals in Mixed-Matrix Membranes: Impact of the Filler Morphology on the Gas Separation Performance, Adv. Funct. Mater. 26 (2016) 3154–3163. doi:10.1002/adfm.201505352.

[35] M.S. Boroglu, A.B. Yumru, Gas separation performance of 6FDA-DAM-ZIF-11 mixed-matrix membranes for H2/CH4 and CO2/CH4 separation, Sep.

Purif. Technol. 173 (2017) 269–279. doi:10.1016/j.seppur.2016.09.037.

[36] T.-H. Bae, J.R. Long, CO2/N2 separations with mixed-matrix membranes containing Mg2(dobdc) nanocrystals, Energy Environ. Sci. 6 (2013) 3565–3569. doi:10.1039/C3EE42394H.

[37] T.-H. Bae, J.S. Lee, W. Qiu, W.J. Koros, C.W. Jones, S. Nair, A High-Performance Gas-Separation Membrane Containing Submicrometer-Sized Metal–Organic Framework Crystals, Angew. Chemie Int. Ed. 49 (2010) 9863–9866. doi:10.1002/anie.201006141.

[38] C. Zhang, Y. Dai, J.R. Johnson, O. Karvan, W.J. Koros, High performance ZIF-8/6FDA-DAM mixed matrix membrane for propylene/propane separations, J. Memb. Sci. 389 (2012) 34–42. doi:10.1016/j.memsci.2011.10.003.

[39] W. Morris, N. He, K.G. Ray, P. Klonowski, H. Furukawa, I.N. Daniels, Y. a. Houndonougbo, M. Asta, O.M. Yaghi, B.B. Laird, A combined experimental-computational study on the effect of topology on carbon dioxide adsorption in zeolitic imidazolate frameworks, J. Phys. Chem. C. 116 (2012) 24084–24090. doi:10.1021/jp307170a.

[40] A.M. Marti, D. Tran, K.J. Balkus, Fabrication of a Substituted Imidazolate Material 1 (SIM-1) membrane using post synthetic modification (PSM) for pervaporation of water/ethanol mixtures, J. Porous Mater. 22 (2015) 1275–1284. doi:10.1007/s10934-015-0005-y.

[41] S. Aguado, C.-H. Nicolas, V. Moizan-Basle, C. Nieto, H. Amrouche, N. Bats, N. Audebrand, D. Farrusseng, Facile synthesis of an ultramicroporous MOF tubular membrane with selectivity towards CO2, New J. Chem. 35 (2011) 41–44. doi:10.1039/C0NJ00667J.

[42] F. Cacho-Bailo, M. Etxeberria-Benavides, O. Karvan, C. Tellez, J. Coronas, Sequential amine functionalization inducing structural transition in an aldehyde-containing zeolitic imidazolate framework: application to gas separation membranes, CrystEngComm. 19 (2017) 1545–1554. doi:10.1039/C7CE00086C.

[43] R.W. Cheary, A. Coelho, A fundamental parameters approach to X-ray line-profile fitting, J. Appl. Crystallogr. 25 (1992) 109–121. doi:10.1107/S0021889891010804.

[44] F. Keilmann, R. Hillenbrand, Near-field microscopy by elastic light scattering from a tip, Philos. Trans. R. Soc. London. Ser. A Math. Phys. Eng. Sci. 362 (2004) 787–805.

[45] N. Ocelic, A. Huber, R. Hillenbrand, Pseudoheterodyne detection for background-free near-field spectroscopy, Appl. Phys. Lett. 89 (2006) 101124.

[46] T. Taubner, R. Hillenbrand, F. Keilmann, Nanoscale polymer recognition by spectral signature in scattering infrared near-field microscopy, Appl. Phys. Lett. 85 (2004) 5064–5066. doi:10.1063/1.1827334.

[47] F. Huth, A. Govyadinov, S. Amarie, W. Nuansing, F. Keilmann, R. Hillenbrand, Nano-FTIR Absorption Spectroscopy of Molecular Fingerprints at 20 nm Spatial Resolution, Nano Lett. 12 (2012) 3973–3978. doi:10.1021/nl301159v.

[48] B. Zornoza, A. Martinez-Joaristi, P. Serra-Crespo, C. Tellez, J. Coronas, J. Gascon, F. Kapteijn, Functionalized flexible MOFs as fillers in mixed matrix membranes for highly selective separation of CO2 from CH4 at elevated pressures, Chem. Commun. 47 (2011) 9522–9524. doi:10.1039/C1CC13431K.

[49] S. Aguado, J. Canivet, D. Farrusseng, Facile shaping of an imidazolate-based MOF on ceramic beads for adsorption and catalytic applications, Chem. Commun. 46 (2010) 7999–8001. doi:10.1039/C0CC02045A.

[50] J. Canivet, S. Aguado, C. Daniel, D. Farrusseng, Engineering the Environment of a Catalytic Metal–Organic Framework by Postsynthetic Hydrophobization, ChemCatChem. 3 (2011) 675–678. doi:10.1002/cctc.201000386.

[51] R. Krutokhvostov, A.A. Govyadinov, J.M. Stiegler, F. Huth, A. Chuvilin, P.S. Carney, R. Hillenbrand, Enhanced resolution in subsurface near-field optical microscopy, Opt. Express. 20 (2012) 593–600. doi:10.1364/OE.20.000593.

[52] I. Amenabar, S. Poly, M. Goikoetxea, W. Nuansing, P. Lasch, R. Hillenbrand, Hyperspectral infrared nanoimaging of organic samples based on Fourier transform infrared nanospectroscopy, Nat. Commun. 8 (2017) 14402. doi:10.1038/ncomms14402.

[53] O.C. David, D. Gorri, A. Urtiaga, I. Ortiz, Mixed gas separation study for the hydrogen recovery from H2/CO/N2/CO2 post combustion mixtures using a Matrimid membrane, J. Memb. Sci. 378 (2011) 359–368. doi:10.1016/j.memsci.2011.05.029.

[54] H. Lin, E. Van Wagner, R. Raharjo, B.D. Freeman, I. Roman, High-Performance Polymer Membranes for Natural-Gas Sweetening, Adv. Mater. 18 (2006) 39–44. doi:10.1002/adma.200501409.

[55] S. Matteucci, Y. Yampolskii, B.D. Freeman, I. Pinnau, Transport of Gases and Vapors in Glassy and Rubbery Polymers, in: Mater. Sci. Membr. Gas Vap. Sep., John Wiley & Sons, Ltd, 2006: pp. 1–47. doi:10.1002/047002903X.ch1.

[56] J.E. Bachman, Z.P. Smith, T. Li, T. Xu, J.R. Long, Enhanced ethylene separation and plasticization resistance in polymer membranes incorporating metal – organic framework nanocrystals, 15 (2016). doi:10.1038/NMAT4621.

[57] T.C. Merkel, B.D. Freeman, R.J. Spontak, Z. He, I. Pinnau, P. Meakin, A.J. Hill, Sorption, Transport, and Structural Evidence for Enhanced Free Volume in

Poly(4-methyl-2-pentyne)/Fumed Silica Nanocomposite Membranes, Chem. Mater. 15 (2003) 109–123. doi:10.1021/cm020672j.

[58] J. Ahn, W.-J. Chung, I. Pinnau, M.D. Guiver, Polysulfone/silica nanoparticle mixed-matrix membranes for gas separation, J. Memb. Sci. 314 (2008) 123–133. doi:10.1016/j.memsci.2008.01.031.

[59] M. Josephine, C. Ordoñez, K.J.B. Jr, J.P. Ferraris, I.H. Musselman, Molecular sieving realized with ZIF-8 / Matrimid ® mixed-matrix membranes, J. Memb. Sci. 361 (2010) 28–37. doi:10.1016/j.memsci.2010.06.017.

[60] S. Qiu, M. Xue, G. Zhu, Metal-organic framework membranes: from synthesis to separation application, Chem. Soc. Rev. 43 (2014) 6116–6140. doi:10.1039/C4CS00159A.

[61] C. Zhang, K. Zhang, L. Xu, Y. Labreche, B. Kraftschik, W.J. Koros, Highly scalable ZIF-based mixed-matrix hollow fiber membranes for advanced hydrocarbon separations, AIChE J. 60 (2014) 2625–2635. doi:10.1002/aic.14496.

[62] B. Zornoza, T. Carlos, Mixed Matrix Membranes Based on 6FDA Polyimide with Silica and Zeolite Microsphere Dispersed Phases, AIChE J. 61 (2015) 4481–4490. doi:10.1002/aic.

[63] L. Ge, W. Zhou, V. Rudolph, Z. Zhu, Mixed matrix membranes incorporated with size-reduced Cu-BTC for improved gas separation, J. Mater. Chem. A. 1 (2013) 6350–6358. doi:10.1039/C3TA11131H.

[64] J. Hu, H. Cai, H. Ren, Y. Wei, Z. Xu, H. Liu, Y. Hu, Mixed-Matrix Membrane Hollow Fibers of Cu3(BTC)2 MOF and Polyimide for Gas Separation and Adsorption, Ind. Eng. Chem. Res. 49 (2010) 12605–12612. doi:10.1021/ie1014958.

[65] A. Car, C. Stropnik, K.V. Peinemann, Hybrid membrane materials with different metal-organic frameworks (MOFs) for gas separation, Desalination. 200 (2006) 424–426. doi:10.1016/j.desal.2006.03.390.

[66] D. Fritsch, K. V Peinemann, D. De Figueiredo Gomes, Composite material, in particular composite membrane, and process for the production of the same, US Pat., 7,658,784, 2010.

[67] A.F. Bushell, M.P. Attfield, C.R. Mason, P.M. Budd, Y. Yampolskii, L. Starannikova, A. Rebrov, F. Bazzarelli, P. Bernardo, J. Carolus Jansen, M. Lanč, K. Friess, V. Shantarovich, V. Gustov, V. Isaeva, Gas permeation parameters of mixed matrix membranes based on the polymer of intrinsic microporosity PIM-1 and the zeolitic imidazolate framework ZIF-8, J. Memb. Sci. 427 (2013) 48–62. doi:10.1016/j.memsci.2012.09.035.

[68] L. Xu, C. Zhang, M. Rungta, W. Qiu, J. Liu, W.J. Koros, Formation of defect-

free 6FDA-DAM asymmetric hollow fiber membranes for gas separations, J. Memb. Sci. 459 (2014) 223–232. doi:10.1016/j.memsci.2014.02.023.

[69] T.C. Merkel, H. Lin, X. Wei, R. Baker, Power plant post-combustion carbon dioxide capture: An opportunity for membranes, J. Memb. Sci. 359 (2010) 126–139. doi:10.1016/j.memsci.2009.10.041.

Appendix A

Table A1. Summary of the CO_2/N_2 separation performance at 25ºC obtained for pure 6FDA-DAM membrane for single gases and CO_2/N_2 gas mixture (15:85) at different transmembrane pressures (1 to 4 bar). Permeate side at atmospheric pressure. The permeability data are average values of two samples and error correspond to standard deviation.

Δp [bar]	Pure gases			Mixed gas (N_2/CO_2=85/15)		
	P CO_2 [Barrer]	P N_2 [Barrer]	α CO_2/N_2 [-]	P CO_2 [Barrer]	P N_2 [Barrer]	α CO_2/N_2 [-]
1	538 ± 1	36.7 ± 0.1	14.7 ± 0.1	768 ± 1	32.1 ± 0.4	23.9 ± 0.3
2	503 ± 1	36.4 ± 0.3	13.8 ± 0.1	714 ± 2	30.0 ± 0.4	23.8 ± 1.3
3	472 ± 1	35.6 ± 0.3	13.2 ± 0.1	687 ± 1	28.2 ± 0.6	24.4 ± 2.2
4	450 ± 1	34.8 ± 0.4	12.9 ± 0.1	670 ± 3	26.4 ± 0.5	25.3 ± 1.8

Table A2. Summary of the mixed gas CO_2/N_2 separation performance at 25ºC obtained for ZIF-94/6FDA-DAM MMMs with different filler loadings at different transmembrane pressures (1 to 4 bar). Permeate side at atmospheric pressure. The permeability data are average values of two samples and error correspond to standard deviation.

MOF loading [wt%]	Membrane Thickness [μm]	Δp [bar]	Mixed gas (N_2/CO_2=85/15)		
			P CO_2 [Barrer]	P N_2 [Barrer]	α CO_2/N_2 [-]
10	32.5 ± 1.2	1	930 ± 40	38 ± 2	24.5 ± 0.1
		2	865 ± 40	35 ± 1	24.8 ± 0.2
		4	780 ± 35	32 ± 2	24.7 ± 0.2
20	24.8 ± 3.9	1	1140 ± 70	50 ± 1	22.6 ±1.0
		2	1070 ± 45	47 ± 1	22.9 ± 0.6
		4	960 ± 5	41 ± 1	23.6 ± 0.6
30	18.7 ± 1.3	1	1225 ± 40	60 ± 0	20.5 ± 0.6
		2	1125 ± 35	57 ± 1	19.7 ± 0.4
		4	1000± 30	56 ± 2	17.8 ± 0.1
40	64.8 ± 7.4	1	2310 ± 120	104 ± 10	22.2 ± 1.0
		2	2165 ± 110	97 ± 10	22.4 ± 1.1
		4	2000 ± 80	88 ± 8	22.9 ± 1.1

Table A3. CO_2 permeability calculated by the Maxwell equation and the experimental permeability for ZIF-94/6FDA-DAM MMMs with different filler loadings at 25 ºC and 1 bar transmembrane pressure. Disperse phase permeability (P_d) was calculated from experimental 10 wt% ZIF-94 MMM permeability (P_d: 4735 Barrer). Continuous phase permeability (P_c) was determined by bare polymer permeation test (P_c: 768 Barrer)

MOF loading [wt%]	CO_2 permeability [Barrer]	
	$P_{maxwell}$	$P_{experimental}$
10	-	930
20	1110	1140
30	1320	1225
40	1565	2310

Chapter 3

PBI mixed matrix hollow fiber membrane: influence of ZIF-8 filler over H_2/CO_2 separation performance at high temperature and pressure

High-performance and commercially attractive mixed-matrix membranes were developed for H_2/CO_2 separation via a scalable hollow fiber spinning process. Thin (~300 nm) and defect-free selective layers were successfully created with a uniform distribution of the nanosized (~60 nm) zeolitic-imidazole framework (ZIF-8) filler within the polymer (polybenzimidazole, PBI) matrix. These membranes could be operated at high temperature (150 ºC) and pressure (up to 30 bar), process conditions required in the treatment of pre-combustion and syngas process gas streams. Compared with neat PBI hollow fibers, filler incorporation into the polymer matrix leads to a strong increase in H_2 permeance from 65 GPU to 107 GPU at 150 ºC and 7 bar, while the ideal H_2/CO_2 selectivity remained constant at 18. In mixed gas permeation, the competition between H_2 and CO_2 transport in the ZIF-8 structure affects the performance. Adsorption of CO_2 in the nanocavities of the filler suppresses the transport of the faster permeating H_2 and consequently decreases the H_2 permeance with increasing total feed pressure down to values equal to the pure PBI hollow fibers for 30 bar. Therefore, the improvement of fiber performance for gas separation with filler addition is compromised at high operating feed pressures, which emphasizes the importance of membrane evaluation under relevant process conditions.

This chapter is based on the following publication:

M. Etxeberria-Benavides, T. Johnson, S. Cao, B. Zornoza, J. Coronas, J. Sanchez-Lainez, A. Sabetghadam, X. Liu, E. Andres-Garcia, F. Kapteijn, J. Gascon, O. David, PBI mixed matrix hollow fiber membrane: influence of ZIF-8 filler over H_2/CO_2 separation performance at high temperature and pressure, Sep. Purif. Technol., 237 (2020) 116347

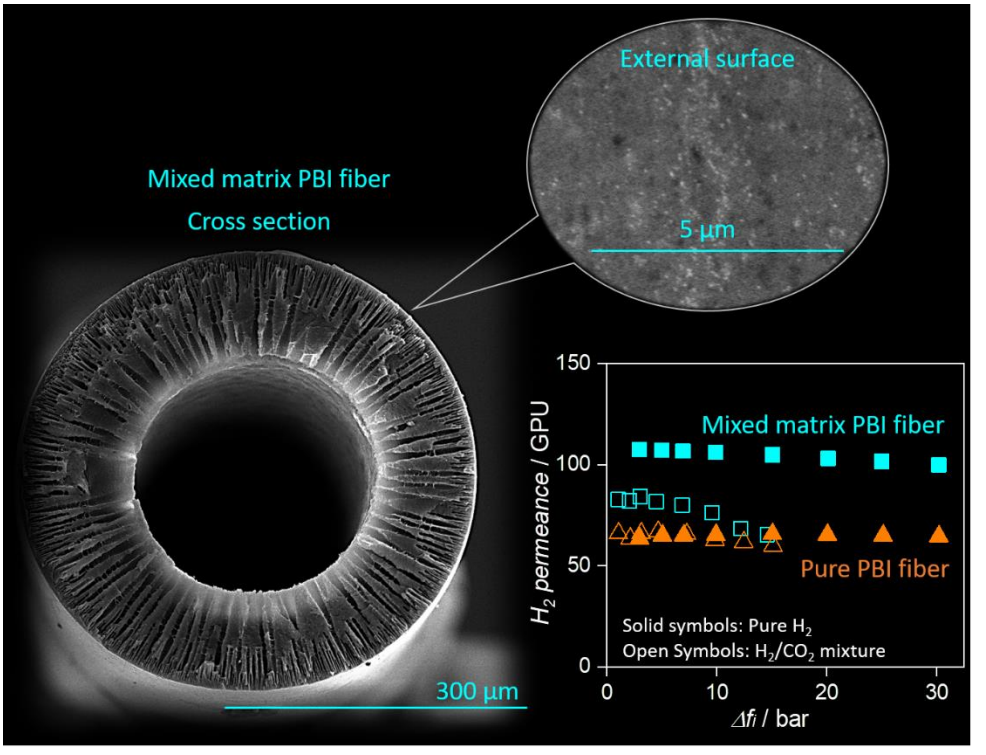
External surface
5 µm
Mixed matrix PBI fiber
Cross section
300 µm
150
100
50
0
H_2 permeance / GPU
Mixed matrix PBI fiber
Pure PBI fiber
Solid symbols: Pure H_2
Open Symbols: H_2/CO_2 mixture
0
10
20
30
Δf_i / bar

3.1. Introduction

There are several major benefits of membrane based gas separation over conventional gas separation technologies like cryogenic distillation, condensation and amine absorption: (1) lower energy cost since there is no gas-liquid phase change of the gas mixture to be separated, (2) relatively small footprint - gas separation membrane units are smaller than other types of plants, like amine stripping plants, (3) low mechanical complexity and (4) operation under continuous, steady-state conditions [1]. Membrane based gas separation finds additional benefits in pre-combustion application (H_2/CO_2 separation) where stripping and adsorption technologies are limited for direct gas processing [2]. The H_2/CO_2 mixture exiting a typical water-gas shift reactor is at high pressure and high temperature (150-250 °C) conditions. Also, depending on the feed, the mixture might contain traces of H_2S and steam. Preferably, a membrane must be able to operate continuously under such challenging process conditions.

The required hydrogen purity and therefore the membrane material, depends on the specific application, *e.g.* high purity hydrogen is required for proton exchange membrane fuel cell applications, whereas a lower hydrogen purity is acceptable for refinery applications. Due to the unique permeation mechanism, palladium-based membranes show high permeability and exclusive selectivity for H_2 and are commonly used when high purity hydrogen is required [3]. However, their implementation at industrial scale has been hampered due to the low mechanical resistance, modest reproducibility, scale-up problems and the high fabrication and material cost of this type of membranes [4,5]. On the other hand, polymeric membranes have been implemented for gas separation on a large scale in industry, mainly due to their easy processing and mechanical strength [6]. Although polymeric membranes are not as selective as inorganic ones, they can be implemented when such a high purity hydrogen is not required. Polymers of intrinsic microporosity (PIMs) have been identified as attractive candidates for gas separation. Their highly rigid and contorted molecular structure leads to inefficient packing of polymer chains and high free volume, and therefore exhibits very high gas permeability [7]. The ultra-high permeability together with interesting CO_2/N_2 and CO_2/CH_4 selectivity, make this PIMs interesting materials for several applications, such as post-combustion CO_2 capture and biogas upgrading. Nonetheless, PIMs present a relatively low selectivity for H_2/CO_2 separation (<5.5), and in some cases even a reverse selectivity. Few glassy polymers can be successfully used as H_2 selective membranes at the high temperature required in the pre-combustion applications. Polybenzimidazole (PBI) has a rigid polymeric backbone (glass transition temperature of 420 ºC) and close chain packing [8], and has already

been identified as a good candidate for this application [9–12]. In addition, PBI has shown to exhibit the highest H_2/CO_2 selectivity among the polymer family. Nevertheless, the gas permeation rate through PBI polymer is low [13]. Mixed matrix membranes (MMMs, consisting of a dispersion of filler particles in a polymeric matrix) combine the good processability of polymers with high gas flux and selectivity of the inorganic filler [14,15]. The use of metal-organic frameworks (MOFs) as filler is attractive because of good chemical compatibility with polymers, a high surface area and pore volume, and their porosity is, in general, higher than that of their inorganic counterpart, zeolites. MOFs can be fine-tuned by selecting the appropriate building blocks [16] or by post-synthetic modification [17]. Their partially organic nature improves the polymer/MOF affinity, helping to overcome compatibility issues and avoiding the so-called *sieve-in-a-cage morphology* [18,19]. ZIF-8 is one of the most studied zeolitic imidazolate frameworks, and consists of a metal cation of Zn^{2+} coordinated with the organic linker 2-methylimidazole. ZIF-8 forms a SOD zeolitic topology with large cavities of 11.6 Å size connected through smaller windows of 3.4 Å [20].

Large-scale gas separation applications demand highly productive membranes. Therefore, commercial gas separation membranes are processed into asymmetric structures where a porous support is covered by a very thin dense layer that governs gas permeation. The asymmetric membrane can be a flat film or a hollow fiber. For high productivity, when membranes are packed into modules, a high membrane area/unit volume ratio, *i.e.* packing density, is desired. Hollow fiber modules offer high packing density (over 10000 $m^2\ m^{-3}$) [21–23], about ten times higher than for flat sheet (plate and frame) membranes. In addition, hollow fiber membranes can handle very high transmembrane pressure differences (up to 70 bar) and their fabrication costs are 5 to 20 times lower than those of equivalent membranes for spiral wound modules [24].

This work is focused on the development of commercially relevant membranes (hollow fiber membranes) for CO_2 capture application in pre-combustion processes with a strong focus on performance evaluation under relevant process conditions (30 bar, 150 ºC and gas mixtures). Also, considering that the low H_2 permeability is among the major drawbacks of PBI membranes [13], we propose an improved structure with the PBI/ZIF-8 based mixed matrix hollow fiber membrane. In this configuration ZIF-8, a MOF with high thermal resistance [25,26], would improve the H_2 permeation rate through the PBI matrix. To this date, PBI based hollow fiber membranes reported in the literature have been applied at limited pressures, less than 8 bar. In this way new knowledge on membrane behavior related to real process conditions revealed in this work, are of extreme importance for chemical process industry.

3.2. Experimental

3.2.1. Materials

PBI was received from PBI Performance Products INC. as 26 wt% solution in DMAc with 1.5 wt% LiCl. Anhydrous N-methylpyrrolidone (NMP) and dimethylacetamide (DMAc) were purchased from Sigma-Aldrich. Hexane and methanol were purchased from Fisher Scientific. Sylgard 184 (Dow Corning) was used for the defect healing process. $Zn(NO_3)_2 \cdot 6H_2O$, and methanol for ZIF-8 synthesis were purchased from Alfa Aesar. 2-methylimidazole was purchased from Sigma Aldrich. All materials were used without further purification.

3.2.2 Synthesis of ZIF-8 crystals

ZIF-8 was synthetized as follows. $Zn(NO_3)_2 \cdot 6H_2O$ (98.7 mmol, 29.33 g) and 2-methylimidazole (790.4 mmol, 64.89 g) were dissolved in 2 L methanol at room temperature. The two precursor solutions were then rapidly mixed and stirred for 30 min. The solution turned turbid gradually. The formed ZIF-8 nanoparticles were collected by centrifugation and washed with fresh methanol three times. The products were dried in ambient air for 16 h. Reaction yield was 8.8 g, 40 % based on Zn^{2+}. The samples were activated by subjecting to vacuum at 50 °C for 12 h before N_2 sorption measurement.

3.2.3 Characterization of ZIF-8 crystals

Powder X-ray diffraction (PXRD) data were collected in reflection geometry using a Bruker AXS D8 diffractometer using Cu *Ka* radiation (λ = 1.5406 and 1.54439 Å) over the 2θ range 3-130° range in 0.02° steps.

Thermogravimetric analysis (TGA) was conducted between room temperature and 1000 ºC heating at 3 ºC min^{-1} in an N_2 atmosphere on a Netzsch TG 209 F1 Libra instrument. Infra-red (IR) spectra were collected on a Perkin Elmer Spectrum One instrument utilizing an UATR attachment. The powder was analyzed directly with no special preparation.

ZIF-8 was subjected to CO_2 and N_2 physisorption analysis. Adsorption/desorption isotherms were collected on a Quantachrome Autosorb iQ instrument. Experiments were conducted at -196 ºC (77 K) for N_2 isotherm and 0 ºC for CO_2. Both isotherms were subject to BET analysis for surface area calculation. Samples were degassed under vacuum at 125 ºC for 16 h.

High-pressure adsorption experiments (up to 35 bar) were performed on a BELSORP-HP. The adsorption/desorption isotherm for CO_2 was obtained with an equilibration time of 1500 seconds (deviation lower than 0.1% F.S pressure). Temperature ranged from 50 ºC to 150 ºC. Samples were outgassed overnight under vacuum conditions at 150 ºC.

The sample powder was dusted directly onto SEM stubs. The sample was carbon coated prior to analysis to provide a conductive layer for charge dissipation. The sample was analyzed using a Zeiss ultra 55 Field emission electron microscope equipped with in-lens secondary electron and backscatter detectors.

3.2.4 Preparation of PBI based hollow fiber membranes

The fabrication of PBI based hollow fiber membranes was based on a dry jet followed by wet quench spinning process [23,27–31]. Two types of hollow fibers have been fabricated: (1) hollow fibers based on pure PBI and (2) hollow fibers containing PBI and ZIF-8 filler. This was done by co-extrusion of polymer dope and a bore fluid into a quench bath containing water after a short residence in an air gap. Pure PBI dope was prepared by diluting the 26 wt% starting solution to the desired concentration. Filler containing polymer dope was prepared by dispersing ~10 wt% ZIF-8 into PBI polymer solution under ultrasonic mixing in a bath. ZIF-8 was dried in a vacuum oven at 60 ºC for 16 h before use. Dope was loaded into the syringe pump and degassed for 24 h at room temperature before spinning. Polymer dopes were filtered in-line with a 90 μm filter for the pure polymer dopes and 140 μm filter for the filler-containing polymer dopes. At the end, fiber was collected on a drum. Spinning conditions were varied in order to find the optimal combination of spinning parameters for achieving best performance for gas permeation. The studied parameter range and optimal spinning parameters for pure PBI and mixed matrix hollow fiber batches are listed in Table 3.1. Is important to mention that MOF addition causes an important increase in spinning dope viscosity. The addition of ZIF-8 to the dope containing 20.4 wt% PBI significantly increases dope viscosity, from 55465 cP for the pure polymer dope to 76106 cP for 10 wt% ZIF-8 loading. With the objective to have similar viscosity for the two spinning dopes, the optimal PBI concentration was lowered for mixed matrix hollow fiber preparation. Dope viscosity was measured by a Thermo Haake Scientific RS6000 rheometer with 20 mm parallel plate at 25 ºC and 10 s^{-1} shear rate. After spinning, fibers were kept in DI water for four days. Water was refreshed every day. Then fibers were washed further in a methanol bath followed by a hexane bath and dried at 70 ºC overnight. Hollow fibers were dip-coated for defect healing using a 3 wt% solution of polydimethylsiloxane (PDMS) in hexane before permeation testing.

Table 3.1. Spinning parameters for pure PBI and mixed matrix hollow fiber membrane fabrication.

Spinning parameter		Studied range	Pure PBI	10 wt% ZIF-8/PBI
MOF loading	(wt%)	0-10	-	10
PBI concentration	(wt%)	20-22	21.7	20.4
Dope viscosity	cP	-	85000	76000*
Bore composition	-	-	65 DMAc / 35 H_2O	85 NMP/ 15 H_2O
Spinneret temperature	(ºC)	20-25	25	20
Outer Dope flow rate	(ml h^{-1})	180-300	240	180
Bore flow rate	(ml h^{-1})	60-80	60	80
Air gap height	(cm)	3.4-20	10	3.4
Quench bath temperature	(ºC)	25	25	24
Take up rate	(m min^{-1})	10-30	20	14

Spinneret dimensions: 460 μm inner diameter / 820 μm outer diameter

* Viscosity for non ZIF-8 loaded dope at same PBI concentration is 55000 cP

3.2.5 Hollow fiber membrane characterization

The surface and cross-section morphology of the hollow fiber membranes were characterized by scanning electron microscopy (SEM) (Quanta 250 ESEM) equipped with energy dispersive X-ray spectroscopy (EDX). Cross-sections of the membranes were prepared by freeze-fracturing after immersion in liquid nitrogen and subsequently coated with gold/palladium. The low voltage high contrast backscatter electron detector (vCD) and the Everhart Thornley detector (ETD) were used for the analysis of the membranes.

High-pressure adsorption experiments (up to 35 bar) were performed, the same as for ZIF-8 crystals as described in section 2.3. The adsorption/desorption isotherms for CO_2 were obtained with an equilibration time of 1500 s (deviation lower than 0.1% full scale pressure). Temperature ranged from 50 ºC to 150 ºC. Samples were outgassed overnight under vacuum conditions at 150 ºC.

Hollow fiber gas permeation properties were determined using an experimental set-up based on constant pressure technique [30]. Hollow fiber membrane modules were built by insertion of 1-22 fibers of ~18 cm active length within a tubular stainless-steel container using a method reported in literature [32]. Pure (H_2 and CO_2) and mixed gas permeation experiments (H_2/CO_2 = 50/50 vol%) were carried out in the total feed pressure range of 3.5 to 30 bar at 150 ºC. Feed gas flow and pressure was controlled with a Coriolis mass flowmeters (Bronkhorst). Permeate gas flow was measured using a film flow meter (Horiba). To be able to measure the permeate flow of the less permeable component, *i.e.* CO_2, one module containing 22 pure PBI hollow fibers and one module containing 6 10 wt% ZIF-8/PBI hollow fibers were tested for pure gases. For mixed gas permeation studies, an equimolar H_2/CO_2 gas mixture was fed from the shell side of the fiber and permeate mixture was collected from the lumen side of the fibers in a counter-current flow configuration. During the mixed gas experiments, the stage cut (the ratio between permeate flow rate and feed flow rate) was kept below 1 % to avoid concentration polarization phenomena and ensure a constant gas composition at the feed side. This means that maximum permeate flow rate to measure is 100 times lower than the maximum feed flow rate that the permeation system can supply, *i.e.* maximum 100 mL min^{-1} in our case. Therefore, the membrane area was decreased and instead of testing one module with several fibers we tested several modules with one fiber each to have a statistically significant result. An online gas chromatograph (Bruker Scion 456-GC) was used to analyze the permeate stream composition over time. Permeance was calculated once the steady state was reached in the permeate stream of the membrane. The permeance for gas *i* was calculated by the following equation:

$$P_i = \frac{F_i}{\Delta f_i \cdot A}$$

where P_i is the gas permeance in gas permeation units (1 GPU = 10^{-6} cm^3 (STP) cm^{-2} s^{-1} $cmHg^{-1}$), F_i is the volumetric flow rate of component *i* (cm^3 (STP) s^{-1}), Δf_i is the partial fugacity difference of component *i* across the membrane (cmHg) and A is the effective membrane area (cm^2). The use of penetrant fugacity is preferred due to the non-ideal behavior of gases at high pressure [33].

The separation factor or mixed gas selectivity α_{ij} was calculated as the ratio of the permeance of the more permeable compound *i* to the permeance of the less permeable compound *j*:

$$\alpha_{ij} = \frac{P_i}{P_j}$$

3.3. Results and discussion

3.3.1 ZIF-8 characterization

Highly porous ZIF-8 with good crystal structure was successfully synthesized. Main properties are summarized in Table 3.2. PXRD, TGA, IR and CO_2 and N_2 physisorption results are found in the Appendix B.

The experimental PXRD pattern for synthesized ZIF-8 nanoparticles (Figure 3.2) resembles the simulated pattern, showing that it possesses the right crystal structure. The TG analysis (Figure 3.3) shows that the synthesized ZIF-8 nanoparticles are thermally stable up to ~480 °C, above which temperature a gradual decomposition is observed. Infra-red (IR) spectroscopy (Figure 3.4) shows the expected bands at ca. 1150 and 1180 cm^{-1} attributed to C-N ring vibrations. The SEM image in Figure 3.1 indicates individual primary particle sizes of ~60 nm. Ideally, for a highly permeable and gas selective fiber, the outer top layer should be as thin as possible, *i.e.* ~100 nm. Therefore, ZIF-8 particles with a particle size below the desired selective layer thickness have been synthesized and used for hollow fiber preparation.

From the N_2 isotherm (Figure 3.5) a BET area of 1830 $m^2 g^{-1}$ was obtained. The CO_2 isotherm presented in the same figure shows that the material has a CO_2 uptake at atmospheric pressure of 1.3 mmol g^{-1}.

Table 3.2. Review of main properties of ZIF-8 particles

Parameter	ZIF-8
Crystal structure	Pure phase
Thermal stability	up to ~480 ºC
Particle size	~60 nm
Surface area	1830 $m^2 g^{-1}$

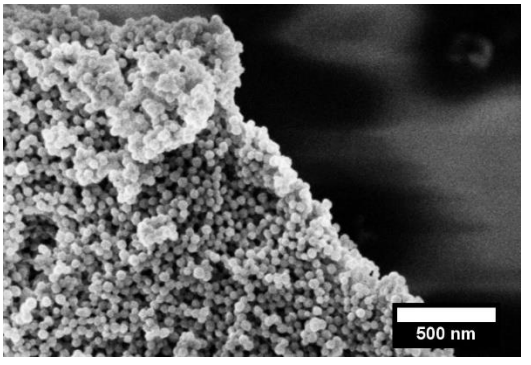

Figure 3.1. SEM image of ZIF-8 particles

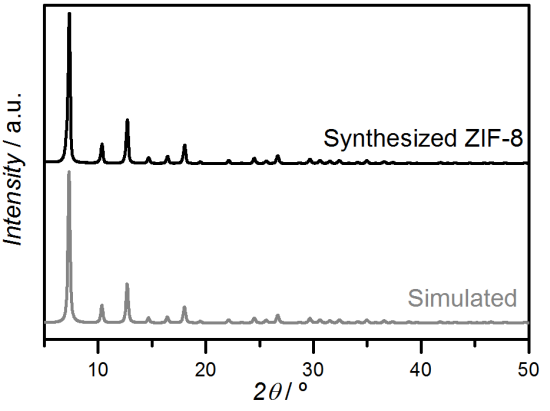

Figure 3.2. PXRD pattern of synthesized ZIF-8 and simulation.

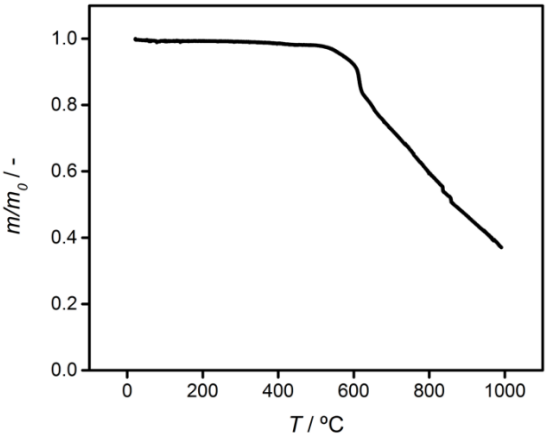

Figure 3.3. TGA profile of ZIF-8 particles conducted in N_2 atmosphere at heating rate 3 °C min^{-1}.

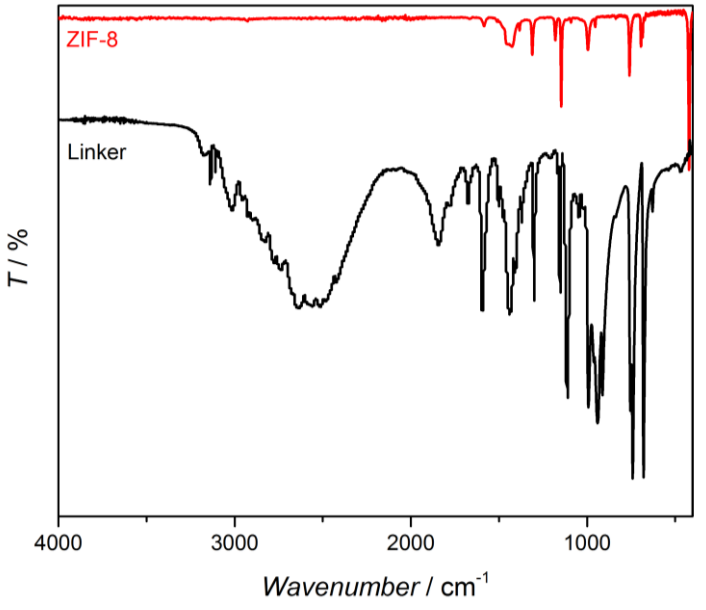

Figure 3.4. Transmission IR spectrum of ZIF-8 and 2-methylimidazole linker.

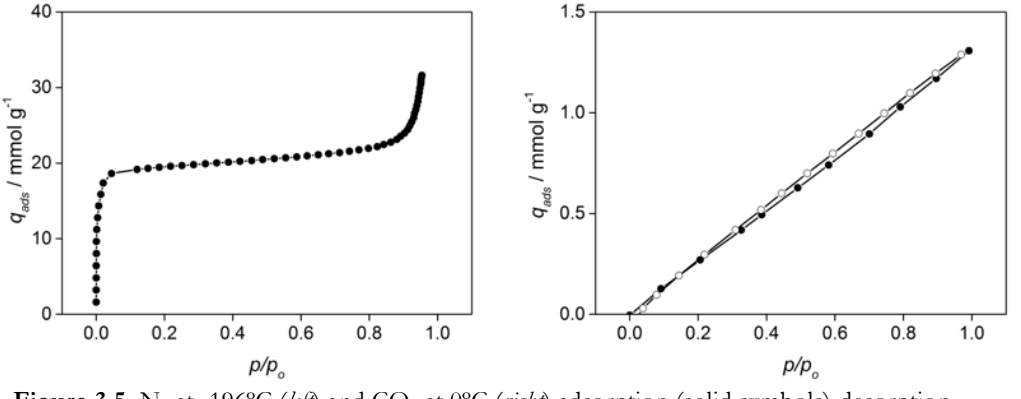

Figure 3.5. N_2 at -196ºC (*left*) and CO_2 at 0ºC (*right*) adsorption (solid symbols)-desorption (open symbols) isotherms of ZIF-8.

3.3.2 Hollow fibers morphological and structural characterization

SEM images of the outer surface and cross-section of the pure PBI and 10 wt% ZIF-8/PBI mixed matrix hollow fibers are shown in Figure 3.6. Both fibers show good circularity and concentricity between the inner and outer diameter (Figure 3.6b, e). A porous substructure with small pores and finger-like type macrovoids was obtained (Figure 3.6c and f). Both fibers have an outer top layer with a densified structure (Figure 3.6a, c). Ideally, for a highly permeable and gas selective fiber, the outer top layer should be as thin as possible, *i.e.* ~100 nm and completely dense. The substructure of the fiber acts just as support with little resistance to gas transport. For a composite MOF-polymer hollow fiber, the MOF particles should be homogeneously dispersed within the top layer and their size should be smaller than the thickness of the top layer. Therefore, the surface of the mixed matrix hollow fibers was analyzed by the vCD detector at the SEM. The compositional contrast provided by the vCD detector enables observation of the MOF distribution just beneath the surface of the membrane (see Chapter 2). Small ZIF-8 particles appear with bright contrast in the SEM image of the 10 wt% ZIF-8/PBI hollow fiber outer surface (Figure 3.6d). The presence of MOF particles in the outer layer of the fiber was also confirmed by EDX analysis (3.38 wt% Zn).

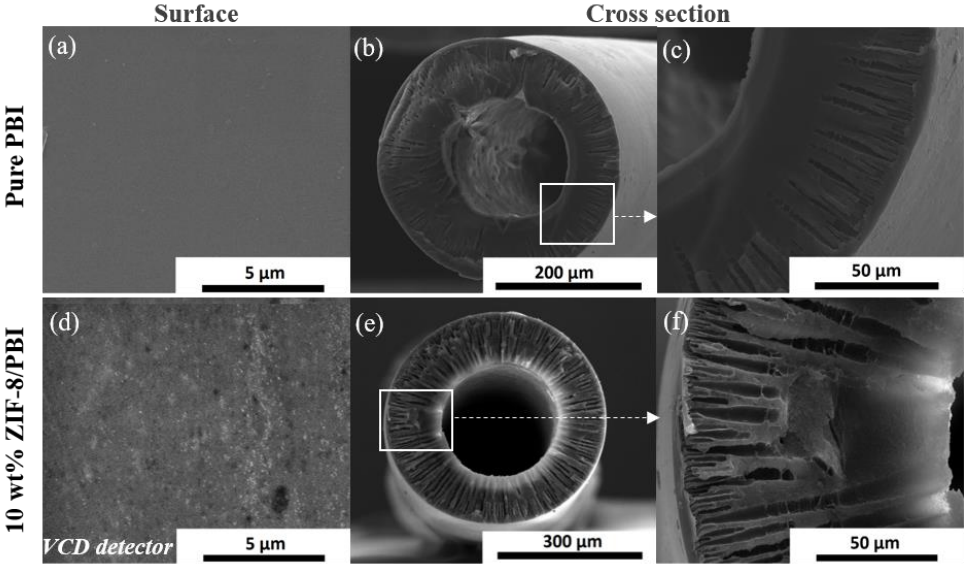

Figure 3.6. SEM images of the outer surface and cross-section of the: (a-c) pure PBI hollow fiber, (d-f) 10 wt% ZIF-8/PBI mixed matrix hollow fiber. Surface image of the mixed matrix fiber (d) was obtained by the vCD detector.

3.3.3 Hollow fibers gas permeation

3.3.3.1 Pure gas permeation -overall analysis

Pure gas transport properties of pure PBI and 10 wt% ZIF-8/PBI mixed matrix hollow fibers are shown in Table 3.3. A summary of gas permeation results of PBI hollow fiber membranes from literature is included. Pure PBI hollow fibers developed in this work had a permeance of H_2 of 65 GPU and a H_2/CO_2 ideal selectivity of 17.6 at 150 ºC and 7 bar transmembrane total fugacity. Asymmetric membranes are defined to be "defect-free" if the ideal selectivity is greater than 80% of the intrinsic selectivity of dense films [34]. If these results are compared with gas permeation through a dense flat film made of pure PBI from the same provider [35] at similar operational conditions (20 Barrer H_2; 20 H_2/CO_2 ideal selectivity), the outer selective top layer has an estimated effective thickness of ~307 nm and the fibers are selective with few or no defects (17.6 versus 20 H_2/CO_2 selectivity). In the calculation of selective layer thickness phenomenon like ageing is not considered, and the resulting value is an estimation. Direct measurement of the selective thickness cannot be performed. Measuring the thickness from SEM pictures only gives a local value (not an average) and in most cases is not easy to identify the borderline between selective layer/transition layer/porous support. A value of ~307 nm for the thickness of the selective top layer is remarkably good. In principle, thinner, up to 100 nm, top layers could be obtained but would require extensive optimization of the spinning recipe. If our results are compared with pure PBI hollow fiber membranes developed by Kumbharkar *et al.* [10], we obtained an ~100 times higher permeance and 1.4 times higher H_2/CO_2 selectivity. At 250 ºC Berchtold *et al.* [36] achieved 1.7 times higher permeance than us. It is known that temperature has a strong influence over gas permeance through membranes showing an Arrhenius type dependency [12]. The activation energy of H_2 permeability through PBI is 19.35 kJ mol^{-1} which would predict a 4 times higher permeance at 250 ºC than at 150 ºC as shown in dense flat sheet PBI membranes [35]. Therefore, if we extrapolate our results to 250 ºC a permeance of 260 GPU is expected.

Upon addition of ZIF-8, the H_2 permeance was increased from 65 GPU for the pure PBI to 107 GPU of H_2 for the PBI-10wt % ZIF-8 fiber, at almost constant H_2/CO_2 ideal selectivity of ~17. This increase in gas permeance could be given by the contribution of following factors: (1) achievement of an even thinner selective top layer when spinning the mixed matrix dope, and/or (2) the contribution from ZIF-8 filler porosity found in the dense top layer and/or (3) a support layer with a more open porous structure. Differences in the pure and mixed gas permeation (see section 3.3.2) can only be attributed to ZIF-8 contribution. The similar ideal selectivity for H_2/CO_2

Table 3.3. Transport properties of developed pure PBI and mixed matrix PBI hollow fiber membranes. PBI based hollow fiber membranes reported in literature are also included.

	H_2 permeance (GPU)	H_2/CO_2 selectivity	Testing conditions	Ref.
PBI dense film	20 Barrer	20	150ºC, 3.5 bar, SG	[35]
PBI	65	17.6	150 ºC, 7 bar, SG	This work
PBI	0.62	12.8	200 ºC, 5-8 bar, SG	[10]
PBI	108	23.7	250 ºC, unsp, SG	[36]
10 wt% ZIF-8/PBI	107	16.1	150 ºC, 7 bar, SG	This work
10 wt%ZIF-8-PBI/Matrimid	50	11.5	150 ºC, 7 bar, MG	[37]
33 wt%ZIF-8-PBI/Matrimid	140	7		
PBI/PdNPs	80	10	60 ºC, 1 bar, SG	[38]

SG: single gas test. MG: mixed gas test (50/50 H_2/CO_2). Unsp: unspecified

1 GPU = 10^{-6} (cm^3(STP))/(cm^2·s·cmHg)

separation of 10 wt% ZIF-8/PBI hollow fiber compared with pure PBI hollow fiber shows that the ZIF-8 filler does not act as molecular sieve between the H_2 and CO_2 molecules. The ZIF-8 addition in the selective top layer improves, however, the overall gas permeance. Other composite hollow fiber PBI membranes have been reported before [37,38]. Asymmetric ZIF-8-PBI/Matrimid dual layer hollow fibers were fabricated by Yang *et al.* [37]. Villalobos *et al.* [38] proposed a novel scheme to fabricate PBI hollow fiber membranes with a thin skin loaded with fully dispersed palladium nanoparticles. Only modest H_2/CO_2 selectivities are reported compared with the archivable selectivity of PBI material and our results.

3.3.3.2 Influence of transmembrane fugacity on pure and mixed gas permeations

The influence of transmembrane fugacity (Δf) over gas separation performance of pure PBI and 10 wt% ZIF-8/PBI hollow fiber was evaluated at 150 ºC and 3 - 30 bar using pure and equimolar CO_2/H_2 mixtures (Figure 3.7). H_2 and CO_2 permeances and H_2/CO_2 selectivity are presented as a function of transmembrane fugacity for pure gases (closed symbols) and transmembrane partial fugacity for mixed gas experiments (open symbols). All numeric data are included in Table B1 and B2, Appendix B. The H_2 and CO_2 pure gas permeances of pure PBI hollow fibers exhibit little or no dependency on transmembrane fugacity; they stay constant at a level of ~65 GPU and ~3.5 GPU respectively. Therefore, a constant ideal H_2/CO_2 selectivity of ~18 is obtained over the studied fugacity range. It is worth mentioning that considering the

constant CO_2 permeance the typical plasticization phenomenon observed for other polyimides like P84® or Matrimid [39,40] did not occur. In the case of 10 wt% ZIF-8/PBI hollow fiber, the H_2 permeance exhibits little or no dependency on transmembrane fugacity, while a slight decrease in CO_2 permeance is observed as fugacity increases. As a result, a slight increase in the ideal H_2/CO_2 selectivity is observed as transmembrane fugacity increases (from 16.6 at 3 bar to 17.7 at 30 bar).

For mixed gas permeation, the same separation performance is obtained for pure PBI hollow fibers. It shows that neither H_2 permeance nor CO_2 permeance is affected by the presence of the other gas. However, a significant deviation of mixed gas permeation from pure gas permeation is observed when adding 10 wt% ZIF-8. The H_2 mixed gas permeance is much lower than the H_2 pure gas permeance (23 % lower at 3 bar total fugacity). At the same time, the H_2 permeance remains constant at a value of ~83 GPU up to 5 bar partial fugacity, above which it starts to decrease to the level of pure PBI hollow fibers at 15 bar (~65 GPU). There is a smaller effect of fugacity on the CO_2 mixed gas permeance which starts from the same value as for pure gas permeance and decreases from 6.2 to 4.8 GPU as the fugacity increases. This phenomenon is attributed to the competitive sorption between H_2 and CO_2 gas molecules. CO_2 molecules are adsorbed in the cavities of ZIF-8 particles and therefore transportation of H_2 molecules through ZIF-8 diffusion pathways is reduced [37,41]. Adsorption and diffusion of gases in ZIF-8 by molecular simulation studies have been reported in literature, where enhanced adsorption in specific sites was determined [42]. Two preferred adsorption sites were identified for H_2. The first adsorption site is located on top of the imidazolate ring over the C=C bond and the second adsorption site at the center of the hexagonal window. For CO_2, the preferred adsorption site may depend on CO_2 loading [43]. At low loading, CO_2 is adsorbed in the vicinity of the C=C bond of the 2-methylimidazolate linker. At high loading CO_2 is also adsorbed near the aperture and in the central cage. It means that as the pressure increases, the nanocages of ZIF-8 are saturated (mainly by CO_2) and therefore both pathways for CO_2 and H_2 diffusion through ZIF-8 may be hindered. The stronger adsorption of CO_2 (see section 3.4) suppresses the H_2 permeation in the mixture, yielding a lower mixture selectivity, but compensates partly for the hindered diffusivity, explaining the smaller CO_2 permeance reduction. This result shows, unlike other MOF fillers, the active role of ZIF-8 in the MMM and also demonstrates that a possible void space between filler and polymer does not play a role in this system [44], otherwise a selectivity equal to the pure PBI would have been observed. Summarizing, at lower pressures transport through the ZIF-8 contributes to the permeation and to the MMM performance, while at higher pressures this contribution is reduced by strong adsorption of penetrants.

Is worth mentioning that this performance is reversible. When the fugacity was decreased to the initial testing value of 3 bar, the initial permeance values were recovered (see Table B1).

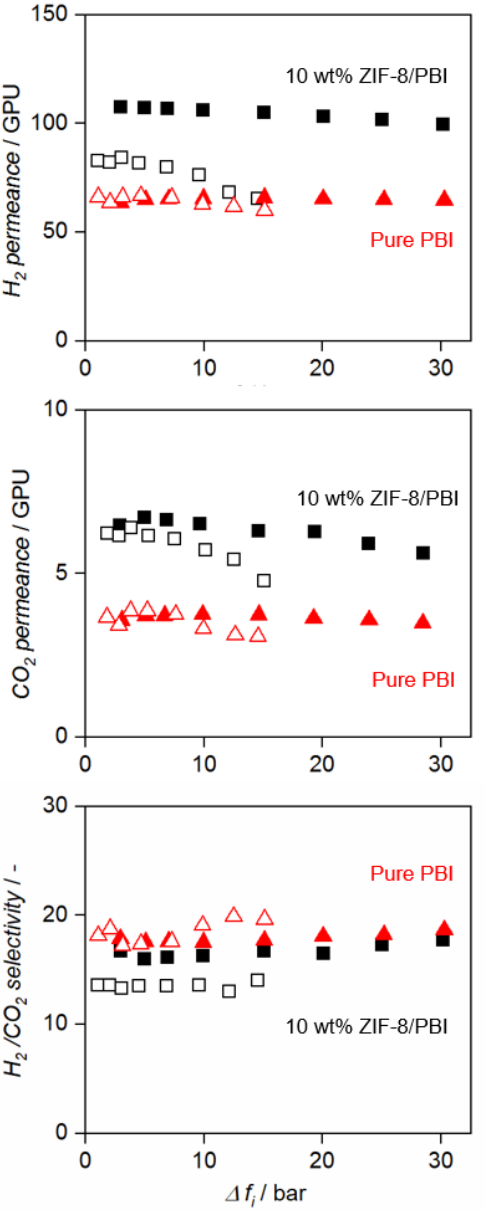

Figure 3.7. H_2 and CO_2 permeance and H_2/CO_2 selectivity of pure PBI (*red triangle*) and 10wt % ZIF-8/PBI (*black square*) hollow fiber membranes as a function of transmembrane partial fugacity of the components at 150 °C. Solid symbols correspond to pure gas experiments and open symbols to mixed gas experiments (H_2/CO_2 = 50/50 vol%).

3.3.4 Hollow fibers gas sorption measurements

Figure 3.8 shows the results from the adsorption measurements of the three samples (ZIF-8 powder, pure PBI hollow fiber and 10 wt% ZIF-8/PBI hollow fiber) at different temperatures (50, 100 and 150 ºC) in a pressure range of 0 to 35 bar.

ZIF-8 powder (Figure 3.8 *left*) exhibits an isotherm that is concave to the pressure axis, with a larger slope in the low-pressure range (0-20 bar). The adsorption uptake decreases with increasing temperature, in agreement with an exothermal adsorption process. As expected, ZIF-8 presents a much higher adsorption than pure PBI, attributed to the high specific surface area of MOF particles.

Interpretation of the pure PBI polymer behavior becomes more complex. Sorption isotherms in glassy polymers can be described as *type II* according to IUPAC [45] with an S-shape character, *i.e.* concave to the pressure axis at the beginning, then almost linear and finally convex to the pressure axis. The complete isotherm (saturation) can be obtained at low temperatures and/or high pressures [46]. In our case only at 50 ºC the isotherm is completed (Figure 3.8 *right*). The adsorbed CO_2 amount decreases with increasing temperature at pressures below 5 bar. However, at higher pressures the profile at 50 ºC lies below the one at 100 ºC. This behavior cannot be explained in terms of thermodynamics, and so kinetic effects, *i.e.* diffusion limitations, must be considered. Mobility of CO_2 and polymer chains is improved at higher temperature. This effect was already reported in literature for polyethyleneimine [47]. The nearly absent CO_2 adsorption at 150 ºC is expected based on thermodynamics.

10 wt% ZIF-8/PBI hollow fiber experimental isotherms are shown in Figure 3.8 *middle*. The adsorption profiles have contributions from both components, but an exact match is not expected due to unknown interaction between the constituents: *i.e.* the interface between polymer and MOF particles, differences in the surface roughness and porosity between the neat PBI and mixed matrix fiber. H_2 adsorption could not be determined within the equipment's accuracy. These results support the picture of the mixed matrix membrane behavior, where the adsorption of CO_2 in the ZIF-8 still plays a role at 150 ºC and high pressure. Therefore, it is expected that operation at higher temperatures can further reduce this adsorption, leading to higher H_2/CO_2 selectivities (next to higher permeances), as is observed in literature for pure PBI [12,37].

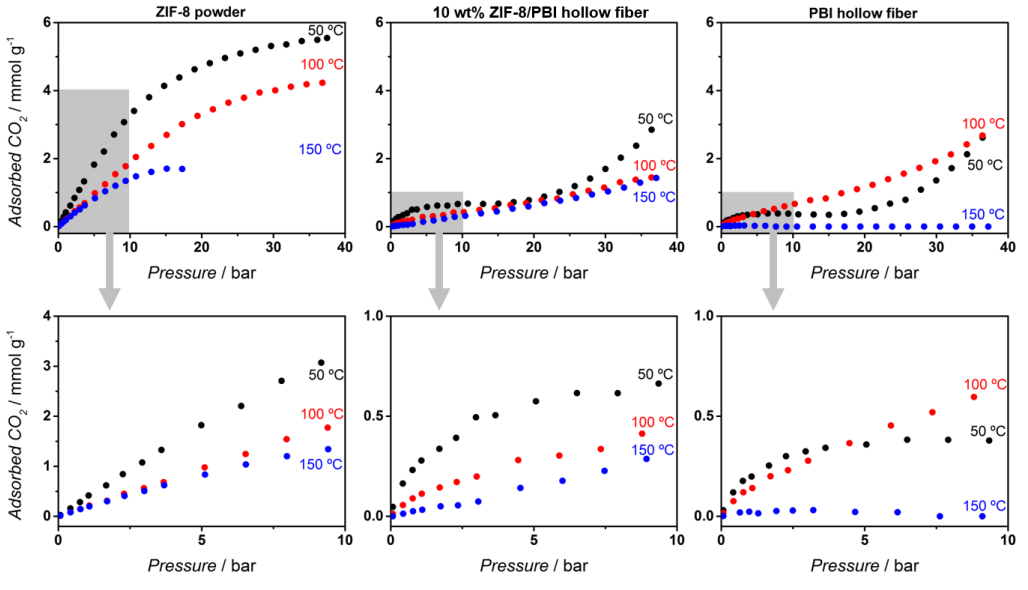

Figure 3.8. High pressure adsorption isotherms (excess adsorption) for carbon dioxide on ZIF-8 powder (*left*), 10 wt% ZIF-8/PBI hollow fiber (*middle*) and pure PBI hollow fiber (*right*), at 50 °C (*black*), 100 °C (*red*) and 150 °C (*blue*).

3.4. Conclusions

Defect-free hollow PBI fibers have been produced with thin (~300 nm) dense mixed matrix top layers containing a uniform distribution of the nanosized (~60 nm) zeolitic-imidazole framework filler (ZIF-8) in the polymer polybenzimidazole (PBI) matrix. The manufacturing protocol developed could be used for the incorporation of any type of porous filler. ZIF-8 incorporation into the PBI polymer matrix strongly influences gas transport, specifically in mixed gas permeation, where the improvement of fiber performance for H_2/CO_2 separation with filler addition at 150 ºC is compromised at high operating feed pressures (30 bar) due to competitive adsorption of CO_2 in ZIF-8, reducing the transport of both components, but H_2 more than CO_2. The ZIF-8 plays an active role in the permeation performance, unlike many other fillers. We expect that at higher temperature the H_2/CO_2 selectivity will improve due to lower CO_2 adsorption in the filler. Our results reveal material performance under conditions relevant to the application and demonstrate the importance of such an evaluation. Future improvement of membrane performance is foreseen by incorporation of porous fillers with lower interaction with CO_2 and higher size exclusion properties for H_2/CO_2, like benzimidazole-linked polymers (BILPs), a new class of porous organic framework [48].

References

[1] P. Bernardo, E. Drioli, G. Golemme, Membrane Gas Separation: A Review/State of the Art, Ind. Eng. Chem. Res. 48 (2009) 4638–4663. doi:10.1021/ie8019032.

[2] O.C. David, D. Gorri, A. Urtiaga, I. Ortiz, Mixed gas separation study for the hydrogen recovery from H2/CO/N2/CO2 post combustion mixtures using a Matrimid membrane, J. Memb. Sci. 378 (2011) 359–368. doi:10.1016/j.memsci.2011.05.029.

[3] E. Fernandez, K. Coenen, A. Helmi, J. Melendez, J. Zuñiga, D.A. Pacheco Tanaka, M. van Sint Annaland, F. Gallucci, Preparation and characterization of thin-film Pd–Ag supported membranes for high-temperature applications, Int. J. Hydrogen Energy. 40 (2015) 13463–13478. doi:10.1016/j.ijhydene.2015.08.050.

[4] J. Gascon, F. Kapteijn, B. Zornoza, V. Sebastián, C. Casado, J. Coronas, Practical Approach to Zeolitic Membranes and Coatings: State of the Art, Opportunities, Barriers, and Future Perspectives, Chem. Mater. 24 (2012) 2829–2844. doi:10.1021/cm301435j.

[5] J. Coronas, Present and future synthesis challenges for zeolites, Chem. Eng. J. 156 (2010) 236–242. doi:10.1016/j.cej.2009.11.006.

[6] M.A. Aroon, A.F. Ismail, T. Matsuura, M.M. Montazer-Rahmati, Performance studies of mixed matrix membranes for gas separation: A review, Sep. Purif. Technol. 75 (2010) 229–242. doi:10.1016/j.seppur.2010.08.023.

[7] Neil B. McKeown, Polymers of Intrinsic Microporosity, ISRN Mater. Sci. 2012 (2012) 16. doi:10.5402/2012/513986.

[8] S.C. Kumbharkar, P.B. Karadkar, U.K. Kharul, Enhancement of gas permeation properties of polybenzimidazoles by systematic structure architecture, J. Memb. Sci. 286 (2006) 161–169. doi:10.1016/j.memsci.2006.09.030.

[9] R.P. Singh, G.J. Dahe, K.W. Dudeck, C.F. Welch, K.A. Berchtold, High Temperature Polybenzimidazole Hollow Fiber Membranes for Hydrogen Separation and Carbon Dioxide Capture from Synthesis Gas, Energy Procedia. 63 (2014) 153–159. doi:10.1016/j.egypro.2014.11.015.

[10] S.C. Kumbharkar, Y. Liu, K. Li, High performance polybenzimidazole based asymmetric hollow fibre membranes for H2/CO2 separation, J. Memb. Sci. 375 (2011) 231–240. doi:10.1016/j.memsci.2011.03.049.

[11] D.R. Pesiri, B. Jorgensen, R.C. Dye, Thermal optimization of polybenzimidazole meniscus membranes for the separation of hydrogen,

methane, and carbon dioxide, J. Memb. Sci. 218 (2003) 11–18. doi:10.1016/S0376-7388(03)00129-7.

[12] J. Sánchez-Laínez, B. Zornoza, C. Téllez, J. Coronas, Asymmetric polybenzimidazole membranes with thin selective skin layer containing ZIF-8 for H2/CO2 separation at pre-combustion capture conditions, J. Memb. Sci. 563 (2018) 427–434. doi:10.1016/j.memsci.2018.06.009.

[13] T.-S. Chung, A Critical Review of Polybenzimidazoles, J. Macromol. Sci. Part C. 37 (1997) 277–301. doi:10.1080/15321799708018367.

[14] P.S. Goh, A.F. Ismail, S.M. Sanip, B.C. Ng, M. Aziz, Recent advances of inorganic fillers in mixed matrix membrane for gas separation, Sep. Purif. Technol. 81 (2011) 243–264. doi:10.1016/j.seppur.2011.07.042.

[15] B. Seoane, J. Coronas, I. Gascon, M.E. Benavides, O. Karvan, J. Caro, F. Kapteijn, J. Gascon, Metal–organic framework based mixed matrix membranes: a solution for highly efficient CO2 capture?, Chem. Soc. Rev. 44 (2015) 2421–2454. doi:10.1039/C4CS00437J.

[16] J. Gascon, U. Aktay, M. Hernandezalonso, G. van Klink, F. Kapteijn, Amino-based metal-organic frameworks as stable, highly active basic catalysts, J. Catal. 261 (2009) 75–87. doi:10.1016/j.jcat.2008.11.010.

[17] Z. Wang, S.M. Cohen, Postsynthetic modification of metal-organic frameworks, Chem. Soc. Rev. 38 (2009) 1315–1329. doi:10.1039/B802258P.

[18] R. Mahajan, R. Burns, M. Schaeffer, W.J. Koros, Challenges in forming successful mixed matrix membranes with rigid polymeric materials, J. Appl. Polym. Sci. 86 (2002) 881–890. doi:10.1002/app.10998.

[19] Rajiv Mahajan, De Q. Vu, William J. Koros, Mixed Matrix Membrane Materials: An Answer to the Challenges Faced by Membrane Based Gas Separations Today?, J. Chinese Inst. Chem. Eng. 33 (2002) 77–86.

[20] K.S. Park, Z. Ni, A.P. Côté, J.Y. Choi, R. Huang, F.J. Uribe-Romo, H.K. Chae, M. O'Keeffe, O.M. Yaghi, Exceptional chemical and thermal stability of zeolitic imidazolate frameworks, Proc. Natl. Acad. Sci. 103 (2006) 10186 LP – 10191. doi:10.1073/pnas.0602439103.

[21] M.F.A. Wahab, A.F. Ismail, S.J. Shilton, Studies on gas permeation performance of asymmetric polysulfone hollow fiber mixed matrix membranes using nanosized fumed silica as fillers, Sep. Purif. Technol. 86 (2012) 41–48. doi:10.1016/j.seppur.2011.10.018.

[22] S. Husain, W.J. Koros, Mixed matrix hollow fiber membranes made with modified HSSZ-13 zeolite in polyetherimide polymer matrix for gas separation, J. Memb. Sci. 288 (2007) 195–207. doi:10.1016/j.memsci.2006.11.016.

[23] N. Peng, N. Widjojo, P. Sukitpaneenit, M.M. Teoh, G.G. Lipscomb, T.-S. Chung, J.-Y. Lai, Evolution of polymeric hollow fibers as sustainable technologies: Past, present, and future, Prog. Polym. Sci. 37 (2012) 1401–1424. doi:10.1016/j.progpolymsci.2012.01.001.

[24] R.W. Baker, Membrane Technology and Applications, 2nd Editio, Wiley, 2004.

[25] P.K. Thallapally, N. Martin, S.K. Nune, P.K. Thallapally, A. Dohnalkova, C. Wang, Synthesis and properties of nano zeolitic imidazolate frameworks, Chem. Commun. 46 (2010) 4878–4880. doi:10.1039/c002088e.

[26] J.B. James, Y.S. Lin, Thermal stability of ZIF-8 membranes for gas separations, J. Memb. Sci. 532 (2017) 9–19. doi:10.1016/j.memsci.2017.02.017.

[27] Y. Li, T. Chung, Z. Huang, S. Kulprathipanja, Dual-layer polyethersulfone (PES)/BTDA-TDI/MDI co-polyimide (P84) hollow fiber membranes with a submicron PES–zeolite beta mixed matrix dense-selective layer for gas separation, J. Memb. Sci. 277 (2006) 28–37. doi:10.1016/j.memsci.2005.10.008.

[28] N. Widjojo, T.-S. Chung, S. Kulprathipanja, The fabrication of hollow fiber membranes with double-layer mixed-matrix materials for gas separation, J. Memb. Sci. 325 (2008) 326–335. doi:10.1016/j.memsci.2008.07.046.

[29] O. David, Y. Gendel, M. Wessling, Tubular macro-porous titanium membranes, J. Memb. Sci. 461 (2014) 139–145. doi:10.1016/j.memsci.2014.03.010.

[30] O.C. David, D. Gorri, K. Nijmeijer, I. Ortiz, A. Urtiaga, Hydrogen separation from multicomponent gas mixtures containing CO, N2 and CO2 using Matrimid® asymmetric hollow fiber membranes, J. Memb. Sci. 419–420 (2012) 49–56. doi:10.1016/j.memsci.2012.06.038.

[31] V.P. Babu, B.E. Kraftschik, W.J. Koros, Crosslinkable TEGMC asymmetric hollow fiber membranes for aggressive sour gas separations, J. Memb. Sci. 558 (2018) 94–105. doi:10.1016/j.memsci.2018.04.028.

[32] D.Q. Vu, W.J. Koros, S.J. Miller, High Pressure CO2/CH4 Separation Using Carbon Molecular Sieve Hollow Fiber Membranes, Ind. Eng. Chem. Res. 41 (2002) 367–380. doi:10.1021/ie010119w.

[33] B.F. Yuri Yampolskii, Ingo Pinnau, Materials Science of Membranes for Gas and Vapor Separation, 2006.

[34] S.C. Pesek, W.J. Koros, Aqueous quenched asymmetric polysulfone membranes prepared by dry/wet phase separation, J. Memb. Sci. 81 (1993) 71–88. doi:10.1016/0376-7388(93)85032-R.

[35] X. Li, R.P. Singh, K.W. Dudeck, K.A. Berchtold, B.C. Benicewicz, Influence of polybenzimidazole main chain structure on H2/CO2 separation at elevated

temperatures, J. Memb. Sci. 461 (2014) 59–68. doi:10.1016/j.memsci.2014.03.008.

[36] G.J. Berchtold Kathryn A, ; Dudeck Kevin W, ; Singh Rajinder P, ; Dahe Ganpat J, ; Berchtold, Kathryn A, ; Dudeck, Kevin W, ; Singh, Rajinder P, ; Dahe, Polybenzimidazole hollow fiber membranes and method for making an asymmetric hollow fiber membrane, US2016375410 (A1), 2016.

[37] T. Yang, G.M. Shi, T.-S. Chung, Symmetric and Asymmetric Zeolitic Imidazolate Frameworks (ZIFs)/Polybenzimidazole (PBI) Nanocomposite Membranes for Hydrogen Purification at High Temperatures, Adv. Energy Mater. 2 (2012) 1358–1367. doi:10.1002/aenm.201200200.

[38] L.F. Villalobos, R. Hilke, F.H. Akhtar, K.-V. Peinemann, Fabrication of Polybenzimidazole/Palladium Nanoparticles Hollow Fiber Membranes for Hydrogen Purification, Adv. Energy Mater. 8 (2018) 1701567. doi:10.1002/aenm.201701567.

[39] A. Bos, I.G.M. Pünt, M. Wessling, H. Strathmann, CO2-induced plasticization phenomena in glassy polymers, J. Memb. Sci. 155 (1999) 67–78. doi:10.1016/S0376-7388(98)00299-3.

[40] J.N. Barsema, G.C. Kapantaidakis, N.F.A. van der Vegt, G.H. Koops, M. Wessling, Preparation and characterization of highly selective dense and hollow fiber asymmetric membranes based on BTDA-TDI/MDI co-polyimide, J. Memb. Sci. 216 (2003) 195–205. doi:10.1016/S0376-7388(03)00071-1.

[41] J.-R. Li, Y. Ma, M.C. McCarthy, J. Sculley, J. Yu, H.-K. Jeong, P.B. Balbuena, H.-C. Zhou, Carbon dioxide capture-related gas adsorption and separation in metal-organic frameworks, Coord. Chem. Rev. 255 (2011) 1791–1823. doi:10.1016/j.ccr.2011.02.012.

[42] B. Assfour, S. Leoni, G. Seifert, Hydrogen Adsorption Sites in Zeolite Imidazolate Frameworks ZIF-8 and ZIF-11, J. Phys. Chem. C. 114 (2010) 13381–13384.

[43] L. Zhang, G. Wu, J. Jiang, Adsorption and Diffusion of CO2 and CH4 in Zeolitic Imidazolate Framework-8 : Effect of Structural Flexibility, J. Phys. Chem. C. 118 (2014) 8788–8794. doi:10.1021/jp500796e.

[44] R. Semino, J.C. Moreton, N.A. Ramsahye, S.M. Cohen, G. Maurin, Understanding the origins of metal–organic framework/polymer compatibility, Chem. Sci. 9 (2018) 315–324. doi:10.1039/C7SC04152G.

[45] K.S.W. Sing, D.H. Everett, R.A.W. Haul, L. Moscou, R.A. Pierotti, J. Rouquerol, T. Siemieniewska, Reporting Physisorption Data for Gas/Solid Systems, Handb. Heterog. Catal. (2008). doi:10.1002/9783527610044.hetcat0065.

[46] M. Lanč, K. Pilnáček, C.R. Mason, P.M. Budd, Y. Rogan, R. Malpass-Evans, M. Carta, B.C. Gándara, N.B. McKeown, J.C. Jansen, O. Vopička, K. Friess, Gas sorption in polymers of intrinsic microporosity: The difference between solubility coefficients determined via time-lag and direct sorption experiments, J. Memb. Sci. 570–571 (2019) 522–536. doi:10.1016/j.memsci.2018.10.048.

[47] R. Sanz, G. Calleja, A. Arencibia, E.S. Sanz-Pérez, CO2 adsorption on branched polyethyleneimine-impregnated mesoporous silica SBA-15, Appl. Surf. Sci. 256 (2010) 5323–5328. doi:10.1016/j.apsusc.2009.12.070.

[48] M. Shan, X. Liu, X. Wang, I. Yarulina, B. Seoane, F. Kapteijn, J. Gascon, Facile manufacture of porous organic framework membranes for precombustion CO2 capture, Sci. Adv. 4 (2018). doi:10.1126/sciadv.aau1698.

Appendix B

Table B1. Summary of the single component and equimolar mixed gas H_2/CO_2 permeation performance at 150ºC obtained for pure PBI hollow fibers at different transmembrane fugacity (3 to 30 bar).

Sample ID	Δf (bar)	Permeance (GPU)		H_2/CO_2 selectivity
		H_2	CO_2	
Single gas experiment				
PBI_M1	3	63	3.6	17.8
(one module with 22 fibers)	5	65	3.7	17.5
	7	65	3.7	17.6
	10	65	3.7	17.5
	15	66	3.7	17.7
	20	65	3.6	18.0
	25	65	3.6	18.2
	30	65	3.5	18.6
Mixed gas experiment				
PBI_M2	3	66	3.6	18.1
(one module with 1 fiber)	5	64	3.4	18.7
	7	66	3.8	17.2
	10	67	3.8	17.3
	15	66	3.7	17.6
	20	63	3.3	19.0
	25	62	3.1	19.9
	30	60	3.1	19.6

Table B2. Summary of the single and mixed gas H_2/CO_2 separation performance at 150ºC obtained for 10 wt% ZIF-8/PBI mixed matrix hollow fiber at different transmembrane fugacity (3 to 30 bar). Error corresponds to standard deviation.

Sample ID	Δf (bar)	Permeance (GPU)		H_2/CO_2 selectivity
		H_2	CO_2	
Single gas experiment				
10 wt% ZIF-8/PBI	3	107	6.5	16.6
	5	107	6.7	16.0
	7	107	6.6	16.1
(one module with 6 fibers)	10	106	6.5	16.2
	15	105	6.3	16.7
	20	103	6.3	16.4
	25	102	5.9	17.2
	30	100	5.6	17.7
Mixed gas experiment				
10 wt% ZIF-8/PBI	3	83 ± 23	6.2 ± 2.0	13.5 ± 1.6
	5	82 ± 20	6.1 ± 1.8	13.5 ± 1.8
(average from testing three modules with one fiber each)	7	84 ± 19	6.4 ± 1.6	13.3 ± 1.3
	10	82 ± 18	6.1 ± 1.6	13.5 ± 1.6
	15	80 ± 10	6.0 ± 1.3	13.5 ± 2.0
	20	76 ± 12	5.7 ± 1.4	13.6 ± 1.8
	25	68.2 ± 7.5	5.4 ± 1.3	12.9 ± 2.2
	30	65 ± 12	4.8 ± 1.4	14.0 ± 1.7
	3 (ref)	80 ± 22	6.1 ± 1.7	13.4 ± 2.8

Chapter 4

Fabrication of Defect-Free P84® Polyimide Hollow Fiber for Gas Separation: Pathway to Formation of Optimized Structure

The elimination of the additional defect healing post-treatment step in asymmetric hollow fiber manufacturing would result in a significant reduction in membrane production cost. However, obtaining integrally skinned polymeric asymmetric hollow fiber membranes with an ultrathin and defect-free selective layer is quite challenging. In this study, polyimide P84® asymmetric hollow fiber membranes with a highly thin (~56 nm) defect-free skin were successfully fabricated by fine-tuning the dope composition and spinning parameters using a volatile additive (tetrahydrofuran, THF) as key parameters. An extensive experimental and theoretical study of the influence of volatile THF addition on the solubility parameter of the N-methyl-2-pyrrolidone/THF solvent mixture was performed. Although THF itself is not a solvent for P84®, in a mixture with a good solvent for the polymer, like N-methyl-2-pyrrolidone (NMP), it can be dissolved at high THF concentrations (NMP/THF ratio > 0.52). The as-spun fibers had a reproducible ideal CO_2/N_2 selectivity of 40, and a CO_2 permeance of 23 GPU at 35 °C. The fiber production can be scaled-up with retention of the selectivity.

This chapter is based on the following publication:

M. Etxeberria-Benavides, O. Karvan, F. Kapteijn, J. Gascon, O. David, Fabrication of Defect-Free P84® Polyimide Hollow Fiber for Gas Separation: Pathway to Formation of Optimized Structure, Membranes 2020, 10, 4

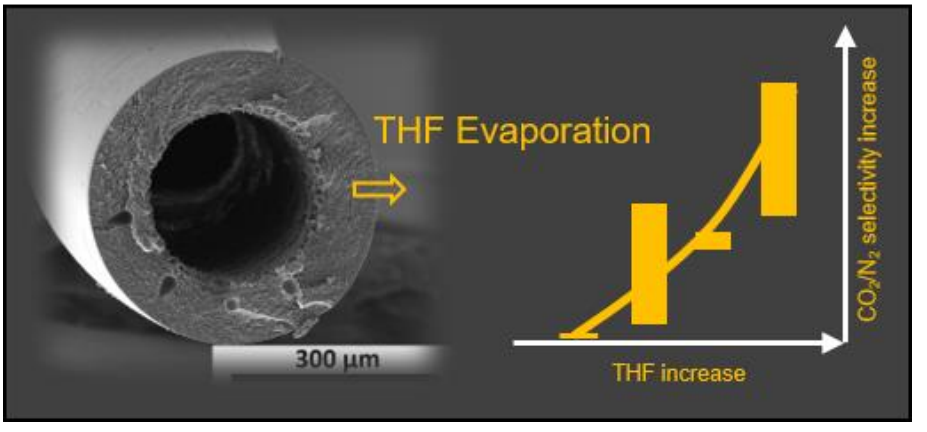
THF Evaporation
300 µm
THF increase
CO_2/N_2 selectivity increase

4.1. Introduction

In order to assess gas separation at large scale, membrane products need to be highly productive. For this reason, there are two features that commercial membranes generally meet. First, the membranes are asymmetric with a dense and thin (100-200 nm) top layer supported by a thicker porous sublayer. The actual membrane is the top layer whose thickness controls the productivity of the membrane. Second, most commercial membranes are processed in the form of a fiber (<500 μm) with a hollow interior, because hollow fibers can be densely packed at over 10,000 m^2 membrane active area in 1 m^3 module volume [1–3], ten times more than for flat sheet membranes in plate and frame packaging.

The manufacture of asymmetric hollow fiber gas separation membranes follows a dry jet spinning and consecutive wet quench process [3–8]. The fabrication of hollow fibers with an ultrathin and defect-free dense selective layer is essential, since permeance and selectivity of the membrane will be determined by the quality of the selective layer. However, the thinner the selective layer is, the greater the probability for the creation of defects [9–11]. Therefore, obtaining ultrathin and defect-free selective layer is quite challenging. Since Henis and Tripodi reported that defects in asymmetric membranes could be repaired with a thin coating layer of a highly permeable polymer such as silicone rubber [12], healing techniques have been widely used to seal the defects. However, the defect healing post-treatment implies an additional step in membrane manufacturing, resulting in an increased membrane production cost. Therefore, significant efforts have been made during the last decades in the development of defect-free as-spun hollow fiber membranes.

One approach was to add a highly volatile additive in the dope to facilitate the skin formation. Following this approach, defect-free Matrimid® 5218 hollow fiber membranes have been developed by several authors [13,14]. An ultra-thin selective layer of around 100 nm was obtained by Clausi and Koros [13] using spinning dopes comprising THF as volatile solvent. Krol *et al.* [14] used another highly volatile additive, *i.e.*, acetone (b.p. = 56 °C). Hollow fibers with an effective top layer thickness of 300-400 nm were produced by tuning the polymer and acetone concentration in the spinning dope. High-flux and almost defect-free asymmetric hollow fiber membranes consisting of a 50/50 wt% P84®/Matrimid-blend were prepared by Visser *et al.* [15]. The volatile additive acetone was also used in the spinning dope to promote the formation of a skin layer of 43–73 nm. Asymmetric Torlon® polyamide-imide hollow fiber membranes with a defect-free selective skin layer of 410 nm were formed by Kosuri and Koros [16] by adding THF in the spinning dope.

Defect-free as-spun Torlon® hollow fibers were successfully produced by Peng *et al.* [17] from a simple polymer/solvent spinning dope, resulting in ultra-thin dense layers of around 54 nm. Variation of the spinneret dimension and the take-up rate they managed to have a proper control of shear-induced and elongation-induced polymer chain orientation during the spinning process.

Polyimides are among the most interesting polymeric materials for gas separation applications due to their good trade-off between perm-selectivity and permeability, high thermal and chemical stability, combined with high mechanical strength, long durability and their suitability to prepare asymmetric structures [18]. P84®, a co-polyimide of 3,3´4,4´-benzophenone tetracarboxylic dianhydride and 80% methylphenylene-diamine + 20% methylene diamine or poly(BTDA-TDI/MDI), has been used for several applications such as organic solvent nanofiltration [19–26], pervaporation [27–31] and gas separation [15,32–36], alone or in a mixture with other polymers.

Pure P84® hollow fiber membranes have been developed for gas separation by several authors [32,36–38]. Barsema *et al.* prepared highly selective P84® hollow fiber membranes and gas permeance, selectivity, and plasticization behaviour of pure and mixed was compared with dense flat sheet membranes. The reported CO_2/N_2, O_2/N_2 and He/N_2 P84® selectivity values are among the highest in the literature [32]. In another publication, chemically cross-linked asymmetric P84® co-polyimide hollow fiber membranes with enhanced separation performance were fabricated by Choi *et al.* [36] using a dry-wet spinning process with an in-line cross linking step. An increased H_2/CO_2 selectivity and mechanical resistance was observed for the crosslinked hollow fiber membranes. In all these studies, however, P84® hollow fibers exhibit the intrinsic polymer selectivity for gas separation only after defect healing by silicone rubber coating.

Therefore, this work focuses on the development of defect-free as-spun ultrathin P84® asymmetric hollow fiber membranes that do not require a silicone rubber coating post-treatment step. For this purpose, the approach reported in literature of using a dope solution comprising volatile and non-volatile solvents was followed. THF, one of the most studied volatile solvents for gas separation hollow fiber preparation, was selected as the volatile component in view of the positive influence on hollow fiber formation of other polyimides. The influence of volatile THF addition on the solubility parameter was extensively investigated, followed by spinning optimization through fine tuning of the dope composition and spinning parameters. The as-spun P84® asymmetric hollow fiber membranes were characterized by their performance in CO_2 and N_2 permeation.

4.2. Materials and Methods

4.2.1. Materials

P84® (BTDA-TDI/MDI) co-polyimide was supplied by HP Polymer GmbH. Anhydrous N-methyl-2-pyrrolidone (NMP, 99.5% purity) and tetrahydrofuran (THF, 99.5% purity) were purchased from Sigma-Aldrich (Madrid, Spain). Anhydrous ethanol (EtOH, ≥99.8% purity) was purchased from Prolabo. Hexane and methanol were purchased from Fisher Scientific (Madrid, Spain). All materials were used without further purification.

4.2.2 Solubility Parameter Calculation

The solubility parameter expresses the nature and magnitude of interaction forces working between polymers and solvents. The group contribution method was used to calculate the overall value of the solubility parameter [39]:

$$\delta = \sqrt{\delta_d^2 + \delta_p^2 + \delta_h^2} \qquad \text{(Eq. 5.1)}$$

where δ_d, δ_p and δ_h are the dispersive, polar and hydrogen bonding solubility parameters, respectively. The solubility parameter components may be calculated by the Hoftyzer and Van Krevelen method [40], using the following equations:

$$\delta_d = \frac{\sum F_{di}}{V}; \qquad \delta_p = \frac{\sqrt{\sum F_{pi}^2}}{V}; \qquad \delta_h = \sqrt{\frac{\sum E_{hi}}{V}} \qquad \text{(Eq. 5.2)}$$

where F_d is the dispersion component of the molar attraction constant, F_p the polar component, E_h the contribution of hydrogen bonding forces to the cohesive energy and V the molar volume.

The solubility of a polymer in an organic liquid can be determined by the total solubility parameter difference between polymer and solvent, *i.e.* the smaller the difference in the solubility parameter, the better the compatibility. It is calculated by the following equation, where each component of the Hansen solubility parameter of pure components (polymer, *P* and solvent, *S*) is taken into consideration:

$$\Delta\delta_{P/S} = \sqrt{\left(\delta_{d,P} - \delta_{d,S}\right)^2 + \left(\delta_{p,P} - \delta_{p,S}\right)^2 + \left(\delta_{h,P} - \delta_{h,S}\right)^2} \qquad \text{(Eq. 5.3)}$$

4.2.3. Ternary Phase Diagram Determination

Ternary phase diagrams were determined via the cloud point technique at room temperature. Dopes containing different non-solvent (ethanol) concentrations were prepared for different polymer concentrations ranging from 15 to 30 wt%. The cloud point was assigned to the non-solvent concentration where the dope changes from one phase into two phases, i.e., when the solution become turbid for more than 5 min. The binodal line is formed joining the cloud points of different polymer concentrations. Ternary diagrams for two polymer/solvent/non-solvent systems (P84®/NMP/EtOH and P84®/NMP+THF/EtOH) were determined and the influence of the incorporation of THF was studied. Ternary diagrams for different NMP/THF ratios were determined. The mixture of NMP and THF is considered as an "effective solvent" to draw the ternary diagram.

4.2.4. Preparation of P84® Hollow Fiber Membranes

The fabrication of P84® hollow fiber membranes was based on a process of dry jet spinning followed by a wet quench [3–8]. The hollow fibers preparation procedure has been described in detail elsewhere [41]. A spinneret with the following dimensions was used: 630 μm inner diameter and 1200 μm outer diameter. After spinning, the fibers were solvent exchanged in a methanol bath for 30 min (3 times) followed by a hexane bath for 30 min (3 times) and dried at 70 °C overnight. Fibers were kept overnight in a vacuum oven at 100 °C to completely remove residual solvent.

4.2.5. Hollow Fiber Membrane Characterization

The surface and cross-section morphology of the hollow fiber membranes were characterized by scanning electron microscopy (SEM) (Quanta 250 ESEM, FEI, The Netherlands). Membrane samples were freeze-fractured after immersion in liquid nitrogen and subsequently coated with gold/palladium to analyse cross sections of the samples.

Hollow fiber membrane modules were prepared and tested using an experimental set-up, based on constant pressure technique [7] described in detail elsewhere [41]. Pure N_2 and CO_2 gas permeation experiments were carried out at a transmembrane pressure of 7 bar at 35 °C. Gas was fed from the lumen side of the fiber and the permeate was collected from the shell side in a dead end, cross-flow configuration. The permeance for gas *i* was calculated by the following equation:

$$P_i = \frac{F_i}{\Delta p_i \cdot A} \quad \text{(Eq. 5.4)}$$

where P_i is the gas permeance in gas permeation units (1 GPU = 10^{-6} cm^3 (STP) cm^{-2} s^{-1} $cmHg^{-1}$), F_i is the volumetric flow rate of component i (cm^3 (STP) s^{-1}), Δp_i is the partial pressure difference of component i across the membrane (cmHg) and A is the effective membrane area (cm^2). The effective membrane area was calculated using the average value for fiber diameter taken from the measurement of 3 fibers at each end of the module and the active membrane length on the feed side.

The ideal selectivity α_{ij} was calculated as the ratio of the permeance of the more permeable compound i to the permeance of the less permeable compound j:

$$\alpha_{ij} = \frac{P_i}{P_j} \quad \text{(Eq. 5.5)}$$

4.3. Results and Discussion

4.3.1. Polymer Dope Optimization

Optimization of polymer solution (dope) composition is a key to success for the formation of defect-free hollow fiber membranes. For this purpose, the dope usually has a complex composition as it contains polymer, solvents and additives (non-solvents) that are miscible with the solvent but not with the polymer. Regarding polymer concentration, one requirement to produce hollow fibers with minimum defects is a high polymer concentration in order to create significant chain entanglement during skin formation. Nevertheless, a too high polymer concentration is not desired because it creates a support layer with lower porosity and higher resistance to gas transport. Therefore, the optimum value is met when the dope has sufficient viscosity to allow extrusion of the polymer dope and take-up at a relevant speed without breaking (*i.e.* a spinnable dope). In a polymer solution, the viscosity increases slightly with polymer concentration, up to a point from where it begins to increase exponentially. The critical polymer concentration (c.p.c.) is extrapolated from the typical viscosity versus polymer concentration curve, more specifically from the back interpolation of the linear part. The optimum polymer concentration in the dope is equal to or slightly above the c.p.c.. The critical P84® concentration of 28 wt% was identified from the viscosity vs polymer concentration curve for a P84®/NMP dope

solution by Peng *et al.* [42]. A P84® concentration of 28 to 28.5 wt% was employed in our spinning experiments.

The other components of the dope and their concentration are important for a rapid formation of a defect-free outer skin layer during the nascent fiber's residence time in the air gap. In that sense, Xu *et al.* presented the qualitative dope composition trajectories in the ternary phase diagram during a dry-jet/wet-quench spinning process and concluded that potentially useful dope composition should be in the one-phase region and close to the binodal line [43]. By the use of a non-solvent the dope solution composition gets closer to the binodal boundary, facilitating a faster phase separation. Due to the strong non-solvent character of water titration of the spinning dope close to the binodal becomes difficult and therefore EtOH is commonly selected as non-solvent. Also, as presented in the introduction section, the evaporation of volatile components in the air gap causes an increase in polymer concentration in the outermost region of the fiber so a dense skin can be formed.

4.3.1.1. Solubility Parameter

The influence of THF in the solubility of P84® in the solvent mixture NMP/THF was studied both theoretically and experimentally. Solubility parameter has been widely used to predict the solubility of polymers in various solvents. The solubility parameter of P84® co-polyimide was calculated by the group contribution method using Equations (1) and (2). The chemical structure of the polymer is shown in Figure 4.1 and the group contributions F_{di}, F_{pi} and E_{hi} of the structural groups composing the co-polyimide are listed in Table 4.1. An overall value of the solubility parameter of 27.46 $MPa^{1/2}$ was obtained for the P84® co-polyimide, in accordance with the value reported in literature for the same polymer [44].

The dispersive, polar and hydrogen bonding solubility parameter components, as well as the overall solubility parameter of components involved in the spinning dopes and phase inversion process, and the solubility parameter difference of P84® with the other components are presented in Table 4.2.

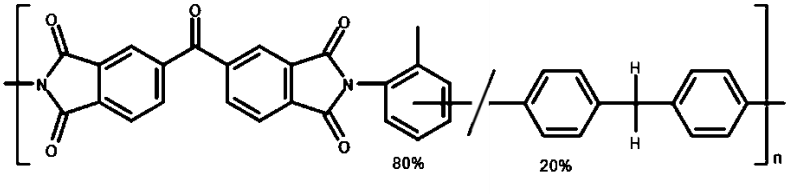

Figure 4.1. Chemical structure of P84® co-polyimide.

Table 4.1. Group contribution to P84® (BTDA-TDI/MDI) co-polyimide [40].

Functional Group	Numbers	F_{di} ($J^{1/2}$ $m^{3/2}$ mol^{-1})	F_{pi} ($J^{1/2}$ $m^{3/2}$ mol^{-1})	E_{hi} (J mol^{-1})	V_i (cm^3 mol^{-1})
$-CH_3$	0.8	420	0	0	21.9
$-CH_2$	0.2	270	0	0	16.4
=CH–	10	200	0	0	13.5
=C–	9.2	70	0	0	0.0
–CO–	5	290	770	2000	13.6
–N=	2	20	800	5000	6.9

Table 4.2. Calculated solubility parameters of components involved in the spinning dopes and coagulation bath [39].

Component	δ_d ($MPa^{1/2}$)	δ_p ($MPa^{1/2}$)	δ_h ($MPa^{1/2}$)	δ ($MPa^{1/2}$)	$\Delta\delta_{P/S}$ ($MPa^{1/2}$)
P84®	19.0	17.5	9.17	27.5	-
NMP	18.0	12.3	7.20	23.0	5.69
THF	16.8	5.7	8.00	19.5	12.1
EtOH	15.8	8.80	19.4	26.5	13.8
Water	15.5	16	42.3	47.8	33.4

The solubility parameter difference of P84® with the other components involved in the spinning dope increases in the order NMP (5.69) < THF (12.1) < EtOH (13.83). Thermodynamic considerations led to the conclusion that the effects of δ_d and δ_p over the $\Delta\delta_{P/S}$ are similar, while the effect of δ_h is of a different nature. Accordingly, the parameter $\delta_v = (\delta_d + \delta_p)^{1/2}$ was introduced, leading to δ_v versus δ_h diagrams [40]. In such diagrams, the interaction between a polymer and a number of solvents is graphically shown, and the "solubility circle" associated with the polymer is determined. The solubility region of the polymer is delimited by the circle, which usually has a radius of about 5δ-units. As a general rule, any liquid lying within the circle is a true solvent for the polymer, while the ones lying outside will act as non-solvents. The $\delta_v - \delta_h$ diagram of P84® is presented in Figure 4.2, where solvent and non-solvent involved in the phase inversion process are included. NMP is situated within the theoretical "solubility circle" of P84® represented by a dashed line, and as consequence has been used as

solvent for P84® membrane preparation in literature [32,42]. On the contrary, THF is out of the circle and therefore this solvent itself is not an appropriate solvent for P84®. However, a polymer could be dissolved in a mixture of two non-solvents or a mixture of a solvent and a non-solvent if the solubility parameter of the mixture is situated inside the circle.

Therefore, the solubility parameter of the NMP/THF solvent mixture was calculated for different NMP/THF ratios. The difference in the solubility parameter of P84® and the solvent mixture ($\Delta\delta_{P84®/Smix}$) is presented as a function on NMP/THF ratio in Figures 4.3a,b. As expected, $\Delta\delta_{P84®/Smix}$ decreases as NMP/THF ratio increases (THF content decreases), showing an exponential decrease up to an NMP/THF ratio of 14 (from 12.1 to 6.1 $MPa^{1/2}$, for pure THF and NMP/THF ratio of 14, respectively). Then, $\Delta\delta_{P84®/Smix}$ continues decreasing more moderately up to 5.75 $MPa^{1/2}$ (NMP/THF ratio of 100).

To experimentally determine the amount of THF that could be added to the spinning solution before it becomes unstable, dopes at different NMP/THF ratios (0.2 to 5.5) were prepared, at a constant P84® concentration of 28.5 wt%. As shown in Figure 4.3c, P84® solution becomes unstable at a THF concentration of ~47 wt%, which corresponds to an NMP/THF ratio of 0.52 ($\Delta\delta_{P84®/Smix}$ value of 9.86 $MPa^{1/2}$). Therefore, an NMP/THF ratio of 0.52 was defined as the boundary region for P84® dissolution and it is represented by a continuous line as the experimental "solubility circle" in Figure 4.2. In other words, P84® will solubilize in solvent mixtures with an NMP/THP ratio > 0.52. This demonstrated that even if THF itself is not an appropriate solvent for P84®, an NMP/THF mixture can be used to dissolve the polymer. The addition of THF weakens the solubilization capacity of the mixture. Nevertheless, still a wide solubility window was identified for the NMP/THF solvent mixture, as reflected in green in Figure 4.3b.

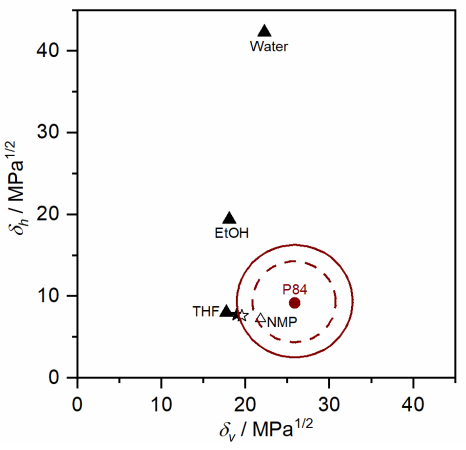

Figure 4.2. $\delta_v - \delta_h$ diagram of P84® at room temperature. Solvents are represented by open symbols, and non-solvents by close symbols. Star symbols represent solvent mixture with an NMP/THF ratio of 1 (☆) and 0.52 (★). Theoretical (dashed line) and experimental (continuous line) "solubility circles" are represented.

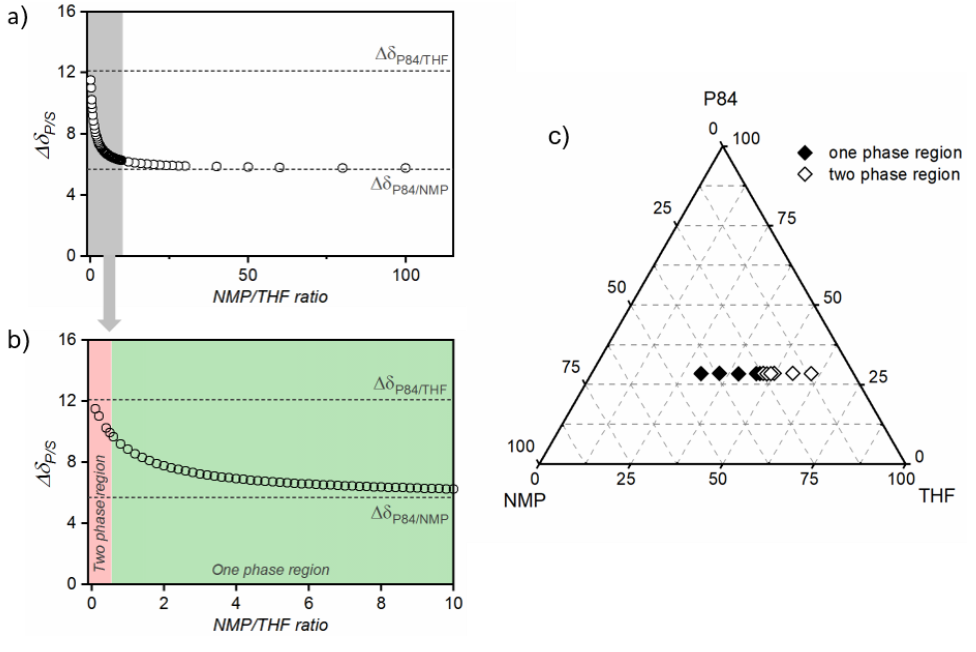

Figure 4.3. The difference in the solubility parameter of P84® and the solvent mixture ($\Delta\delta_{P84®/Smix}$) as a function on NMP/THF ratio for (**a**) an NMP/THF ratio range of 0 to 120, and (**b**) a magnification of the 0 to 10 range. (**c**) Ternary phase diagram of P84®/NMP/THF system at room temperature. Solid symbols represent solutions situated in the one phase region of the diagram and open symbols represent solutions situated in the two-phase region.

4.3.1.2. Ternary Phase Diagrams

Ternary phase diagrams for P84®/NMP/EtOH and P84®/NMP/THF/EtOH systems are presented in Figure 4.4. For P84®/NMP dope solution ~12 wt% ethanol is required to cause phase separation. As THF is incorporated in the system the binodal line is displaced closer to the polymer-solvent axis. For the P84®/NMP/THF dope solution with an NMP/THF ratio of 4, around 9 wt% of ethanol is required to cause phase separation. A further displacement of the binodal curve is observed as the THF concentration in the system increases, ~8 wt% and ~5 wt% ethanol is required to cause phase separation for a dope solution with an NMP/THF ratio of 2 and 1, respectively. This is in accordance with the solubility parameter study presented in section 3.1. The dope solution becomes more unstable as the THF amount increases ($\Delta\delta_{P84®/Smix}$ increases) and thus it can accommodate less non-solvent.

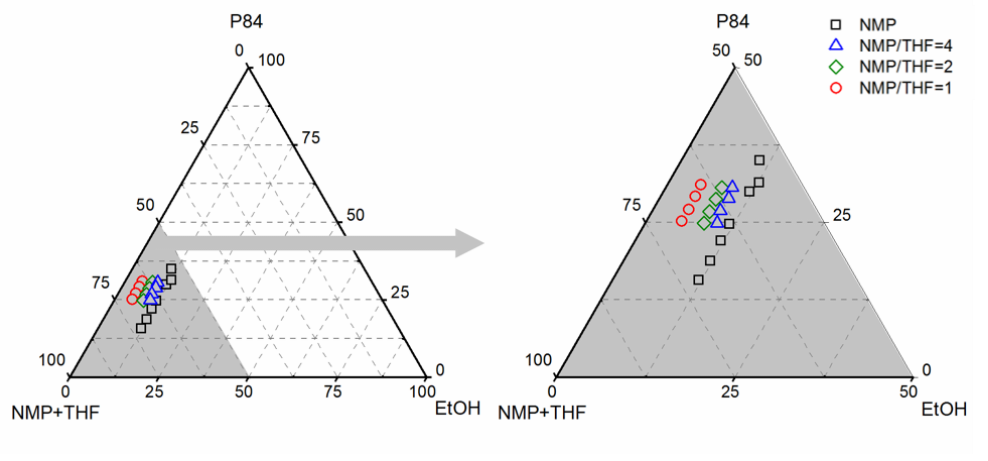

Figure 4.4. Ternary phase diagram of P84®/NMP/EtOH system (□) and P84®/(NMP/THF)/EtOH system at NMP/THF ratio of 4 (Δ), 2 (◊) and 1(○) at room temperature.

4.3.2. P84® Hollow Fiber Spinning Process Optimization

Several spinning sessions were performed (D1–D5), the studied spinning parameter range, as well as separation performance of hollow fibers of each spinning sessions are presented in Table 4.3. For each spinning session a dope composition was established, and the spinning conditions were varied in order to find the optimal combination of spinning parameters for achieving the best performance for gas permeation. The as-spun fiber separation performance was evaluated. These results are compared with gas permeation through a 20 μm thick dense flat film of P84® at similar operational conditions (1.28 Barrer CO_2; 36.6 CO_2/N_2 selectivity at 35 °C) [32]. Asymmetric membranes are defined to be "defect-free" if the ideal selectivity is greater than 80% of the intrinsic selectivity of dense films [45]. In the case of asymmetric P84® hollow fibers this value has been fixed at a CO_2/N_2 selectivity of ~29.3 at 35 °C.

Table 4.3. Spinning conditions and permeation performance for P84® hollow fiber membranes prepared from different dope compositions. Single gas permeation at 35 °C and 7 bar transmembrane pressure. The permeance data are values of two modules of ten fibers each.

Spinning Parameters	Unit	D1	D2	D3	D4	D5
Dope composition	wt% P84®	28.5	28.5	28.5	28	28.5
	wt% NMP	64.5	62.5	58.7	46.9	35.2
	wt% THF	-	-	9.8	19.1	35.3
	wt% EtOH	7	9	3	6	1 *
NMP/THF ratio	-	-	-	6	2.4	1
Dope/bore fluid flow rate	ml h^{-1}	180/60	180/60	180/60	180/60	210/80, 240/90
Bore fluid composition	NMP/H_2O	87.5/12.5	93/7, 85/15	84.5/15.5	84.8/15.2	87/13
Spinneret temperature	°C	25	30–40	25–30	25–30	25–40
Air gap height	cm	5–15	5-15	5-15	5–10	2-10
Quench bath temperature	°C	25	25	25	25	25
Take up rate	m min^{-1}	20–30	20–25	20–30	20–30	20
Membrane Performance	Unit	D1	D2	D3	D4	D5
CO_2 permeance	GPU	2269–1692	784–5692	79.9–193	28.2–34.9	3.53–23.0
Ideal CO_2/N_2 selectivity	-	0.98–1.08	0.87–1.09	3.28–21.4	15.2–17.4	20.6–40.4

* $LiNO_3$.

4.3.2.1. P84®/NMP/EtOH Systems

For the first two spinning sessions (D1 and D2), a simple solvent system similar to that reported by Barsema *et al.* [32] was employed. The same solvent (NMP) and P84® concentration was employed (28.5 wt%), but with the only difference of the incorporation of ethanol to the dope. Ethanol was added into the dopes to be close to the binodal line (7 wt% and 9 wt% of ethanol to D1 and D2, respectively). The high permeance and lack of selectivity of as-spun fibers (>780 GPU of CO_2 and ~1 CO_2/N_2 selectivity) denoted that highly defective fibers were obtained, even when the ethanol concentration was increased for D2 to be even closer to the binodal curve.

4.3.2.2. P84®/NMP/THF/EtOH Systems

The addition of THF to the spinning dope results on the obtention of less defective fibers. Figure 4.5 shows that an increase in ideal CO_2/N_2 selectivity is observed by decreasing the NMP/THF ratio (THF content increases). Dope D3, with an NMP/THF ratio of 6, gives fibers with CO_2 permeances lower than 193 GPU and CO_2/N_2 selectivity ranging from 3.28 to 21.4. A further increase in THF content in D4 (NMP/THF ratio of 2.4) promotes the formation of a tighter skin layer and therefore, less permeable fibers (CO_2 permeance < 35 GPU). However, the obtained selectivity value ranging from 15.2 to 17.4, almost half of the dense film selectivity value, denoted the presence of small defects in the selective layer of the fibers. The THF content was further increased to NMP/THF ratio of 1 for the D5 spinning session. Also, in order to accelerate phase separation $LiNO_3$ was introduced in the system [43]. For all prepared fibers, an ideal CO_2/N_2 selectivity higher than 20 was obtained. Even more, a selectivity of 40.4 was obtained for one of the states, higher than the dense film selectivity values. This phenomenon has been reported before for 6FDA-based polymer spinning [46,47]. It was hypothesized, that it was due to the uniaxial orientation of polymer chains resulting from the high shear rate in the spinneret. This results in a tighter packing of the polymer chains, leading to an increase in selectivity over the unaligned state of polymer chains of the dense film. This demonstrates that as-spun fibers with a small number of defects or even defect-free fibers can be obtained by fine tuning of the dope composition and spinning parameters.

The performance of the four different fibers states obtained from dope D5 are analyzed in detail. Spinning conditions, separation performance and selective layer thickness of the four states of hollow fiber membranes are presented in Table 4.4. The selective layer thickness was estimated from the intrinsic CO_2 permeability of the dense film and the permeance value of the asymmetric hollow fiber membrane. The influence of two spinning parameters was studied: The air gap height and the spinneret temperature.

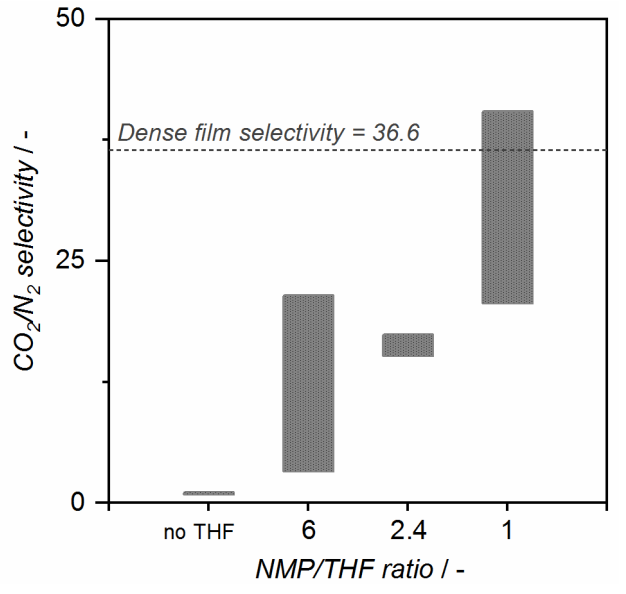

Figure 4.5. Ideal CO_2/N_2 selectivity range obtained at 35 °C for fibers spun from dopes D1 and D2 (no THF), D3 (NMP/THF ratio 6), D4 (ratio 2.4) and D5 (ratio 1).

Table 4.4. Spinning conditions and separation performance of the four states of hollow fiber membranes prepared from dope D5. Membrane performance for single gas permeation at 35 °C and 7 bar transmembrane pressure. The permeance data are average values of two modules of ten fibers each and error correspond to standard deviation.

-	D5	Unit	ST-1	ST-2	ST-3	ST-4
Spinning Parameters	Spinneret temperature	°C	25	25	40	40
	Air gap height	cm	2	10	2	10
Separation Performance	CO_2 permeance	GPU	23.0 ± 1.8	4.9 ± 0.1	12.0 ± 1.5	3.5 ± 0.1
	Ideal CO_2/N_2 selectivity	-	40.4 ± 1.4	25.1 ± 0.4	34.8 ± 2.8	20.6 ± 0.25
	Selective layer thickness (calculated from permeance)	nm	56	262	107	363

Only varied spinning parameters are listed on the table, the rest of the parameters were kept constant: Dope composition (28.5 wt% P84®/35.2 wt% NMP/35.3 wt% THF/1 wt% $LiNO_3$), bore fluid composition (87 wt%/13 wt% NMP/H_2O), quench bath temperature (25 °C) and take up rate (20 m min^{-1}). Dope flow rate and bore flow rate were 210 mL h^{-1} and 80 mL h^{-1}, respectively, except for ST-4 where dope and bore fluid flow rate were increased to 240 mL h^{-1} and 90 mL h^{-1} to avoid pulsing phenomena observed at lower values.

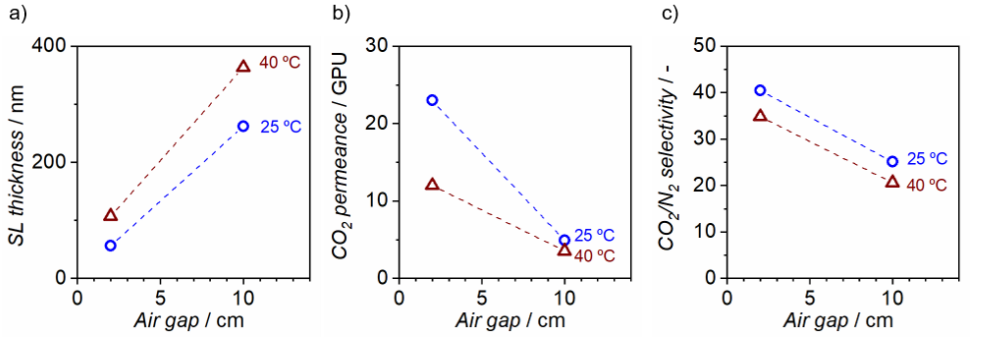

Figure 4.6. Air gap vs (**a**) selective layer thickness, (**b**) CO_2 permeance at 35 °C and (**c**) CO_2/N_2 selectivity for two spinneret temperatures (25 °C and 40 °C)

Selective layer thickness, CO_2 permeance and ideal CO_2/N_2 selectivity as a function of the air gap for two spinneret temperatures (25 and 40 °C) are presented in Figure 4.6. The selective layer thickness is increased by the increase of the air gap (from 2 to 10 cm) for both spinneret temperatures, from 56 to 262 nm and from 107 to 363 nm for a spinneret temperature of 25 and 40 °C, respectively. Correspondingly, a decrease in CO_2 permeance is observed by the increased air gap height. The dense selective layer is formed by the evaporation of the solvent in the air gap, mostly volatile THF. As the air gap height increases, the residence time of the fiber in the air gap increases, and hence, the evaporated solvent amount, increasing the polymer concentration at the outermost region of the fiber. Therefore, an increase in selective layer thickness and a decrease in gas permeance is expected by increasing the air gap. Figure 4.6 also shows that an increased selective layer thickness and a decreased CO_2 permeance is observed for the higher spinneret temperature. The increased spinneret temperature may induce a larger amount of evaporated solvent and therefore an increased selective layer thickness and hence a decreased CO_2 permeance.

SEM images of the cross-section of the overall fiber, fiber wall and the selective layer as well as the outer surface of hollow fiber states prepared at the lowest air gap and spinneret temperature (ST-1) and highest air gap and spinneret temperature (ST-4) are presented in Figure 4.7. Both fibers present an outer diameter of ~430 μm and a similar sponge-like substructure. The trend observed in the estimation of the selective layer thickness from the CO_2 permeance value (i.e., 56 nm for ST-1 and 363 nm for ST-4) is somehow confirmed by the SEM images, showing a thicker selective layer of ~500 nm for the latter. The selective layer thickness measured by SEM is higher than the one given by CO_2 permeance due to bending of the outer layer produced during the freeze-fracturing of the sample in liquid nitrogen. Although a cleaner cut could improve the

estimation of the selective layer thickness by SEM, in most cases it would not be easy to identify the borderline between selective layer/transition layer/porous support. In addition, SEM analysis is local and does not give an average. Although the calculation of selective layer thickness from CO_2 permeance value is also a simple estimation—it does not consider substrate resistance to the overall membrane resistance—it is useful for evaluating if the produced fibers have the thinnest achievable selective layer (*i.e.* ~100 nm) or if there is still room for optimization.

On the other hand, Figure 4.6c shows that the threshold selectivity value to consider P84® fibers as defect-free (CO_2/N_2 ~29.3) is attained only for the lowest air gap height of 2 cm for both spinneret temperatures. This result is in contradiction with the expected increase in selectivity with the increase in solvent evaporation rate at larger air gaps. We speculate that, during the residence time of the spun fiber in the air gap, an early phase separation on the outer surface of the fiber could be induced by water absorption from the ambient humidity. This may cause formation of small defects in the outer dense selective layer. A short air gap helps to minimize the effect of the water vapor within the air gap, and therefore, the number of defects. Nevertheless, the obtained selectivity value of 20–25 for the maximum air gap of 10 cm suggests that the defects could be easily healed by the conventional silicone rubber coatings.

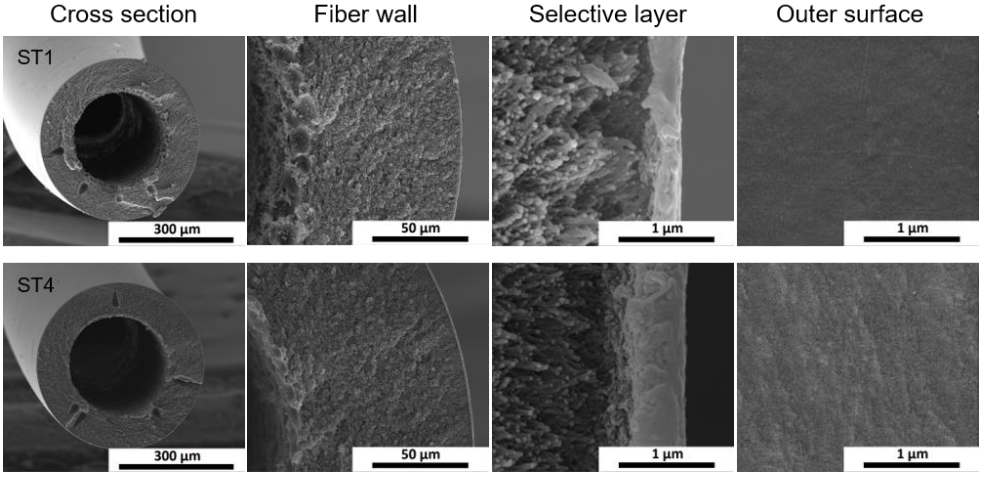

Figure 4.7. SEM images of the cross-section (overall fiber, fiber wall and the selective layer) and outer surface of hollow fibers from ST1 (air gap: 2 cm and spinneret temperature 25 °C) and ST4 (air gap: 10 cm and spinneret temperature 40 °C).

The highest permeability and ideal selectivity were obtained for fibers spun with the smallest air gap (2 cm) and lowest spinneret temperature (25 °C). An ultra-thin selective layer of ~56 nm was obtained, almost ten times lower than the 500 nm thick selective layer obtained by Barsema *et al.* [32]. These hollow fiber membranes present an ideal CO_2/N_2 selectivity of 40.4, and the highest permeance reported in literature for P84® hollow fibers, 23 GPU of CO_2 at 35 °C, against 2.2 GPU at 25 °C reported by Barsema *et al.*

A new spinning process has been performed at a larger scale (~5000 meters of fibers) using the optimal spinning parameters from D5, ST1 with the difference that we used a flow of dry N_2 in the air gap with the objective of eliminating humidity influence. Five modules containing 10 fibers each, taken at different production times have been characterized and the average value is provided in Table 4.5. For comparison purposes, the hollow fiber performance for the reference spinning process is included. The ideal selectivity was reproduced for the scaled up fibers, while the CO_2 permeance was lowered. We assume there was a combination of factors that gave a lower CO_2 permeance, like faster evaporation of solvent induced by forced N_2 flow in the air gap, or small variations in the other spinning parameters such as room temperature (15 °C for spinning D5_ST1 versus 25 °C for up-scale D5_ST-1). SEM images of up-scaled fibers are presented in Figure 4.8. Two fibers were subjected to SEM analysis and several areas of the selective layer were checked. A selective layer thickness of around 200 nm could be estimated from the clearest cut of fiber 2 area B, slightly higher than the one estimated from CO_2 permeance value.

Table 4.5. Separation performance of hollow fiber membranes prepared from dope D5 and spinning conditions ST-1 in two spinning sessions (reference and scaled-up). Separation performance for single gas permeation at 35 °C and 7 bar transmembrane pressure.

Separation performance	Unit	D5_ST-1	Scaled-up D5_ST-1
CO_2 permeance	GPU	23.0 ± 1.8	8.4± 1.7
Ideal CO_2/N_2 selectivity	-	40.4 ± 1.4	39.1 ± 1.0
Selective layer thickness (calculated from permeance)	nm	56	152

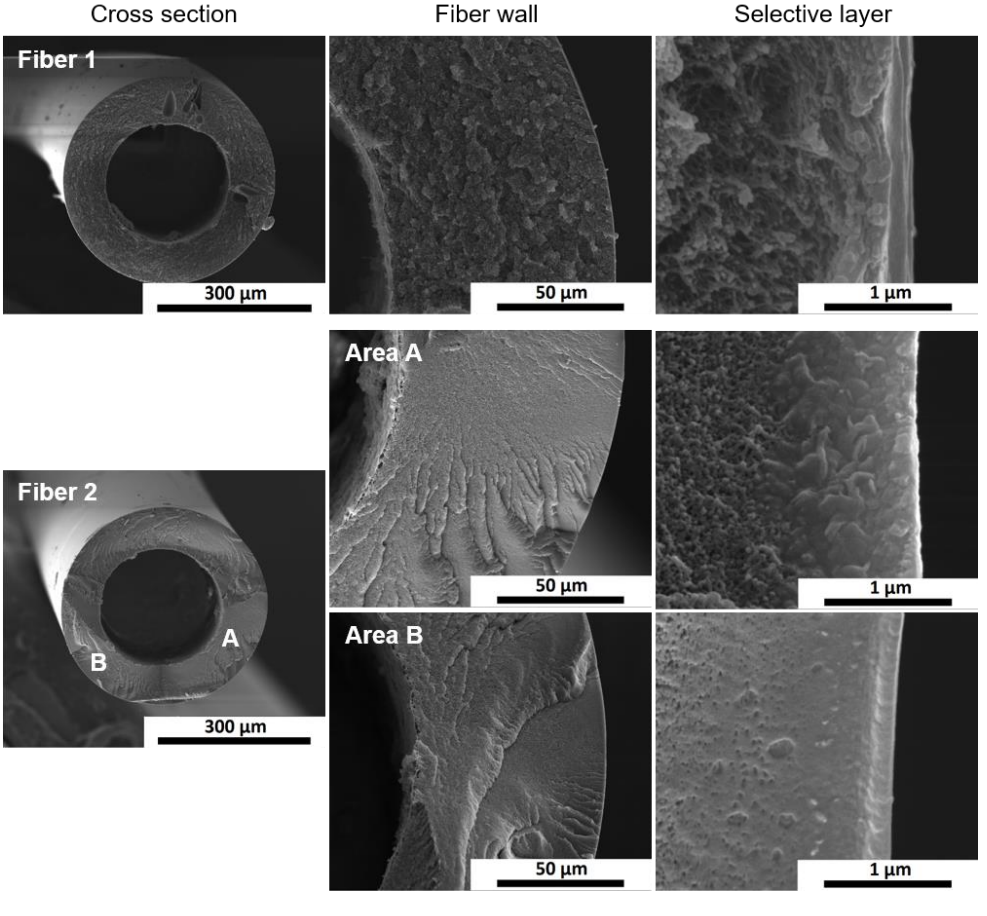

Figure 4.8. SEM images of the cross-section (overall fiber, fiber wall and the selective layer) of scaled-up D5_ST1 hollow fibers.

4.4. Conclusions

Using volatile THF in combination with non-volatile NMP allows the fabrication of defect-free ultra-thin (~56 nm) P84® asymmetric hollow fiber membranes with no need for defect healing post treatment. The elimination of an additional defect healing post-treatment step would result in a significant reduction in membrane production costs. Solubility parameter study demonstrated that even while THF itself is not an appropriate solvent for P84®, an NMP/THF mixture could be used to dissolve the polymer as long as the NMP/THF ratio is kept above 0.52. Defect-free as-spun P84® hollow fiber membranes fibers can be obtained by fine tuning of the dope composition and spinning parameters. The best results were obtained for hollow fibers membranes spun from a spinning dope containing a NMP/THF ratio of 1 and the smallest air gap and spinneret temperature studied (2 cm and 25 °C), resulting in a CO_2 permeance improvement by a factor ten and an ideal CO_2/N_2 selectivity of up to 40. The spinning process is reproducible at a larger scale (~5000 m fibers).

References

[1] M.F.A. Wahab, A.F. Ismail, S.J. Shilton, Studies on gas permeation performance of asymmetric polysulfone hollow fiber mixed matrix membranes using nanosized fumed silica as fillers, Sep. Purif. Technol. 86 (2012) 41–48. doi:10.1016/j.seppur.2011.10.018.

[2] S. Husain, W.J. Koros, Mixed matrix hollow fiber membranes made with modified HSSZ-13 zeolite in polyetherimide polymer matrix for gas separation, J. Memb. Sci. 288 (2007) 195–207. doi:10.1016/j.memsci.2006.11.016.

[3] N. Peng, N. Widjojo, P. Sukitpaneenit, M.M. Teoh, G.G. Lipscomb, T.-S. Chung, J.-Y. Lai, Evolution of polymeric hollow fibers as sustainable technologies: Past, present, and future, Prog. Polym. Sci. 37 (2012) 1401–1424. doi:10.1016/j.progpolymsci.2012.01.001.

[4] Y. Li, T. Chung, Z. Huang, S. Kulprathipanja, Dual-layer polyethersulfone (PES)/BTDA-TDI/MDI co-polyimide (P84) hollow fiber membranes with a submicron PES–zeolite beta mixed matrix dense-selective layer for gas separation, J. Memb. Sci. 277 (2006) 28–37. doi:10.1016/j.memsci.2005.10.008.

[5] N. Widjojo, T.-S. Chung, S. Kulprathipanja, The fabrication of hollow fiber membranes with double-layer mixed-matrix materials for gas separation, J. Memb. Sci. 325 (2008) 326–335. doi:10.1016/j.memsci.2008.07.046.

[6] O. David, Y. Gendel, M. Wessling, Tubular macro-porous titanium membranes, J. Memb. Sci. 461 (2014) 139–145. doi:10.1016/j.memsci.2014.03.010.

[7] O.C. David, D. Gorri, K. Nijmeijer, I. Ortiz, A. Urtiaga, Hydrogen separation from multicomponent gas mixtures containing CO, N2 and CO2 using Matrimid® asymmetric hollow fiber membranes, J. Memb. Sci. 419–420 (2012) 49–56. doi:10.1016/j.memsci.2012.06.038.

[8] V.P. Babu, B.E. Kraftschik, W.J. Koros, Crosslinkable TEGMC asymmetric hollow fiber membranes for aggressive sour gas separations, J. Memb. Sci. 558 (2018) 94–105. doi:10.1016/j.memsci.2018.04.028.

[9] Y. Yampolskii, Polymeric Gas Separation Membranes, Macromolecules. 45 (2012) 3298–3311. doi:10.1021/ma300213b.

[10] N. Peng, T.-S. Chung, J.-Y. Lai, The rheology of Torlon® solutions and its role in the formation of ultra-thin defect-free Torlon® hollow fiber membranes for gas separation, J. Memb. Sci. 326 (2009) 608–617. doi:10.1016/j.memsci.2008.10.038.

[11] I. Pinnau, W.J. Koros, Gas-permeation properties of asymmetric polycarbonate, polyestercarbonate, and fluorinated polyimide membranes

prepared by the generalized dry–wet phase inversion process, J. Appl. Polym. Sci. 46 (1992) 1195–1204. doi:10.1002/app.1992.070460709.

[12] J.M.S. Henis, M.K. Tripodi, Composite hollow fiber membranes for gas separation: the resistance model approach, J. Memb. Sci. 8 (1981) 233–246. doi:10.1016/S0376-7388(00)82312-1.

[13] D.T. Clausi, W.J. Koros, Formation of defect-free polyimide hollow fiber membranes for gas separations, J. Memb. Sci. 167 (2000) 79–89. doi:10.1016/S0376-7388(99)00276-8.

[14] J.J. Krol, M. Boerrigter, G.H. Koops, Polyimide hollow fiber gas separation membranes: preparation and the suppression of plasticization in propane/propylene environments, J. Memb. Sci. 184 (2001) 275–286. doi:10.1016/S0376-7388(00)00640-2.

[15] T. Visser, Mixed gas plasticization phenomena in asymmetric membranes, University of Twente, Enschede, The Netherlands, 2006.

[16] M.R. Kosuri, W.J. Koros, Defect-free asymmetric hollow fiber membranes from Torlon®, a polyamide–imide polymer, for high-pressure CO2 separations, J. Memb. Sci. 320 (2008) 65–72. doi:10.1016/j.memsci.2008.03.062.

[17] N. Peng, T.S. Chung, The effects of spinneret dimension and hollow fiber dimension on gas separation performance of ultra-thin defect-free Torlon ® hollow fiber membranes, J. Memb. Sci. 310 (2008) 455–465. doi:10.1016/j.memsci.2007.11.018.

[18] Y. Kase, Gas Separation by Polyimide Membranes, Adv. Membr. Technol. Appl. (2008) 581–598. doi:10.1002/9780470276280.ch22.

[19] C. Ba, J. Langer, J. Economy, Chemical modification of P84 copolyimide membranes by polyethylenimine for nanofiltration, J. Memb. Sci. 327 (2009) 49–58. doi:10.1016/j.memsci.2008.10.051.

[20] Y.H. See-Toh, M. Silva, A. Livingston, Controlling molecular weight cut-off curves for highly solvent stable organic solvent nanofiltration (OSN) membranes, J. Memb. Sci. 324 (2008) 220–232. doi:10.1016/j.memsci.2008.07.023.

[21] Y.H. See Toh, F.W. Lim, A.G. Livingston, Polymeric membranes for nanofiltration in polar aprotic solvents, J. Memb. Sci. 301 (2007) 3–10. doi:10.1016/j.memsci.2007.06.034.

[22] P. Vandezande, L.E.M. Gevers, I.F.J. Vankelecom, Solvent resistant nanofiltration: separating on a molecular level, Chem. Soc. Rev. 37 (2008) 365–405. doi:10.1039/B610848M.

[23] R. Han, Y. Xie, X. Ma, Crosslinked P84 copolyimide/MXene mixed matrix membrane with excellent solvent resistance and permselectivity, Chinese J. Chem. Eng. 27 (2019) 877–883. doi:10.1016/j.cjche.2018.10.005.

[24] R. Han, Y. Xie, X. Ma, D. Teng, S. Zhang, X. Jian, Preparation of poly(2,4,6-triaminopyrimidine-TMC)/P84 composite nanofiltration membrane with enhanced chlorine resistance and solvent resistance, J. Chem. Technol. Biotechnol. 94 (2019) 2838–2843. doi:10.1002/jctb.5883.

[25] M.H. Davood Abadi Farahani, T.-S. Chung, Solvent resistant hollow fiber membranes comprising P84 polyimide and amine-functionalized carbon nanotubes with potential applications in pharmaceutical, food, and petrochemical industries, Chem. Eng. J. 345 (2018) 174–185. doi:10.1016/j.cej.2018.03.153.

[26] S.M. Dutczak, C.R. Tanardi, K.K. Kopeć, M. Wessling, D. Stamatialis, "Chemistry in a spinneret" to fabricate hollow fibers for organic solvent filtration, Sep. Purif. Technol. 86 (2012) 183–189. doi:10.1016/j.seppur.2011.11.003.

[27] G. Polotskaya, M. Putintseva, A. Pulyalina, I. Gofman, A. Toikka, Impact of endometallofullerene on P84 copolyimide transport and thermomechanical properties, Polymers (Basel). 10 (2018). doi:10.3390/polym10101108.

[28] G.M. Shi, Y. Wang, T.-S. Chung, Dual-layer PBI/P84 hollow fibers for pervaporation dehydration of acetone, AIChE J. 58 (2012) 1133–1145. doi:10.1002/aic.12625.

[29] R. Liu, X. Qiao, T.-S. Chung, The development of high performance P84 co-polyimide hollow fibers for pervaporation dehydration of isopropanol, Chem. Eng. Sci. 60 (2005) 6674–6686. doi:10.1016/j.ces.2005.05.066.

[30] X. Qiao, T.-S. Chung, K.P. Pramoda, Fabrication and characterization of BTDA-TDI/MDI (P84) co-polyimide membranes for the pervaporation dehydration of isopropanol, J. Memb. Sci. 264 (2005) 176–189. doi:10.1016/j.memsci.2005.04.034.

[31] X. Qiao, T.-S. Chung, Fundamental Characteristics of Sorption, Swelling, and Permeation of P84 Co-polyimide Membranes for Pervaporation Dehydration of Alcohols, Ind. Eng. Chem. Res. 44 (2005) 8938–8943. doi:10.1021/ie050836g.

[32] J.N. Barsema, G.C. Kapantaidakis, N.F.A. van der Vegt, G.H. Koops, M. Wessling, Preparation and characterization of highly selective dense and hollow fiber asymmetric membranes based on BTDA-TDI/MDI co-polyimide, J. Memb. Sci. 216 (2003) 195–205. doi:10.1016/S0376-7388(03)00071-1.

[33] T. Visser, N. Masetto, M. Wessling, Materials dependence of mixed gas plasticization behavior in asymmetric membranes, J. Memb. Sci. 306 (2007) 16–

28. doi:10.1016/j.memsci.2007.07.048.

[34] M. Omidvar, C.M. Stafford, H. Lin, Thermally stable cross-linked P84 with superior membrane H2/CO2 separation properties at 100 °C, J. Memb. Sci. 575 (2019) 118–125. doi:10.1016/j.memsci.2019.01.003.

[35] A. Guo, Y. Ban, K. Yang, W. Yang, Metal-organic framework-based mixed matrix membranes: Synergetic effect of adsorption and diffusion for CO2/CH4 separation, J. Memb. Sci. 562 (2018) 76–84. doi:10.1016/j.memsci.2018.05.032.

[36] S.-H. Choi, J.C. Jansen, F. Tasselli, G. Barbieri, E. Drioli, In-line formation of chemically cross-linked P84® co-polyimide hollow fibre membranes for H2/CO2 separation, Sep. Purif. Technol. 76 (2010) 132–139. doi:10.1016/j.seppur.2010.09.031.

[37] E.P. Favvas, S.K. Papageorgiou, J.W. Nolan, K.L. Stefanopoulos, A.C. Mitropoulos, Effect of air gap on gas permeance/selectivity performance of BTDA-TDI/MDI copolyimide hollow fiber membranes, J. Appl. Polym. Sci. 130 (2013) 4490–4499. doi:10.1002/app.39677.

[38] L. Sheng, J. Ren, K. Hua, H. Li, Y. Feng, M. Deng, The enhancement of mechanical properties of P84 hollow fiber membranes by thermally annealing below and above Tg, J. Memb. Sci. (2019) 117580. doi:10.1016/j.memsci.2019.117580.

[39] C.M. Hansen, Hansen Solubility Parameters: A User's Handbook, Second Edi, CRC Press, 2007. doi:10.1201/9781420006834.

[40] D.W. van Krevelen, K. te Nijenhuis, Properties of Polymers: Their Correlation with Chemical Structure; their Numerical Estimation and Prediction from Additive Group Contributions, 4th Editio, Elsevier Science, 2009.

[41] M. Etxeberria-Benavides, T. Johnson, S. Cao, B. Zornoza, J. Coronas, J. Sanchez-Lainez, A. Sabetghadam, X. Liu, E. Andres-Garcia, F. Kapteijn, J. Gascon, O. David, PBI mixed matrix hollow fiber membrane: Influence of ZIF-8 filler over H2/CO2 separation performance at high temperature and pressure, Sep. Purif. Technol. 237 (2019) 116347. doi:10.1016/j.seppur.2019.116347.

[42] N. Peng, T.S. Chung, K.Y. Wang, Macrovoid evolution and critical factors to form macrovoid-free hollow fiber membranes, J. Memb. Sci. 318 (2008) 363–372. doi:10.1016/j.memsci.2008.02.063.

[43] L. Xu, C. Zhang, M. Rungta, W. Qiu, J. Liu, W.J. Koros, Formation of defect-free 6FDA-DAM asymmetric hollow fiber membranes for gas separations, J. Memb. Sci. 459 (2014) 223–232. doi:10.1016/j.memsci.2014.02.023.

[44] I. Soroko, M.P. Lopes, A. Livingston, The effect of membrane formation

parameters on performance of polyimide membranes for organic solvent nanofiltration (OSN): Part A. Effect of polymer/solvent/non-solvent system choice, J. Memb. Sci. 381 (2011) 152–162. doi:10.1016/j.memsci.2011.07.027.

[45] S.C. Pesek, W.J. Koros, Aqueous quenched asymmetric polysulfone membranes prepared by dry/wet phase separation, J. Memb. Sci. 81 (1993) 71–88. doi:10.1016/0376-7388(93)85032-R.

[46] T.-S. Chung, W.-H. Lin, R.H. Vora, The effect of shear rates on gas separation performance of 6FDA-durene polyimide hollow fibers, J. Memb. Sci. 167 (2000) 55–66. doi:10.1016/S0376-7388(99)00278-1.

[47] R.P. Lively, M.E. Dose, L. Xu, J.T. Vaughn, J.R. Johnson, J.A. Thompson, K. Zhang, M.E. Lydon, J.-S. Lee, L. Liu, Z. Hu, O. Karvan, M.J. Realff, W.J. Koros, A high-flux polyimide hollow fiber membrane to minimize footprint and energy penalty for CO2 recovery from flue gas, J. Memb. Sci. 423–424 (2012) 302–313. doi:10.1016/j.memsci.2012.08.026.

Chapter 5

PBI hollow fiber membranes: Influence of PVP additive on manufacturing scalability

Defect-free asymmetric hollow fiber membranes for H_2/CO_2 separation in pre-combustion CO_2 capture processes have been developed based on blending polybenzimidazole (PBI) and polyvinylpyrrolidone (PVP). The main advantage of PVP addition was the possibility to increase the as spun fiber elasticity, reaching industrially relevant take up rate values (as high as 50 m/min), and significantly reducing fibers outer diameter (< 300 μm). Defect-free fibers were prepared at PVP concentrations below 30 wt.%. DSC analysis confirmed the formation of a homogeneous PBI and PVP blend. TGA analysis showed thermal stability of blend fibers up to ~340 °C. Developed PBI/PVP blend fibers show a H_2 permeance of 56 GPU and a H_2/CO_2 mixed gas selectivity of 16.6 at 150 ºC.

This chapter is based on the following publication:

M. Etxeberria-Benavides, S. Miguel, M. Díaz de Guereñu, F. Kapteijn, J. Gascon, O. David, PBI hollow fiber membranes: Influence of PVP additive on manufacturing scalability, *Submitted*

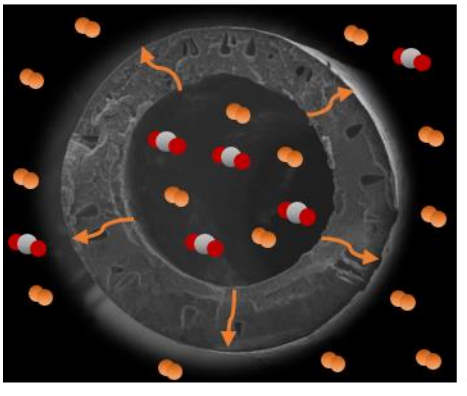

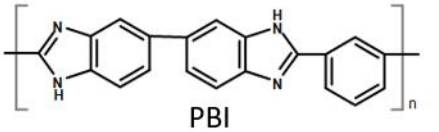

PBI

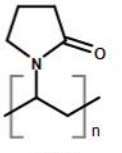

PVP

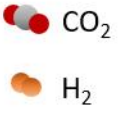

5.1. Introduction

Membrane gas separation processes have gained much attention in the past few decades. Compared to conventional gas separation technologies like cryogenic distillation, condensation and amine absorption, membrane separation processes have lower energy consumption, relatively small footprint, low mechanical complexity and the main advantage of operating under continuous, steady state conditions [1]. Pre-combustion CO_2 capture is one of the three major ways to reduce CO_2 emissions in combustion processes, next to post-combustion CO_2 capture and oxyfuel combustion.

Polybenzimidazole (PBI) has been identified as a good polymeric material for the high temperature membrane separation required in the pre-combustion application [2–5]. It exhibits the highest H_2/CO_2 selectivity among the polymer family, together with a high chemical and thermal stability (glass transition temperature of 420 ºC) and resistance against plasticization. Nevertheless, low permeability and brittleness are among its major drawbacks [6]. Other polymeric materials present higher H_2 permeability but a relatively low H_2/CO_2 permselectivity. In addition, sorption of highly condensable CO_2 can plasticize the other polymeric materials. Several strategies have been proposed to overcome these disadvantages, such as mixed matrix membrane preparation [5,7–12], polymer blending [13–18] and PBI crosslinking [17,19–21]. Blending of PBI has been extensively studied in literature. The presence of both donor and acceptor hydrogen bonding sites in the PBI repeating unit favour the formation of miscible blends with other polymers. Several works on flat sheet membranes from PBI blends have been reported in literature where an improvement on separation properties was achieved. For instance, PBI/Matrimid® blend membranes showed a 1.5 fold increase in H_2/CO_2 and H_2/N_2 selectivity [22]. The O_2/N_2 and CO_2/CH_4 selectivity of polyimide DPPD-IMM was doubled when it was blended with PBI [23]. PBI/Torlon® and PBI/P84® blend membranes showed a 1.6 and 1.15 times increase in H_2/CO_2 selectivity [24]. H_2 permeability was greatly increased by the combination of PIM and PBI [15]. In another study PBI was blended with a thermally rearrangeable polyimide (HAB-6FDA-CI), the H_2 permeability was doubled at constant H_2/CO_2 selectivity [16].

The hollow fiber configuration is the preferred one for commercial gas separation application, since hollow fibers can be densely packed yielding membrane modules with a high surface area (over 10,000 m^2/m^3) [25–27]. Surface area/volume ratio for a given packing density will be dependent on hollow fiber outer diameter: the smaller the diameter the higher the surface area/volume ratio. The hollow fiber outer diameter will be determined by several spinning parameters, with the production rate (take up rate on the final drum) being the most influential. Several polymers such us

polyethersulfone [28], polyamide-imide [29,30] and polyimide [31–36] have been spun at commercially relevant take up rates, resulting in hollow fibers with an outer diameter of less than 300 μm. The preparation of PBI hollow fiber membrane has been extensively studied [3,8,9,11,37–39]. PBI blended hollow fiber membranes have been also reported. For instance, hollow fibers were prepared from PBI and Matrimid® blend and subsequently crosslinked, resulting on improvement of both plasticization resistance and H_2/CO_2 selectivity [14]. PBI was also blended with sulfonated polyphenylsulfone. The hollow fibers were then subjected to a crosslinking reaction and heat treatment to enhance the gas separation performance for H_2/CO_2 separation [18]. However, low take up rates values were employed during spinning of bare PBI and PBI blends, below 10 m/min in most of the cases and therefore PBI hollow fiber with relatively large outer diameter (> 370 μm) were obtained (see Table 5.8).

In the present work, PBI was blended with a low molecular weight polymer (polyvinylpyrrolidone, PVP K30) and the expected main contribution of PVP was to increase the production rate of PBI hollow fiber membranes and improve their mechanical properties. PVP addition significantly increases the as spun fiber elasticity and therefore enables to increase the take up rate during the spinning process, resulting in a significant reduction of fiber outer diameter (< 300 μm). Nevertheless, considering that PVP is normally used as additive in the production of porous hollow fiber membranes for ultrafiltration [40] and reverse osmosis [41,42] where it acts as pore forming agent and viscosity enhancer, PVP addition can be detrimental for the formation of a dense top layer, selective for gas separation. In this paper, we show a comparative study of optimization of spinning parameters for pure PBI and PBI/PVP blended fibers using two typical phase inversion solvents (N-Methyl-2-pyrrolidone (NMP) and dimethylacetamide (DMAc)). We identify the threshold PVP concentration below which the formation of the selective layer is not compromised. Thermal and mechanical properties of the hollow fiber membranes were studied, as well as mixed gas performance at typical temperature conditions of pre-combustion H_2/CO_2 separation.

5.2. Experimental

5.2.1. Materials

Fumion® AP poly(2,2'-(m-phenylene))5,5'-bisbenzimidazole (PBI, M_w = 48000 g mol^{-1}) was supplied by Fumatech BWT GmbH. Polyvinylpyrrolidone K30 (PVP), anhydrous N-methylpyrrolidone (NMP, 99.5% purity), anhydrous dimethylacetamide (DMAc, 99.5% purity) and lithium chloride (LiCl) were purchased from Sigma-Aldrich. Hexane and methanol were purchased from Fisher Scientific. Sylgard 184 (Dow Corning) was used for the defect healing process.

5.2.2. Spinning dope preparation and viscosity measurement

PBI, PVP and LiCl were dried in a vacuum oven at 100ºC for 16 h before dope preparation. PBI was dissolved by mechanical stirring at 80ºC overnight. PBI dopes were filtered through a 15 μm sintered metal fiber matrix from Bekaert before loading in the spinning system. For PBI/PVP dopes preparation, each polymer was firstly dissolved in the solvent (NMP or DMAc) and then mixed at room temperature in a glass flask. Viscosity measurements of polymer solution dopes were performed by a Thermo Haake Scientific RS6000 rheometer with 20 mm parallel plate geometry at 25ºC and 10 s^{-1} shear rate.

5.2.3. Preparation of PBI based hollow fiber membranes

The fabrication of PBI based hollow fiber membranes was based on a dry jet followed by wet quench spinning process [27,43–47]. The dope was loaded into the syringe pump and degassed applying vacuum for 24 h at room temperature before spinning. Polymer dope was filtered in-line with a 90 μm filter and spun from a spinneret with 460 μm inner diameter and 820 μm outer diameter. At the end, the fiber was collected on a drum. Fibers were kept in deionized water for several days after spinning to remove LiCl and residual solvent, refreshing the water every day, followed by a solvent exchange procedure (3 times in a methanol bath and 3 times in a hexane bath). After that, the fibers were dried in a vacuum oven at 100 ºC for 12 h.

5.2.4. Hollow fiber membrane characterization

The surface and cross-section morphology of the hollow fiber membranes were characterized by scanning electron microscopy (SEM) (Quanta 250 ESEM) equipped with energy dispersive X-ray spectroscopy (EDX). Cross-sections of the membranes were prepared by freeze-fracturing after immersion in liquid nitrogen and subsequently

coated with gold/palladium. The Everhart Thornley detector (ETD) were used for the analysis of the membranes.

Thermogravimetric analysis (TGA) of the hollow fiber membranes were conducted by a Setaram TG-DTA92 thermo balance in an N_2 atmosphere at a heating rate of 10 ºC min^{-1} between room temperature and 1200 ºC.

Differential scanning calorimetry (DSC) was performed on a TA-Q100 instrument. The samples were heated from 30 ºC to 400 ºC at a 10 ºC min^{-1} rate. Three cooling/heating runs were performed, the first one with the aim of remove the thermal history. The T_g data were collected from the second run.

Mechanical properties were tested on a Multitest 5-i Mecmesin apparatus. Samples with an effective length of 5 cm were tested using a 10 N load cell and at constant deformation rate of 50 mm/min. The Young modulus, yield stress, tensile stress at break and elongation at break were calculated from stress-strain curves. 8 Samples of each fiber sample were tested and the average value and standard deviation were reported.

Hollow fiber gas permeation properties were determined using an experimental set-up based on constant pressure technique [46]. Hollow fiber membrane modules were built by insertion of 2-20 fibers of ~18 cm active length within a tubular stainless-steel container using a method reported in literature [48]. When required, hollow fibers were dip-coated for defect healing using a 3 wt.% of polydimethylsiloxane (PDMS) in hexane before permeation testing. Mixed gas permeation experiments (H_2/CO_2 = 50/50 vol%) were carried 150 ºC and 3 bar feed pressure. Feed gas flow and pressure was set with Coriolis mass flow controllers and pressure controllers (Bronkhorst). Permeate gas flow was measured using a film flow meter (Horiba). The gas mixture was fed from the shell side of the fiber and permeate mixture was collected from the lumen side of the fibers in a counter current flow configuration. The stage cut (the ratio between permeate flow rate and feed flow rate) was kept below 1 % to avoid concentration polarization phenomena and ensure a constant gas composition at the feed side. An online gas chromatograph (Agilent 3000 micro GC) was used to analyze the permeate stream composition over time. Permeance was calculated once the steady state was reached in the permeate stream of the membrane.

The permeance for gas *i* was calculated by the following equation:

$$P_i = \frac{F_i}{\Delta p_i \cdot A}$$

where P_i is the gas permeance in gas permeation units (1 GPU = 10^{-6} cm^3 (STP) cm^{-2} s^{-1} $cmHg^{-1}$), F_i is the volumetric flow rate of component i (cm^3 (STP) s^{-1}), Δp_i is the partial pressure difference of component i across the membrane (cmHg) and A is the effective membrane area (cm^2).

The separation factor or mixed gas selectivity α was calculated as the ratio of the permeance of the more permeable compound i to the permeance of the less permeable compound j:

$$\alpha_{ij} = \frac{P_i}{P_j}$$

5.3. Results and discussions

5.3.1. Determination of critical polymer concentration

Optimization of polymer solution (dope) composition is a key to success for the formation of defect-free hollow fiber membranes. Regarding the polymer concentration, one requirement to produce hollow fibers with minimum defects is a high polymer concentration in order to create significant chain entanglement during skin formation [49]. The critical polymer concentration for gas separation hollow fiber spinning is extrapolated from the viscosity versus polymer concentration relationship. In a polymer solution, the viscosity increases slightly with polymer concentration, up to a point from where it begins to increase exponentially. This point is called the critical polymer concentration (c.p.c.) and the optimum polymer concentration in the dope is equal to or slightly above this point. Viscosity versus polymer concentration curves were constructed for the two most common solvents used in the phase inversion process: DMAc and NMP. Figure 5.1 shows that at similar polymer concentration dopes in NMP exhibit a much higher viscosity than dopes in DMAc. Therefore, a lower critical polymer concentration was identified for NMP than for DMAc (Table 5.1). LiCl is usually used in PBI solutions to facilitate the polymer dissolution and to stabilise the solution against gelation. The necessary LiCl concentration in order to prevent gelation was higher in NMP than when DMAc is used as solvent, LiCl/PBI ratio of 0.115 compared to 0.015, respectively. In NMP, there is a stronger interaction between PBI polymer chains than in DMAc.

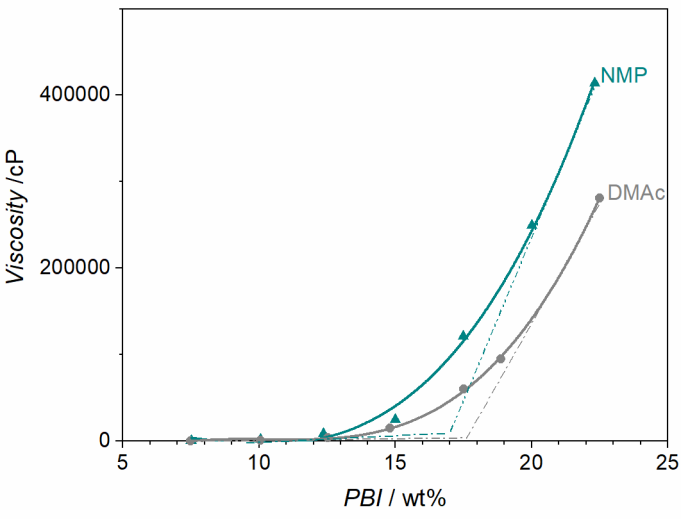

Figure 5.1. Viscosity versus PBI Fumion AP concentration for PBI/NMP and PBI/DMAc dope solutions at 25ºC and 10 s^{-1} rheometer shear rate.

Table 5.1. Critical polymer concentration and dope viscosity corresponding to c.p.c dopes for NMP and DMAc.

	Units	DMAc	NMP
Critical PBI concentration	(wt.%)	17.5	17
Dope viscosity at c.p.c	(cP)	60 000	100 000

5.3.2. PBI hollow fiber spinning from DMAc

First the PBI hollow fiber fabrication has been optimized using DMAc as solvent. Spinning dope composed of PBI, DMAc and LiCl were used for three different spinning sessions. Dopes with a PBI concentration of 18 wt.%, 18.5 wt.% and 19 wt.% were used and spinning parameters were varied in the range reported in Table 5.2. In all cases it was not possible to increase the take up rate beyond 5 m/min since the fiber broke at higher take up rate values, and hollow fibers with a relatively high diameter were obtained (> 700 μm). SEM images of the fiber cross sections are shown in Figure 5.2. A porous substructure with small pores in the middle of the cross section and finger-like macrovoids starting both from the outer and inner side of the fiber was obtained for all the dopes. The low selectivity presented by the as spun hollow fibers (α H_2/CO_2 < 8) denoted that defective fibers were obtained and a PDMS defect healing post-treatment was applied. Mixed gas H_2/CO_2 permeation performance at 150 ºC of

PDMS healed hollow fibers is presented in Table 5.3. The highest H_2/CO_2 selectivity was obtained for the dope solution containing 18.5 wt.% PBI. This fiber presents a H_2 permeance of 62 GPU and a H_2/CO_2 selectivity of 16.2, similar as the separation performance reported in our previous work [9] for PBI hollow fibers prepared from another polymer supplier (H_2 permeance of 66 GPU and a H_2/CO_2 selectivity of 17.2).

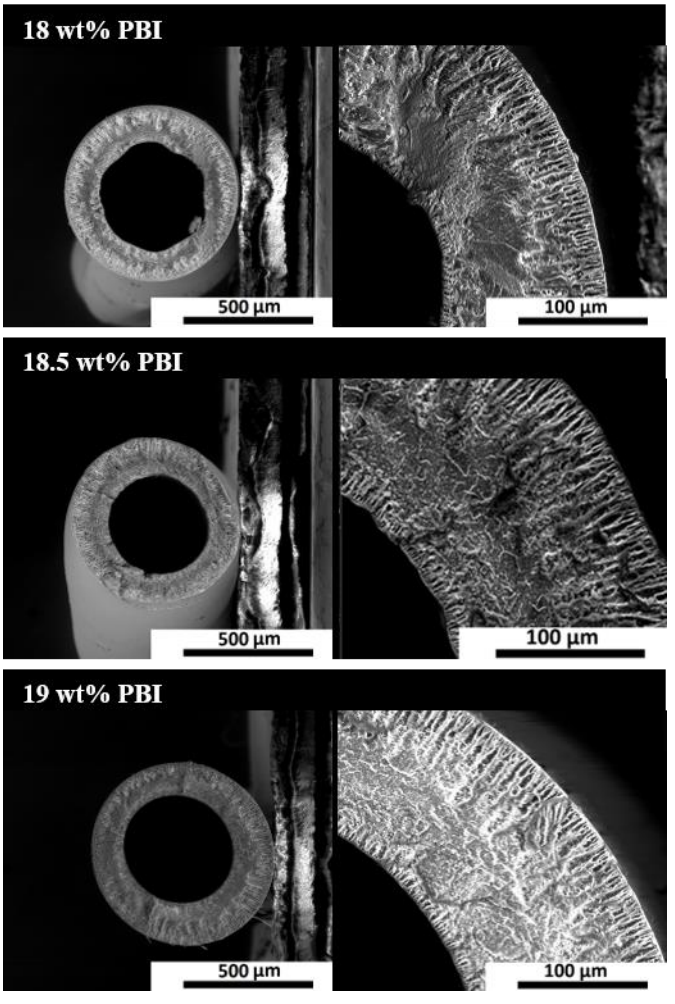

Figure 5.2. SEM images of the cross-section (overall fiber, fiber wall) of fiber spun from dope solution prepared in DMAc.

Table 5.2. Spinning parameters for PBI hollow fiber membrane fabrication prepared from dopes using DMAc as solvent.

Spinning parameter	Studied range
PBI concentration	18 - 18.5 – 19 wt.%
Bore composition	35 wt.% DMAc / 65 wt.% H_2O
Spinneret temperature	25-35ºC
Outer Dope flow rate	180 ml/h
Bore flow rate	60 ml/h
Air gap height	3.5-10 cm
Quench bath temperature	25 ºC
Take up rate	5 m/min

Table 5.3. Equimolar mixed gas H_2/CO_2 permeation performance at 150ºC and 3 bar feed pressure of PBI hollow fibers prepared from PBI/DMAc dopes. PDMS defect healed fibers. OD and ID correspond to the outer diameter and inner diameter of the fiber respectively.

Dope PBI concentration	H_2 permeance (GPU)	H_2/CO_2 selectivity	OD/ID (μm)
18 wt.%	139	8.36	745 / 440
18.5 wt.%	62	16.2	760 / 440
19 wt.%	65	12.0	720 / 425

5.3.3. PBI hollow fiber spinning from NMP

Some manufacturers prefer NMP as solvent instead of DMAc, therefore PBI hollow fiber fabrication has also been optimized using NMP as solvent.

5.3.3.1. PBI hollow fiber spinning without PVP

A spinning dope composed of PBI, NMP and LiCl was used in the first spinning session, with a PBI concentration slightly higher than c.p.c. determined from the viscosity versus polymer concentration curve, 18.5 wt.%. The spinning conditions were varied in order to find the optimal combination of spinning parameters. Studied spinning parameter range are presented in Table 5.4. During the optimization process it was not possible to increase the take up rate beyond 6 m/min since at higher take up rates the fiber broke. Although the take up rate is slightly higher than the maximum achieved for fibers spun from DMAc, it is still quite far from industrially relevant take up rate values. Solvent proportion of the bore fluid was increased compared to PBI spinning with DMAc in order to avoid the formation of macrovoids at the inner side of the fiber. Cross section SEM images in Figure 5.3a and b shows a sponge like substructure with the presence of some finger-like macrovoids starting from the outer part of the fiber. Macrovoids on the inner side of the fiber were eliminated by adjusting the bore fluid composition to 50 wt.% NMP/50 wt.%. These fibers present a H_2 permeance of 7.5 GPU and a H_2/CO_2 selectivity of 12.8 for mixed gas at 150ºC (Table 5.5). As spun fibers were already selective without PDMS coating, unlike PBI fibers spun from DMAc dopes. However, the selectivity is below the 16.2 value obtained for PBI fibers spun from DMAc, denoting the presence still of small defects in the selective layer. The low permeance was attributed to the relatively thick selective layer, ~2 μm based on SEM observation (Figure 5.3d), and the resistance to gas transport of the tight substructure (Figure 5.3c).

Table 5.4. Spinning parameters for PBI and PBI/PVP hollow fiber membrane fabrication prepared from dopes using NMP as solvent.

Spinning parameter	Studied range
Dope PBI/PVP (wt.%/wt.%)	18.5/0, 9.1/8, 11/7.1, 12/5, 14/2.5
Dope viscosity	116 000 – 177 000 cP
Bore composition	50 wt.% NMP / 50 wt.% H_2O
Spinneret temperature	25-50 ºC
Outer Dope flow rate	140-180 ml/h
Bore flow rate	50-100 ml/h
Air gap height	5-15 cm
Quench bath temperature	25 ºC
Take up rate	6-50 m/min

Table 5.5. Equimolar mixed gas H_2/CO_2 permeation performance at 150ºC and 3 bar feed pressure of PBI and PBI/PVP hollow fibers prepared from PBI/NMP dopes.

Dope PBI/PVP (wt.%/wt.%)	Fiber PBI/PVP** (wt.%/wt.%)	H_2 permeance (GPU)	H_2/CO_2 selectivity	OD/ID (μm)
18.5/0	100/-	7.5	12.8	540/340
9.1/8	53/47	41*	4.3*	175/115
11/7.1	61/39	28*	10.7*	195/110
12/5	70/30	56	16.6	275/165
14/2.5	85/15	64	14.2	270/175

* PDMS defect healed fibers

** Fiber PBI/PVP correspond to the theoretical solid content of the fiber, calculated based on polymer added into the spinning dope

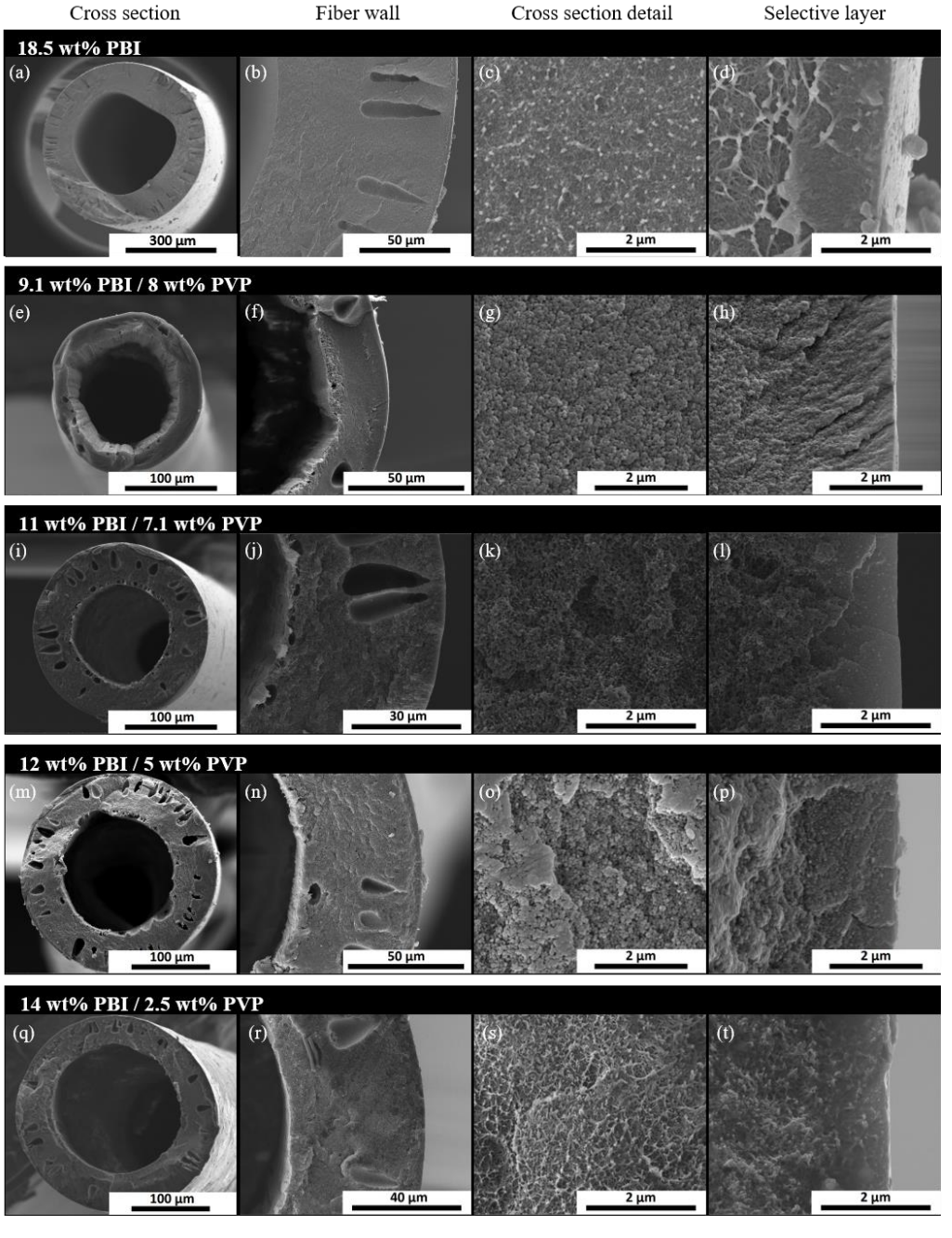

Figure 5.3. SEM images of the overall fiber cross-section, cross section detail, fiber wall, and the selective layer of fibers spun from dope solutions containing different PVP content.

5.3.3.2. PVP influence on PBI hollow fiber spinning

PVP is a polymer of low molecular weight commonly used as pore forming agent for water filtration hollow fiber preparation. The aim of incorporating this additive was to obtain a more open porous structure and consequently decrease gas transport resistance of the substructure. At the same time PVP increases the viscosity of the dope solution and the as-spun fiber elasticity. A PVP concentration of 8 wt.% was selected as starting point and the PBI concentration was reduced to 9.1 wt.% to keep the viscosity above the c.p.c. dope viscosity (100 000 cP, see Table 5.1). One of the major advantages of the addition of PVP was that it enabled increasing the take up rate. The as-spun fiber elasticity was increased by the addition of PVP and higher take up rates up to 50 m/min were reached. This increased the take up rate led to a significant reduction on fiber dimensions (<200 μm outer diameter). Moreover, as Figure 5.3e-g show macrovoids were almost eliminated by the increase of the take up rate. The as-spun hollow fibers presented a low selectivity and therefore a PDMS defect healing post-treatment was applied. Nevertheless, a selectivity value of 4.3 suggest that fibers were too defective, and the silicone rubber coating was not enough to heal the defects. The PBI content was increased and PVP content decreased for the next spinning session, to 11 wt.% and 7.1 wt.% respectively. This change in dope composition resulted in less defective fibers with a H_2 permeance of 28 GPU and H_2/CO_2 selectivity of 10.7 for PDMS coated fibers. In any case, this selectivity is still below the intrinsic selectivity of the material. The presence of defects was believed to be due to the low PBI content of the final fiber, the theoretical amount in the fiber was 53 wt.% PBI / 47 wt.% PVP (for dope containing 8 wt.% PBI / 9.1 wt.% PVP) and 61 wt.% PBI / 39 wt.% PVP (for dope containing 11 wt.% PBI / 7.1 wt.% PVP). Therefore, the PBI content was increased and PVP content decreased for the following two spinning dopes to 70/30 and 85/15 PBI/PVP. A spinning dope containing 12 wt.% PBI / 5 wt.% PVP and another one containing 14 wt.% PBI / 2.5 wt.% PVP were employed. Although in both cases a take up rate value of 50 m/min was feasible, the best performance was obtained with a take up rate of 25 m/min. Fibers with an outer diameter of ~270 μm and a cross section with a sponge like substructure with the presence of few finger-like macrovoids in the outer part of the fiber were obtained (Figure 5.3m-n and q-r). Figure 5.3p and t shows that thinner selective layers than for PBI membranes without PVP (Figure 5.3d) were obtained, resulting in higher permeance values. The fibers present a H_2 permeance of 56 GPU and a H_2/CO_2 selectivity of 16.6 for 12 wt.% PBI / 5 wt.% PVP spinning dope and a H_2 permeance of 64 GPU and H_2/CO_2 selectivity of 14.2 for 14 wt.% PBI / 2.5 wt.% PVP spinning dope (see Table 5.5). No PDMS coating was required for these fibers since they were

already selective. The selectivity value was similar to the one obtained for fibers spun using DMAc solvent and to the one reported in our previous work [9] for PBI hollow fibers prepared from other polymer supplier.

All the fibers prepared from PBI/PVP blends seems to be homogeneous by visual observation. In order to verify the proper miscibility on the molecular level, DSC analysis of the fibers was performed. The presence of a single T_g on a polymer blend is indicative of the formation of a homogeneous blend. All PBI/PVP blend fibers present a single T_g, situated between the T_g of individual components (421 and 163 ºC for PBI and PVP, respectively). Figure 5.4 shows the experimental T_g and theoretical T_g of the blend, calculated by the Fox equation [50]:

$$\frac{1}{T_{g,blend}} = \frac{W_{PBI}}{T_{g,PBI}} + \frac{W_{PVP}}{T_{g,PVP}}$$

where $T_{g,PBI}$ and $T_{g,PVP}$ are the glass transition temperature in K of the individual polymers and W_{PBI} and W_{PVP} the mass fraction of each component in the blend.

Experimental results for PBI/PVP blend fibers show a deviation from theoretical data, being more pronounced as PVP fraction on the blend increses. This is a common behaviour on majority of polymer blends since the Fox equation does not take into account any kind of interaction between polymers [50]. In our case, hydrogen bonds are formed between the N-H group of PBI and the C=O group of PVP, resulting in a higher experimental T_g of the blend than this theoretical prediction.

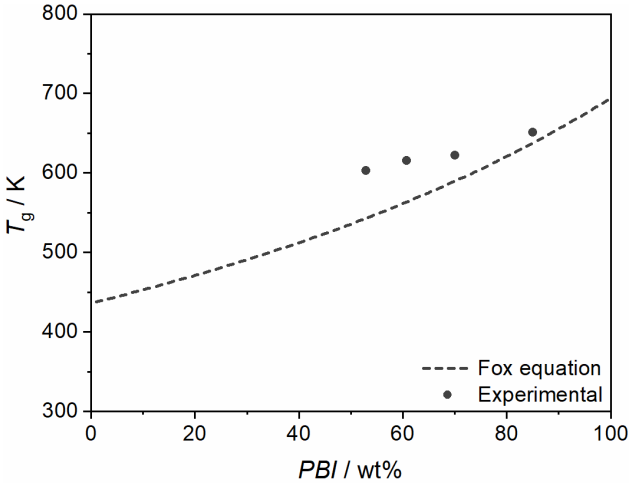

Figure 5.4. Experimental glass transition temperature (T_g) of PBI/PVP blend fibers as function of PBI mass fraction (close symbols) and theoretical values predicted by the Fox equation (dashed line)

The thermogravimetric (TG) profiles and corresponding derivative thermogravimetric (DTG) curves of the hollow fiber membranes are presented on Figure 5.5. TGA analysis of the pure PBI and PVP K30 polymer powders is also included. Table 5.6 summarizes data collected from TG/DTG curves used to evaluate the effect of PVP addition on the thermal stability of PBI hollow fiber membranes. The PVP K30 polymer powder shows a single stage degradation with an onset temperature of 342 ºC corresponding to the degradation of the polymer backbone through the release of the pyrrolidone side group [51]. No residue is remained from PVP decomposition reaction. On the other hand, the PBI polymer powder exhibits a two-stage degradation pattern with a first stage onset temperature of 575 ºC. The degradation of PBI in an inert atmosphere starts with the cleavage of the polymer backbone preferentially between adjacent aromatic rings as well as the imide ring, followed by further condensation reactions and cleavage of nitrogen from the structure as the temperature is increased [52]. A graphite-like residue remained at the end of the decomposition reaction. The degradation stage corresponding to the PVP and PBI polymers is distinguished in the TG/DTG curves of hollow fibers prepared from a blend of both polymers. Blend fibers showed a thermal stability up to ~340 °C with an initial weight loss at ~100 ºC due to water removal and then exhibit a three-step degradation pattern. The first stage that takes place at ~345 ºC corresponds to the degradation of PVP. A weight loss slightly lower than the theoretical wt.% PVP was observed for all samples, ~13 wt.%, 26 wt.%, 33 wt.% and 40 wt.% for 85/15, 70/30, 61/39 and 53/47 PBI/PVP blend fibers, respectively. The second (~575 ºC) and third stage correspond to the degradation of PBI. Because of blending of PBI with PVP the thermal stability of the fibers was reduced in respect to pure PBI. Nevertheless, blend fibers are thermally stable up to ~340 °C and therefore are stable at typical temperature conditions of pre-combustion H_2/CO_2 separation (150–250 °C).

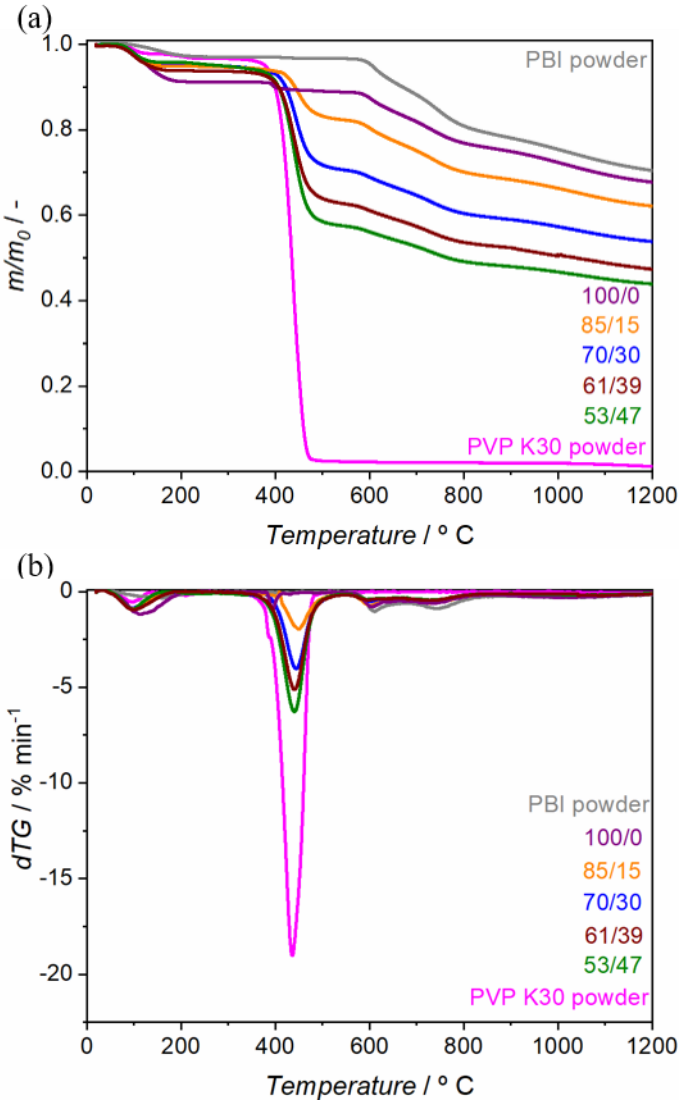

Figure 5.5. (a) TG and (b) DTG curves of pure components and 100/0, 85/15, 70/30, 61/39 and 53/47 PBI/PVP blend (wt.%/wt.%) fibers.

Table 5.6. Onset temperatures of thermal degradation curves of pure PBI and 85/15, 61/39, 70/30 and 53/47 PBI/PVP blend fibers.

Sample	Fiber PBI/PVP (wt.%/wt.%)	PVP T_{onset} (ºC)	PBI T_{onset} (ºC)
PVP K30 powder	0/100	342	-
9.1 wt.% PBI / 8 wt.% PVP	53/47	342	580
11 wt.% PBI / 7.1 wt.% PVP	61/39	345	577
12 wt.% PBI / 5 wt.% PVP	70/30	351	575
14 wt.% PBI / 2 .5 wt.% PVP	85/15	350	573
18.5 wt.% PBI	100/0	-	580
PBI Fumion AP powder	100/0	-	575

Mechanical properties and stress-strain curves of PBI and PBI/PVP blend fibers are presented in Table 5.7 and Figure 5.6, showing the influence of PVP addition on the mechanical properties of the hollow fibers. The Young modulus measures the stiffness of a material. PBI is well known for having excellent mechanical properties. Pure PBI fiber shows a Young modulus of 1.72 GPa, which is in accordance with the value reported in literature for PBI hollow fiber membranes [3]. This value is at least twice the Young moduli presented by gas separation hollow fiber membranes made with other polymers such as cellulose acetate (CA), polyimide (PI), polyetherimide (PEI) or polyether sulfone (PES) [53–55]. The Young moduli of the hollow fibers exhibits a linear decrease with increasing PVP content, and therefore a loss of hollow fiber stiffness. Nevertheless, the stiffness of blend PBI/PVP hollow fibers is still above those presented by the conventional polymers used for gas separation. Hollow fibers show more plastic deformation as PVP content increases, as shown by the increase of elongation at break. The feasibility to increase the take up rate for PBI/PVP blend fibers was attributed to the increase in the elasticity of the fibers by the incorporation of PVP.

Table 5.7. Mechanical properties of pure PBI and PBI/PVP blend fibers.

Dope PBI/PVP (wt.%/wt.%)	Fiber PBI/PVP (wt.%/wt.%)	Young modulus (GPa)	Yield stress (MPa)	Tensile stress at break (MPa)	Elongation at break (%)
9.1/8	53/47	0.94 ± 0.08	24.8 ± 0.7	31.3 ± 1.0	27.4 ± 5.4
11/7.1	61/39	1.01 ± 0.08	28.4 ± 1.4	34.6 ± 0.9	23.2 ± 2.5
12/5	70/30	1.15 ± 0.03	30.3 ± 1.4	34.9 ± 1.2	25.1 ± 2.3
14/2.5	85/15	1.39 ± 0.15	35.7 ± 2.9	38.4 ± 2.2	10.6 ± 2.7
18.5/0	100/0	1.72 ± 0.12	57.1 ± 1.9	61.8 ±1.5	9.7 ± 3.1

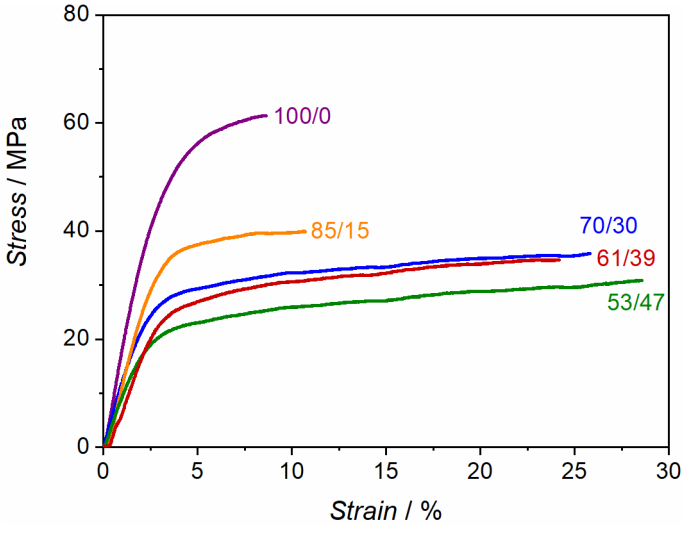

Figure 5.6. Stress-strain curves of pure PBI and PBI/PVP blend fibers.

The work discussed here demonstrated the advantage of blending PVP with PBI for the scalability of PBI based membranes for pre-combustion CO_2 capture. In contrast with other studies on PBI blend hollow fibers, where issues regarding H_2/CO_2 separation performance are addressed (discussed in the introduction); blending in the present study is focused on manufacturing scalability. It was observed that, due to PVPs pore forming properties, a too high PVP content (i.e. 47 and 39 wt.%) leads to defective fibers and therefore PVP content needs to be decreased to obtain defect free fibers. Defect-free fibers were prepared at PVP concentrations below 30 wt.%. Figure 5.7 shows Robeson plot [56] for the separation of H_2 from CO_2 for PBI based hollow fiber membranes. The upper bound in GPU was calculated using the Roberson upper

bound in Barrer and assuming a selective layer thickness of 0.5 micrometer. Compared to PBI based hollow fibers reported in literature, PBI/PVP blend fibers present a H_2/CO_2 separation performance similar as bare PBI membranes tested at similar temperature (*i.e.* 150 ºC). Direct comparison with PBI blends reported in literature is not possible, since separation experiments in literature were performed at lower temperature. The main advantage of PVP addition was the possibility to increase the as spun fiber elasticity, reaching industrially relevant take up rate values and significantly reducing fibers outer diameter (< 300 μm). The outer diameter of PBI/PVP blend fibers obtained in this work is the smallest reported in literature for PBI based hollow fiber membranes [3,8,9,11,14,18,38], significantly smaller than the 370 μm outer diameter reported in literature for the best case (see table 5.8).

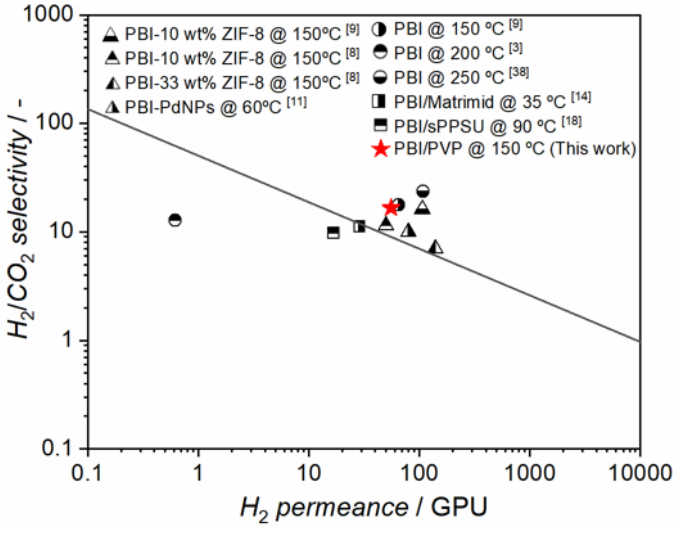

Figure 5.7. Robeson plot for the separation of H_2 from CO_2. The graph contains the most relevant results reported in literature for PBI based hollow fiber membranes: bare PBI (*circles*), PBI blends (*squares*) and PBI mixed matric membranes (*triangles*). Separation performance of PBI/PVP blend fibers prepared in this work is represented by a *red star*.

Table 5.8. Transport properties results reported in literature for PBI based hollow fiber membranes (bare PBI, PBI blends and PBI mixed matrix membranes). Take up rate used during the spinning process and outer diameter of the fibers is included.

Selective layer material	Take-up rate (m/min)	Fiber diameter (μm)	H_2 permeance (GPU)	H_2/CO_2 selectivity (-)	Testing conditions	Ref.
PBI	20	370	65	17.6	150 ºC, 7 bar, SG	[9]
PBI	unsp	600	0.62	12.8	200 ºC, 5-8 bar, SG	[3]
PBI	2.5	430	108	23.7	250 ºC, unsp, SG	[38]
PBI/Matrimid®	Free fall	450	29	11.1	35 ºC, 3.5 bar, SG	[14]
PBI/sPPSU	Free fall	800	16.7	9.7	90 ºC, 14 bar, MG	[18]
PBI/PVP	25	275	56	16.6	150 ºC, 3 bar, MG	This work
PBI-10 wt% ZIF-8	14	450	107	16.1	150 ºC, 7 bar, SG	[9]
PBI-10 wt% ZIF-8	16	600	50	11.5	150 ºC, 7 bar, MG	[8]
PBI-33 wt% ZIF-8	16	600	140	7		
PBI/PdNPs	unsp	540	80	10	60 ºC, 1 bar, SG	[11]

SG: single gas test. MG: mixed gas test (50/50 H_2/CO_2). Unsp: unspecified

1 GPU = 10^{-6} $(cm^3(STP))/(cm^2 \cdot s \cdot cmHg)$

5.4. Conclusions

Mechanically robust and small diameter (< 300 μm) PBI/PVP blend asymmetric hollow fiber membranes have been successfully prepared. The as spun fibers were defect free and therefore defect healing post treatment of the fibers was not required. Developed fibers show a H_2 permeance of 56 GPU and a H_2/CO_2 mixed gas selectivity of 16.6 at 150 ºC. At a PVP concentration lower than 30 wt% the use of PVP as additive was beneficiary to fiber formation since it allowed to: (1) obtain a more open porous substructure and (2) increase as spun fiber elasticity and therefore reach industrially relevant take up rate values (take up rate as high as 50 m/min). The existence of a single T_g on blend fibers demonstrated the proper miscibility of PBI and PVP at the molecular level and the formation a homogeneous blend. Blend fibers are thermally stable up to ~340 °C and therefore can be used at typical temperature conditions of pre-combustion H_2/CO_2 separation.

References

[1] P. Bernardo, E. Drioli, G. Golemme, Membrane Gas Separation: A Review/State of the Art, Ind. Eng. Chem. Res. 48 (2009) 4638–4663. doi:10.1021/ie8019032.

[2] R.P. Singh, G.J. Dahe, K.W. Dudeck, C.F. Welch, K.A. Berchtold, High Temperature Polybenzimidazole Hollow Fiber Membranes for Hydrogen Separation and Carbon Dioxide Capture from Synthesis Gas, Energy Procedia. 63 (2014) 153–159. doi:10.1016/j.egypro.2014.11.015.

[3] S.C. Kumbharkar, Y. Liu, K. Li, High performance polybenzimidazole based asymmetric hollow fibre membranes for H2/CO2 separation, J. Memb. Sci. 375 (2011) 231–240. doi:10.1016/j.memsci.2011.03.049.

[4] D.R. Pesiri, B. Jorgensen, R.C. Dye, Thermal optimization of polybenzimidazole meniscus membranes for the separation of hydrogen, methane, and carbon dioxide, J. Memb. Sci. 218 (2003) 11–18. doi:10.1016/S0376-7388(03)00129-7.

[5] J. Sánchez-Laínez, B. Zornoza, C. Téllez, J. Coronas, Asymmetric polybenzimidazole membranes with thin selective skin layer containing ZIF-8 for H2/CO2 separation at pre-combustion capture conditions, J. Memb. Sci. 563 (2018) 427–434. doi:10.1016/j.memsci.2018.06.009.

[6] T.-S. Chung, A Critical Review of Polybenzimidazoles, J. Macromol. Sci. Part C. 37 (1997) 277–301. doi:10.1080/15321799708018367.

[7] T. Yang, T.-S. Chung, High performance ZIF-8/PBI nano-composite membranes for high temperature hydrogen separation consisting of carbon monoxide and water vapor, Int. J. Hydrogen Energy. 38 (2013) 229–239. doi:https://doi.org/10.1016/j.ijhydene.2012.10.045.

[8] T. Yang, G.M. Shi, T.-S. Chung, Symmetric and Asymmetric Zeolitic Imidazolate Frameworks (ZIFs)/Polybenzimidazole (PBI) Nanocomposite Membranes for Hydrogen Purification at High Temperatures, Adv. Energy Mater. 2 (2012) 1358–1367. doi:10.1002/aenm.201200200.

[9] M. Etxeberria-Benavides, T. Johnson, S. Cao, B. Zornoza, J. Coronas, J. Sanchez-Lainez, A. Sabetghadam, X. Liu, E. Andres-Garcia, F. Kapteijn, J. Gascon, O. David, PBI mixed matrix hollow fiber membrane: Influence of ZIF-8 filler over H2/CO2 separation performance at high temperature and pressure, Sep. Purif. Technol. 237 (2019) 116347. doi:10.1016/j.seppur.2019.116347.

[10] J. Sánchez-laínez, B. Zornoza, S. Friebe, J. Caro, S. Cao, A. Sabetghadam, B. Seoane, J. Gascon, F. Kapteijn, C. Le, G. Clet, M. Daturi, C. Téllez, J. Coronas, Influence of ZIF-8 particle size in the performance of polybenzimidazole

mixed matrix membranes for pre-combustion CO 2 capture and its validation through interlaboratory test, J. Memb. Sci. 515 (2016) 45–53. doi:10.1016/j.memsci.2016.05.039.

[11] L.F. Villalobos, R. Hilke, F.H. Akhtar, K.-V. Peinemann, Fabrication of Polybenzimidazole/Palladium Nanoparticles Hollow Fiber Membranes for Hydrogen Purification, Adv. Energy Mater. 8 (2018) 1701567. doi:10.1002/aenm.201701567.

[12] J. Sanchez-Lainez, B. Zornoza, C. Tellez, J. Coronas, On the chemical filler-polymer interaction of nano- and micro-sized ZIF-11 in PBI mixed matrix membranes and their application for H2/CO2 separation, J. Mater. Chem. A. 4 (2016) 14334–14341. doi:10.1039/C6TA06438H.

[13] T.-S. Chung, Z.-L. Xu, Asymmetric hollow fiber membranes prepared from miscible polybenzimidazole and polyetherimide blends, J. Memb. Sci. 147 (1998) 35–47. doi:https://doi.org/10.1016/S0376-7388(98)00115-X.

[14] S.S. Hosseini, N. Peng, T.S. Chung, Gas separation membranes developed through integration of polymer blending and dual-layer hollow fiber spinning process for hydrogen and natural gas enrichments, J. Memb. Sci. 349 (2010) 156–166. doi:10.1016/j.memsci.2009.11.043.

[15] J. Sánchez-Laínez, B. Zornoza, M. Carta, R. Malpass-Evans, N.B. McKeown, C. Téllez, J. Coronas, Hydrogen Separation at High Temperature with Dense and Asymmetric Membranes Based on PIM-EA(H2)-TB/PBI Blends, Ind. Eng. Chem. Res. 57 (2018) 16909–16916. doi:10.1021/acs.iecr.8b04209.

[16] J.D. Moon, A.T. Bridge, C. D'Ambra, B.D. Freeman, D.R. Paul, Gas separation properties of polybenzimidazole/thermally-rearranged polymer blends, J. Memb. Sci. 582 (2019) 182–193. doi:https://doi.org/10.1016/j.memsci.2019.03.067.

[17] A. Naderi, A. Asadi Tashvigh, T.-S. Chung, M. Weber, C. Maletzko, Molecular design of double crosslinked sulfonated polyphenylsulfone /polybenzimidazole blend membranes for an efficient hydrogen purification, J. Memb. Sci. 563 (2018) 726–733. doi:https://doi.org/10.1016/j.memsci.2018.06.033.

[18] A. Naderi, T.-S. Chung, M. Weber, C. Maletzko, High performance dual-layer hollow fiber membrane of sulfonated polyphenylsulfone/Polybenzimidazole for hydrogen purification, J. Memb. Sci. 591 (2019) 117292. doi:https://doi.org/10.1016/j.memsci.2019.117292.

[19] L. Zhu, M.T. Swihart, H. Lin, Tightening polybenzimidazole (PBI) nanostructure via chemical cross-linking for membrane H2/CO2 separation, J. Mater. Chem. A. 5 (2017) 19914–19923. doi:10.1039/C7TA03874G.

[20] L. Zhu, M.T. Swihart, H. Lin, Unprecedented size-sieving ability in polybenzimidazole doped with polyprotic acids for membrane H2/CO2

separation, Energy Environ. Sci. 11 (2018) 94–100. doi:10.1039/C7EE02865B.

[21] A. Naderi, A. Asadi Tashvigh, T.-S. Chung, H2/CO2 separation enhancement via chemical modification of polybenzimidazole nanostructure, J. Memb. Sci. 572 (2019) 343–349. doi:https://doi.org/10.1016/j.memsci.2018.11.020.

[22] S.S. Hosseini, M.M. Teoh, T.S. Chung, Hydrogen separation and purification in membranes of miscible polymer blends with interpenetration networks, Polymer (Guildf). 49 (2008) 1594–1603. doi:https://doi.org/10.1016/j.polymer.2008.01.052.

[23] J.M. Pérez-Francisco, J.L. Santiago-García, M.I. Loría-Bastarrachea, M. Aguilar-Vega, Evaluation of Gas Transport Properties of Highly Rigid Aromatic PI DPPD-IMM/PBI Blends, Ind. Eng. Chem. Res. 56 (2017) 9355–9366. doi:10.1021/acs.iecr.7b02074.

[24] S.S. Hosseini, T.S. Chung, Carbon membranes from blends of PBI and polyimides for N2/CH4 and CO2/CH4 separation and hydrogen purification, J. Memb. Sci. 328 (2009) 174–185. doi:https://doi.org/10.1016/j.memsci.2008.12.005.

[25] M.F.A. Wahab, A.F. Ismail, S.J. Shilton, Studies on gas permeation performance of asymmetric polysulfone hollow fiber mixed matrix membranes using nanosized fumed silica as fillers, Sep. Purif. Technol. 86 (2012) 41–48. doi:10.1016/j.seppur.2011.10.018.

[26] S. Husain, W.J. Koros, Mixed matrix hollow fiber membranes made with modified HSSZ-13 zeolite in polyetherimide polymer matrix for gas separation, J. Memb. Sci. 288 (2007) 195–207. doi:10.1016/j.memsci.2006.11.016.

[27] N. Peng, N. Widjojo, P. Sukitpaneenit, M.M. Teoh, G.G. Lipscomb, T.-S. Chung, J.-Y. Lai, Evolution of polymeric hollow fibers as sustainable technologies: Past, present, and future, Prog. Polym. Sci. 37 (2012) 1401–1424. doi:10.1016/j.progpolymsci.2012.01.001.

[28] K.Y. Wang, D.F. Li, T.S. Chung, S.B. Chen, The observation of elongation dependent macrovoid evolution in single-and dual-layer asymmetric hollow fiber membranes, Chem. Eng. Sci. 59 (2004) 4657–4660. doi:10.1016/j.ces.2004.06.035.

[29] N. Peng, T.S. Chung, The effects of spinneret dimension and hollow fiber dimension on gas separation performance of ultra-thin defect-free Torlon ® hollow fiber membranes, J. Memb. Sci. 310 (2008) 455–465. doi:10.1016/j.memsci.2007.11.018.

[30] M.R. Kosuri, W.J. Koros, Defect-free asymmetric hollow fiber membranes from Torlon®, a polyamide–imide polymer, for high-pressure CO2 separations, J. Memb. Sci. 320 (2008) 65–72. doi:10.1016/j.memsci.2008.03.062.

[31] D.T. Clausi, W.J. Koros, Formation of defect-free polyimide hollow fiber membranes for gas separations, J. Memb. Sci. 167 (2000) 79–89. doi:10.1016/S0376-7388(99)00276-8.

[32] G.L.R.W.J.K. Seth B. Carruthers, Morphology of integral-skin layers in hollow-fiber gas-separation membranes, J. Appl. Polym. Sci. 90 (2003) 399–411. doi:Doi 10.1002/App.12623.

[33] R.P. Lively, M.E. Dose, L. Xu, J.T. Vaughn, J.R. Johnson, J.A. Thompson, K. Zhang, M.E. Lydon, J.-S. Lee, L. Liu, Z. Hu, O. Karvan, M.J. Realff, W.J. Koros, A high-flux polyimide hollow fiber membrane to minimize footprint and energy penalty for CO2 recovery from flue gas, J. Memb. Sci. 423–424 (2012) 302–313. doi:10.1016/j.memsci.2012.08.026.

[34] C.C. Chen, W. Qiu, S.J. Miller, W.J. Koros, Plasticization-resistant hollow fiber membranes for CO2/CH4 separation based on a thermally crosslinkable polyimide, J. Memb. Sci. 382 (2011) 212–221. doi:10.1016/j.memsci.2011.08.015.

[35] C. Ma, W.J. Koros, High-performance ester-crosslinked hollow fiber membranes for natural gas separations, J. Memb. Sci. 428 (2013) 251–259. doi:10.1016/j.memsci.2012.10.024.

[36] O.M. Ekiner, G. Vassilatos, Polyaramide hollow fibers for H2/CH4 separation: II. Spinning and properties, J. Memb. Sci. 186 (2001) 71–84. doi:http://dx.doi.org/10.1016/S0376-7388(00)00665-7.

[37] X. Li, R.P. Singh, K.W. Dudeck, K.A. Berchtold, B.C. Benicewicz, Influence of polybenzimidazole main chain structure on H2/CO2 separation at elevated temperatures, J. Memb. Sci. 461 (2014) 59–68. doi:10.1016/j.memsci.2014.03.008.

[38] G.J. Berchtold Kathryn A,; Dudeck Kevin W,; Singh Rajinder P,; Dahe Ganpat J,; Berchtold, Kathryn A,; Dudeck, Kevin W,; Singh, Rajinder P,; Dahe, Polybenzimidazole hollow fiber membranes and method for making an asymmetric hollow fiber membrane, US2016375410 (A1), 2016.

[39] Indira Jayaweera; Gopala N. Krishnan; Angel Sanjurjo; Palitha Jayaweera; Srinivas Bhamidi, Process for fabricating PBI hollow fiber asymmetric membranes for gas separation and liquid separation, 14/190,100, 2014.

[40] M.C. Nayak, A.M. Isloor, A. Moslehyani, N. Ismail, A.F. Ismail, Fabrication of novel PPSU/ZSM-5 ultrafiltration hollow fiber membranes for separation of proteins and hazardous reactive dyes, J. Taiwan Inst. Chem. Eng. 82 (2018) 342–350. doi:https://doi.org/10.1016/j.jtice.2017.11.019.

[41] X. Wang, P. Jayaweera, A.R. Alrasheed, A.S. Aljlil, M.Y. Alyousef, M. Alsubaei, H. AlRomaih, I. Jayaweera, Preparation of Polybenzimidazole Hollow-Fiber

Membranes for Reverse Osmosis and Nanofiltration by Changing the Spinning Air Gap, Membranes (Basel). 8 (2018). doi:10.3390/membranes8040113.

[42] T. Wang, C. Zhao, P. Li, Y. Li, J. Wang, Effect of non-solvent additives on the morphology and separation performance of poly(m-phenylene isophthalamide) (PMIA) hollow fiber nanofiltration membrane, Desalination. 365 (2015) 293–307. doi:https://doi.org/10.1016/j.desal.2015.03.016.

[43] Y. Li, T. Chung, Z. Huang, S. Kulprathipanja, Dual-layer polyethersulfone (PES)/BTDA-TDI/MDI co-polyimide (P84) hollow fiber membranes with a submicron PES–zeolite beta mixed matrix dense-selective layer for gas separation, J. Memb. Sci. 277 (2006) 28–37. doi:10.1016/j.memsci.2005.10.008.

[44] N. Widjojo, T.-S. Chung, S. Kulprathipanja, The fabrication of hollow fiber membranes with double-layer mixed-matrix materials for gas separation, J. Memb. Sci. 325 (2008) 326–335. doi:10.1016/j.memsci.2008.07.046.

[45] O. David, Y. Gendel, M. Wessling, Tubular macro-porous titanium membranes, J. Memb. Sci. 461 (2014) 139–145. doi:10.1016/j.memsci.2014.03.010.

[46] O.C. David, D. Gorri, K. Nijmeijer, I. Ortiz, A. Urtiaga, Hydrogen separation from multicomponent gas mixtures containing CO, N2 and CO2 using Matrimid® asymmetric hollow fiber membranes, J. Memb. Sci. 419–420 (2012) 49–56. doi:10.1016/j.memsci.2012.06.038.

[47] V.P. Babu, B.E. Kraftschik, W.J. Koros, Crosslinkable TEGMC asymmetric hollow fiber membranes for aggressive sour gas separations, J. Memb. Sci. 558 (2018) 94–105. doi:10.1016/j.memsci.2018.04.028.

[48] D.Q. Vu, W.J. Koros, S.J. Miller, High Pressure CO2/CH4 Separation Using Carbon Molecular Sieve Hollow Fiber Membranes, Ind. Eng. Chem. Res. 41 (2002) 367–380. doi:10.1021/ie010119w.

[49] M. Etxeberria-Benavides, O. Karvan, F. Kapteijn, J. Gascon, O. David, Fabrication of Defect-Free P84® Polyimide Hollow Fiber for Gas Separation: Pathway to Formation of Optimized Structure, Membranes (Basel). 10 (2019) 4. doi:10.3390/membranes10010004.

[50] A.K. Kulshreshtha, C. Vasile, Handbook of Polymer Blends and Composites, Volume 3, Rapra Technology Limited, Shawbury, 2003.

[51] C. Peniche, D. Zaldívar, M. Pazos, S. Páz, A. Bulay, J.S. Román, Study of the thermal degradation of poly(N-vinyl-2-pyrrolidone) by thermogravimetry–FTIR, J. Appl. Polym. Sci. 50 (1993) 485–493. doi:10.1002/app.1993.070500312.

[52] D.A. Chatfield, I.N. Einhorn, Stepwise thermal degradation of a polybenzimidazole foam, J. Polym. Sci. Polym. Chem. Ed. 19 (1981) 601–618.

doi:10.1002/pol.1981.170190301.

[53] L. Sheng, J. Ren, K. Hua, H. Li, Y. Feng, M. Deng, The enhancement of mechanical properties of P84 hollow fiber membranes by thermally annealing below and above Tg, J. Memb. Sci. 595 (2020) 117580. doi:10.1016/j.memsci.2019.117580.

[54] Xiao Yuan Chen, S. Kaliaguine, D. Rodrigue, A Comparison between Several Commercial Polymer Hollow Fiber Membranes for Gas Separation, J. Membr. Sep. Technol. 6 (2017) 1–15. doi:http://dx.doi.org/10.6000/1929-6037.2017.06.01.1.

[55] A. Tawari, B. Brika, S. Bradshaw, E. Jacobs, Development of a cellulose acetate hollow-fine-fibre membrane, Acta Chem. Malaysia. 2 (2018) 29–44. doi:http://doi.org/10.26480/acmy.02.2018.29.44.

[56] L.M. Robeson, The upper bound revisited, J. Memb. Sci. 320 (2008) 390–400. doi:10.1016/j.memsci.2008.04.030.

Chapter 6

Summary and outlook

Summary and Outlook

Membrane based gas separation has gained a great deal of industrial interest mainly due to its energy efficiency, relatively small physical footprint, low mechanical complexity and continuous operation. Due to their easy processing and mechanical strength, mainly polymeric membranes have been implemented for gas separation at a large scale in industry. However, polymeric membranes suffer from a trade-off between permeability and selectivity. Mixed matrix membranes (MMMs) have been identified to go beyond the upper-bound trade-off limit of polymeric membranes, with metal organic frameworks (MOFs) as one of the most promising filler materials for MMMs preparation. In addition, among different membrane configurations, hollow fiber membranes are the most desired ones due to high packing density, *i.e.* membrane area per module volume. The development of membranes with higher selectivity and sufficient permeance and membranes with zero defects have been identified as two main challenges to be addressed for gas and vapour separation membranes [1].

In part I of the thesis (Chapter 2 and 3), mixed matrix membranes based on MOFs for post-combustion and pre-combustion CO_2 separation are developed. Part II (Chapter 4 and 5) is focused on the scalability of two different polymers with particular attention on the preparation of defect free asymmetric hollow fibers.

Chapter 2 describes the preparation and testing of dense MMMs. The intrinsic gas separation properties of the 6FDA-DAM/ZIF-94 polymer-filler pair have been determined. Prior to membrane preparation, ZIF-94 metal organic framework crystals were synthetized in a scalable process. MOF particles smaller than 500 nm were obtained using a nonhazardous solvent (tetrahydrofuran and methanol) instead of dimethylformamide. Dense MMMs have been successfully prepared up to 40 wt% filler loading, showing a very good dispersion and interaction of the filler in the polymer layer. For the first time membranes were characterized by non-invasive infrared scattering type scanning near field optical microscopy (IR s-SNOM), which provides nanoscale-resolved chemical information that complements standard analysis methods. The CO_2 membrane permeability was increased by the addition of the ZIF-94 particles, maintaining a constant CO_2/N_2 selectivity of ~22. The largest increase in CO_2 permeability (~200%) was observed for 40 wt% ZIF-94 loading. 6FDA-DAM polyimide and ZIF-94 filler present the potential to be spun into a hollow fiber membrane configuration, reaching the region of optimal membrane properties for the separation of CO_2 from flue gas identified by Merkel *et al.* [2].

In Chapter 3 a step forward in the membrane development process was taken by the development of mixed matrix hollow fiber membranes for pre-combustion CO_2 capture. Nanosized ZIF-8 filler particles (~60 nm) were synthesized and incorporated into PBI. Asymmetric mixed matrix membranes were prepared with a thin selective layer where ZIF-8 particles were uniformly distributed. Single and mixed gas experiments were performed at 150 ºC over a wide pressure range (3-30 bar). Compared with neat PBI hollow fibers, filler incorporation into the polymer matrix leads to a strong increase in H_2 permeance from 65 GPU to 107 GPU at 150 ºC and 7 bar, while the ideal H_2/CO_2 selectivity remained constant at 18. ZIF-8 incorporation into the PBI polymer matrix strongly influences gas transport in mixed gas permeation. The improvement of fiber performance for H_2/CO_2 separation with filler addition is compromised at high operating feed pressures due to the competition between H_2 and CO_2 transport inside ZIF-8 structure due to the CO_2 adsorption properties. Our results reveal the material performance under conditions relevant to the application and demonstrate the importance of such an evaluation.

Part II focuses on the fabrication of defect-free asymmetric hollow fiber membranes by phase inversion. P84® co-polyimide asymmetric hollow fiber membranes with a highly thin (~56 nm) defect-free skin were successfully fabricated as described in Chapter 4. First, an extensive experimental and theoretical study of the influence of volatile tetrahydrofuran (THF) addition on the solubility parameter of the N-methylpyrrolidone/THF solvent mixture was performed. We demonstrated that although THF itself is not a solvent for P84®, in a mixture with a good solvent for the polymer, like NMP, it can be dissolved at high THF concentrations. Later, defect-free as-spun P84® hollow fiber membranes fibers were obtained by fine tuning of the dope composition and spinning parameters. The as-spun fibers showed a reproducible ideal CO_2/N_2 selectivity of 40, and a CO_2 permeance of 23 GPU at 35 °C. These fibers do not need the usual PDMS coating for defect healing, which results in the elimination of the additional defect healing post-treatment step in asymmetric hollow fiber manufacturing. Furthermore, the spinning process was reproducible at large scale (up to ~5000 m fibers).

In Chapter 5, the development of defect free PBI/PVP blend asymmetric hollow fiber membranes for H_2/CO_2 separation in pre-combustion CO_2 capture processes is shown. PVP was used as additive to improve the scalability in the production of PBI hollow fiber membranes. The addition of PVP significantly increased as-spun fiber elasticity and therefore increased the take up rate during the spinning process, resulting in a significant reduction on fiber dimensions (outer fiber diameter < 300 μm). The existence of a single glass transition temperature T_g of blend fibers demonstrated the

proper miscibility of PBI and PVP at the molecular level and the formation of a homogeneous blend. The PBI membrane separation performance is preserved by the addition of PVP. Developed PBI/PVP blend fibers shows a H_2 permeance of 56 GPU and a H_2/CO_2 mixed gas selectivity of 16.6 at 150 ºC and thermal stability up to ~340 °C. Therefore, this membrane can be used at typical temperature levels of pre-combustion H_2/CO_2 separation.

The overall conclusion of the first part of this work is that MOF addition should also contribute to selectivity enhancement, not only to permeability improvement. For post-combustion, selection of MOFs based on CO_2 sorption capacity is a good approach because CO_2 should preferentially permeate through the MOF structure [3,4]. Nevertheless, is not enough to ensure an increase in selectivity because the higher sorption capacity in many cases also implies the reduction in diffusivity in MOF channels. A wise selection of the filler must take into consideration both sorption and diffusion. For H_2/CO_2 separation in pre-combustion CO_2 capture, CO_2 remains in the retentate. Therefore, in this case MOF selection should be based on size exclusion, and porous fillers with lower interaction with CO_2 are preferred.

On the second part of this thesis, the guidelines for creating defect free as-spun hollow fibers have been revealed for spinnable polymers for pre- and post-combustion applications. The next step would be to transfer this knowledge to mixed matrix hollow fiber using selective fillers. In the case of mixed matrix hollow fibers, the addition of filler particles is usually accompanied by the creation of small defects in the thin selective skin layer possibly due to residual filler agglomerates found in the filler/polymer dope solutions. In order to avoid this, is highly important to prepare nano-scale homogeneously distributed filler/polymer dope solutions and a nanosize filler with good interaction with the polymer, possibly provided by side groups, is required.

CO_2 capture has been the target application of this thesis. Nevertheless, membrane materials developed in this study could be also applied for gas separation applications where CO_2 or H_2 selective membranes are required, such as natural gas treatment and biogas upgrading or hydrogen recovery, respectively. In addition, olefin-paraffin separation is one of the most important processes in the petrochemical industry. Membrane separation is a much less energy intensive alternative to distillation and therefore has been extensively studied. Nevertheless, due to similar molecular size between olefins and paraffins, their separation with membranes is challenging and, further investigation is required to obtain a membrane with required properties. The addition of fillers with preferential interaction with olefin might improve membrane

separation. For instance, Cu_3BTC_2 MOF showed selective interaction with the olefin an its incorporation in P84® polyimide has been proven to improve the separation ability of dense flat sheet membranes [5]. Future development of olefin/paraffin separation membrane would imply fabrication of thin film asymmetric membranes, where defect-free P84® hollow fiber membranes developed in this thesis would be a good starting point

Samenvatting en vooruitzichten

Gasscheiding met membranen heeft veel industriële interesse gekregen, voornamelijk vanwege de energie-efficiëntie, de relatief kleine fysieke voetafdruk, geringe mechanische complexiteit en continue procesvoering. Vanwege hun gemakkelijke verwerking en mechanische sterkte zijn voornamelijk polymeermembranen geïmplementeerd voor gasscheiding op grote schaal in de industrie. Een nadeel van polymere membranen is dat tegenover hogere permeabiliteit een lagere selectiviteit staat, en omgekeerd. Van mixed-matrixmembranen (MMM's) is het vastgesteld dat ze de bovengrens van permeabiliteit en selectiviteit van polymeermembranen doorbreken, waarbij metaal-organische roosters (MOF's, Metal Organic Frameworks) als een van de meest veelbelovende vulmaterialen gelden voor MMM's. Bovendien zijn van de verschillende membraanconfiguraties holle-vezelmembranen de meest gewenste vanwege hun hoge pakkingsdichtheid, d.w.z. membraanoppervlak per modulevolume. De ontwikkeling van membranen met een hogere selectiviteit en voldoende flux en membranen zonder defecten zijn de twee hoofduitdagingen die moeten worden aangepakt voor de scheiding van gas- en dampmengsels [1].

In deel I van dit proefschrift (Hoofdstuk 2 en 3) worden mixed-matrixmembranen ontwikkeld op basis van MOF's voor de afscheiding van CO_2 uit verbrandingsgassen ('post-combustion capture') en uit synthesegas (pre-combustion capture'). Deel II (Hoofdstuk 4 en 5) richt zich op de opschaalbaarheid van membranen op basis van twee verschillende polymeren met bijzondere aandacht voor de bereiding van defectvrije asymmetrische holle vezels.

Hoofdstuk 2 beschrijft de synthese en het testen van 6FDA-DAM/ZIF-94 MMM's. De intrinsieke gasscheidingseigenschappen van dit polymeer-vullerpaar zijn bepaald. De ZIF-94 kristallen werden gesynthetiseerd in een opschaalbaar proces. MOF-deeltjes kleiner dan 500 nm werden met een relatief ongevaarlijk oplosmiddel verkregen (tetrahydrofuraan en methanol) in plaats van met dimethylformamide. MMM's zijn met succes bereid tot een vulgewicht van 40 gew.%, waarbij een zeer goede dispersie van de MOF in en interactie met de polymeerlaag toont. Voor het eerst werden membranen gekarakteriseerd door *non-invasive infrared scattering type scanning near field optical microscopy* (IR s-SNOM), dat op nanoschaal chemische informatie biedt als aanvulling op standaard-analyse-methoden. De permeabiliteit van het CO_2-selectieve membraan werd door de toevoeging van de ZIF-94-deeltjes verhoogd, met behoud van een constante CO_2/N_2-selectiviteit van ~ 22. De grootste toename in CO_2-permeabiliteit (~200%) werd waargenomen bij een ZIF-94 belading van 40 gew.%. De combinatie 6FDA-DAM-polyimide en ZIF-94 biedt de mogelijkheid om te worden gesponnen in

een holle-vezelmembraanconfiguratie, waarmee het gebied van optimale membraaneigenschappen voor de scheiding van CO_2 uit rookgas, zoals geïdentificeerd door Merkel *et al.* [2], wordt bereikt.

In hoofdstuk 3 is een stap vooruit gezet in het membraanontwikkelingsproces door de ontwikkeling van MMM holle-vezelmembranen voor het afvangen van CO_2 uit synthesegas ('pre-combustion'). ZIF-8 kristallen van nanoafmetingen (~60 nm) werden gesynthetiseerd en geïntegreerd in PBI. Asymmetrische MMM holle-vezelmembranen werden bereid met een dunne selectieve laag waar ZIF-8-deeltjes uniform waren gedispergeerd. Puur-component- en gemengd-gasexperimenten werden uitgevoerd bij 150 ºC over een breed drukbereik (3-30 bar). In vergelijking met zuivere PBI-holle vezels leidt de inbedding van ZIF-8 in de polymeermatrix tot een sterke toename van de H_2-flux van 65 GPU tot 107 GPU bij 150 ºC en 7 bar, terwijl de ideale H_2/CO_2-selectiviteit constant bleef op 18. ZIF-8 opname in de PBI-polymeermatrix heeft een sterke invloed op het gastransport bij permeatie van gemengd gas. De verbetering van de holle-vezelprestaties voor H_2/CO_2-scheiding door toevoeging van ZIF-8 komt in het gedrang bij hoge bedrijfsvoeringdrukken als gevolg van de concurrentie tussen H_2- en CO_2-transport binnen de ZIF-8-structuur vanwege de CO_2-adsorptie-eigenschappen. Onze resultaten laten de prestaties van dit materiaal zien onder omstandigheden die relevant zijn voor de toepassing en tonen het belang van een dergelijke evaluatie.

Deel II richt zich op de fabricage van defectvrije asymmetrische holle-vezelmembranen door fase-inversie. Asymmetrische holle-vezelmembranen van P84® co-polyimide met een zeer dunne (~56 nm) defectvrije laag werden met succes vervaardigd zoals beschreven in hoofdstuk 4. Eerst is de invloed van toevoeging van het vluchtige tetrahydrofuraan (THF) op de oplosbaarheidsparameter van het N-methylpyrrolidon/THF-oplosmiddelmengsel uitgebreide experimenteel en theoretisch onderzocht. Hoewel THF zelf geen oplosmiddel is voor P84®, is aangetoond dat in een mengsel met een goed oplosmiddel voor het polymeer, zoals NMP, P84® wel kan worden opgelost bij hoge THF-concentraties. Daardoor konden defectvrije holle P84®-vezelmembranen gesponnen worden na optimalisering van de dopesamenstelling en spinparameters. De gesponnen holle-vezelmembranen vertoonden een reproduceerbare 'ideal' CO_2/N_2-selectiviteit (op basis van één-components-metingen) van 40 en een CO_2-flux van 23 GPU bij 35 °C. Deze holle-vezelmembranen hebben niet de gebruikelijke PDMS-coating nodig voor het helen van defecten, wat resulteert in het elimineren van een extra stap in de productie. Bovendien was het spinproces reproduceerbaar op grote schaal (getest tot een lengte van ~5000 m).

In Hoofdstuk 5 wordt de ontwikkeling van defectvrije PBI/PVP gemengde asymmetrische holle-vezelmembranen voor de H_2/CO_2-scheiding in pre-combustion CO_2-afvangprocessen getoond. PVP werd gebruikt als additief om de opschaalbaarheid bij de productie van PBI-hollevezelmembranen te verbeteren. De toevoeging van PVP verhoogde de elasticiteit van gesponnen vezels aanzienlijk en daardoor de snelheid tijdens het spinproces, wat resulteerde in een significante afname van de vezelafmetingen (buitendiameter <300 μm). Het bestaan van een enkele glasovergangstemperatuur T_g van deze vezels toonde de goede mengbaarheid van PBI en PVP op moleculair niveau aan en de vorming van een homogene blend. De PBI-membraanscheiding blijft behouden bij de toevoeging van PVP. De ontwikkelde PBI/PVP-blendvezels vertonen een H_2-permeance van 56 GPU, een H_2/CO_2-menggasselectiviteit van 16,6 bij 150 ºC en thermische stabiliteit tot ~340 ° C. Daarom kan dit membraan worden gebruikt bij de temperatuurniveaus die karakteristiek zijn voor pre-combustion H_2/CO_2-scheiding.

De algemene conclusie van het eerste deel van dit werk is dat toevoeging van MOF's ook moet bijdragen aan selectiviteitsverhoging, en niet alleen aan verbetering van de permeabiliteit. Voor post-combustion CO_2-scheiding is de selectie van MOF's op basis van CO_2-sorptiecapaciteit een goede aanpak, omdat CO_2 bij voorkeur door de MOF-structuur zou permeëren [3,4]. Desalniettemin is het niet voldoende om een verhoogde selectiviteit te waarborgen, omdat de hogere sorptiecapaciteit in veel gevallen ook een lagere diffusiviteit in de MOF inhoudt. Een verstandige selectie van de MOF houdt rekening met zowel sorptie als diffusie. Voor de H_2/CO_2-scheiding bij pre-combustion CO_2-capture, blijft CO_2 in het retentaat. Daarom moet de MOF-selectie in dit geval worden gebaseerd op selectie op basis van afmeting (molecular sieving), en waarbij MOF's met lagere interactie met CO_2 de voorkeur hebben.

In het tweede deel van dit proefschrift zijn richtlijnen voor het creëren van defectvrije gesponnen holle membraanvezels aan het licht gebracht voor spinbare polymeren voor toepassingen in pre- en post-combustion CO_2-capture. De volgende stap zou zijn om deze kennis toe te passen voor mixed-matrix holle-vezelmembranen. Toevoeging van 'filler' gaat vaak gepaard met het ontstaan van kleine defecten in de dunne selectieve toplaag, mogelijk als gevolg van resterende MOF-agglomeraten in de MOF/polymeer dispersies. Om dit te voorkomen, is het zeer belangrijk om een op nanoschaal homogene MOF/polymeer dispersie te bereiden en is een MOF van nanoafmetingen met een goede interactie met het polymeer, mogelijk versterkt door functionele groepen, vereist.

CO_2-afvangst was de beoogde toepassing van dit proefschrift. Desalniettemin kunnen membraanmaterialen die in deze studie zijn ontwikkeld ook worden gebruikt voor gasscheidingsapplicaties waar CO_2- of H_2-selectieve membranen nodig zijn, zoals aardgasbehandeling en het opwaarderen van biogas of het terugwinnen van waterstof. Daarnaast is olefine-paraffinescheiding één van de belangrijkste èn energie-intensiefste processen in de petrochemische industrie. Membraanscheiding is een veel minder energie-intensief alternatief voor destillatie en wordt daarom uitgebreid bestudeerd. Echter, vanwege de vergelijkbare moleculaire grootte van olefinen en paraffinen, is hun scheiding met membranen nog steeds een uitdaging en is verder onderzoek nodig om een membraan met de vereiste eigenschappen te verkrijgen. De toevoeging van vulstoffen met preferentiële interactie met olefine zou de membraanscheiding kunnen verbeteren. Cu_3BTC_2 MOF vertoont bijvoorbeeld selectieve interactie met het olefine en het is bewezen dat de inbedding ervan in P84®-polyimide het scheidingsvermogen van vlakke-plaat-membranen verbetert [5]. De verdere ontwikkeling van een olefine/paraffine scheidingsmembraan zou de fabricage van dunne-film asymmetrische membranen vereisen, waarbij defectvrije P84® holle vezelmembranen die in dit proefschrift zijn ontwikkeld een goed startpunt zouden zijn.

References

[1] S.P. Nunes, P.Z. Culfaz-Emecen, G.Z. Ramon, T. Visser, G.H. Koops, W. Jin, M. Ulbricht, Thinking the future of membranes: Perspectives for advanced and new membrane materials and manufacturing processes, J. Memb. Sci. 598 (2020) 117761. doi:https://doi.org/10.1016/j.memsci.2019.117761.

[2] T.C. Merkel, H. Lin, X. Wei, R. Baker, Power plant post-combustion carbon dioxide capture: An opportunity for membranes, J. Memb. Sci. 359 (2010) 126–139. doi:10.1016/j.memsci.2009.10.041.

[3] M. Mihaylov, K. Chakarova, S. Andonova, N. Drenchev, E. Ivanova, E.A. Pidko, A. Sabetghadam, B. Seoane, J. Gascon, F. Kapteijn, K. Hadjiivanov, Adsorption of CO2 on MIL-53(Al): FTIR evidence of the formation of dimeric CO2 species, Chem. Commun. 52 (2016) 1494–1497. doi:10.1039/C5CC08677A.

[4] A. Sabetghadam, X. Liu, A.F. Orsi, M.M. Lozinska, T. Johnson, K.M.B. Jansen, P.A. Wright, M. Carta, N.B. McKeown, F. Kapteijn, J. Gascon, Towards High Performance Metal–Organic Framework–Microporous Polymer Mixed Matrix Membranes: Addressing Compatibility and Limiting Aging by Polymer Doping, Chem. – A Eur. J. 24 (2018) 12796–12800. doi:10.1002/chem.201803006.

[5] J. Ploegmakers, S. Japip, K. Nijmeijer, Mixed matrix membranes containing MOFs for ethylene/ethane separation—Part B: Effect of Cu3BTC2 on membrane transport properties, J. Memb. Sci. 428 (2013) 331–340. doi:https://doi.org/10.1016/j.memsci.2012.11.013.

List of publications

Publications related to this thesis

Beatriz Seoane, Joaquin Coronas, Ignacio Gascon, **Miren Etxeberria Benavides**, Oğuz Karvan, Jürgen Caro, Freek Kapteijn and Jorge Gascon, Metal Organic Framework based Mixed Matrix Membranes: a solution for highly efficient CO_2 capture?, Chem. Soc. Rev., 44 (2015) 2421-2454

M. Etxeberria-Benavides, O. David, T. Johnson, M. M. Łozińska, A. Orsi, P. A. Wright, S. Mastel, R. Hillenbrand, F. Kapteijn, J. Gascon, High Performance Mixed Matrix Membranes (MMMs) Composed of ZIF-94 Filler and 6FDA-DAM Polymer, J. Membr. Sci, 550 (2018) 198-207

M. Etxeberria-Benavides, O. Karvan, F. Kapteijn, J. Gascon, O. David, Fabrication of Defect-Free P84® Polyimide Hollow Fiber for Gas Separation: Pathway to Formation of Optimized Structure, Membranes 2020, 10, 4

M. Etxeberria-Benavides, T. Johnson, S. Cao, B. Zornoza, J. Coronas, J. Sanchez-Lainez, A. Sabetghadam, X. Liu, E. Andres-Garcia, F. Kapteijn, J. Gascon, O. David, PBI mixed matrix hollow fiber membrane: influence of ZIF-8 filler over H_2/CO_2 separation performance at high temperature and pressure, Sep. Purif. Technol., 237 (2020) 116347

M. Etxeberria-Benavides, S. Miguel, M. Díaz de Guereñu, F. Kapteijn, J. Gascon, O. David, PBI hollow fiber membranes: Influence of PVP additive on manufacturing scalability, *Submitted*

Other publications

Fernando Cacho-Bailo, Silvia Catalán-Aguirre, **Miren Etxeberría-Benavides**, Oğuz Karvan, Victor Sebastiana, Carlos Téllez, Joaquín Coronas, Metal-organic framework membranes on the inner-side of a polymeric hollow fiber by microfluidic synthesis, J. Membr. Sci, 476 (2015) 277-285

Fernando Cacho-Bailo, Guillermo Caro, **Miren Etxeberría-Benavides**, Oğuz Karvan, Carlos Téllez, Joaquín Coronas, High selectivity ZIF-93 hollow fiber membranes for gas separation, Chem. Commun., 2015,51, 11283-11285

Fernando Cacho-Bailo, Guillermo Caro, **Miren Etxeberría-Benavides**, Oğuz Karvan, Carlos Téllez, Joaquín Coronas, MOF–polymer enhanced compatibility: post-annealed zeolite imidazolate framework membranes inside polyimide hollow fibers, RSC Adv., 2016,6, 5881-5889

Fernando Cacho-Bailo, **Miren Etxeberría-Benavides**, Oğuz Karvan, Carlos Téllez, Joaquín Coronas, Sequential amine functionalization inducing structural transition in an aldehyde-containing zeolitic imidazolate framework: application to gas separation membranes, CrystEngComm, 2017,19, 1545-1554

Fernando Cacho-Bailo, **Miren Etxeberría-Benavides**, Oana David, Carlos Téllez, Joaquín Coronas, Structural Contraction of Zeolitic Imidazolate Frameworks: Membrane Application on Porous Metallic Hollow Fibers for Gas Separation, ACS Appl. Mater. Interfaces 2017, 9, 24, 20787-20796

Fernando Cacho-Bailo, Ismael Matito-Martos, Julio Perez-Carbajo, **Miren Etxeberría-Benavides**, Oğuz Karvan, Víctor Sebastián, Sofía Calero, Carlos Téllez, Joaquín Coronas, On the molecular mechanisms for the H_2/CO_2 separation performance of zeolite imidazolate framework two-layered membranes, Chem. Sci., 2017,8, 325-333

Francois-Marie Allioux, Oana David, **Miren Etxeberria Benavides**, Lingxue Kong, David Alfredo Pacheco Tanaka, Ludovic F. Dumée, Preparation of Porous Stainless Steel Hollow-Fibers through Multi-Modal Particle Size Sintering towards Pore Engineering, Membranes 2017, 7(3), 40

Francois-Marie Allioux, Oana David, Andrea Merenda, James W. Maina, **Miren Etxeberria-Benavides**, Alfredo Pacheco Tanaka, Ludovic F. Dumée, Catalytic nickel and nickel-copper alloy hollow-fiber membranes for the remediation of organic pollutants by electrocatalysis, J. Mater. Chem. A, 2018,6, 6904-6915

Acknowledgements

Finally, this journey reaches the end. It was June 2015 when I travelled for the first time to Delft to start this PhD. This experience gave me the opportunity to meet many great people on the way. In the following paragraphs I would like to thank all the people that have supported me in one way or another during these years.

First of all, I would like to thank my promotors Jorge and Freek for the opportunity to perform my PhD between TU Delft and Tecnalia. Thanks for your guidance and support during these years. Jorge, thanks for opening the doors of the Catalysis Engineering group. Thanks for the warm welcome to Delft, it has been my privilege to perform the PhD at such a great group. Freek, I would like to thank your guidance during this thesis and also your help on M4CO2 project. It has been my first European project; it has been a pleasure to participate in such a great consortium where I have learned a lot about several aspects of MOFs.

I would like to thank my daily supervisor at Tecnalia and friend Oana. Thank you for being always there to advise and support me when I most needed it. It has been a pleasure to work closely with you, I have learned a lot from you. And of course, thanks for the nice moments after work, I really enjoyed our walks, climb and sky sessions. I will never forget our funny (and I would say at some point scary) adventure in Rila mountains after the M4CO2 meeting in Sofia!

I thank all my colleagues from the Membrane Technology and Process Intensification group at Tecnalia. Sara, thanks for being always there supporting and helping me, you have been there from the beginning when we started preparing membranes almost from zero. And thanks for the nice picture of the hollow fibers I have used for the design of the front and back covers of this thesis. You are a great photographer! Mari Mar, thanks for your help and support during these last two years, for your patience with my "infinite" permeation experiment, and for showing me many things about gas chromatography. I would like to take the opportunity to thank Oguz, without whose help it would not have been possible to start this PhD. Thanks for revealing to me the spinning world! My warm thanks go to all members of the group, Alba, Jon Melendez, Jon Z, Nerea, Ekain, Pepe, Margot, Alfredo, Jorge and Iñigo, for the great music and moments in the lab, and your willingness to help me when I needed.

During this thesis project I have had the opportunity to stay in two occasions at Delft. I would like to thank all the nice people from the Catalysis Engineering group I have met, in particular Anahid, my M4CO2 project PhD colleague and friend. Thanks for the moments we have shared during project meetings and at Delft, you have been a

great support during the project and my stay at Delft. Beba thanks for helping me during my first days in the laboratory, for showing how to use the permeation set up and for introducing me to the group. Meixa and Xinlei thanks for nice chats and recommendations about membranes. Eduardo, Lide and Maria Jose thanks for making me feel like at home, Els for helping me with all the administrative and housing issues. Jara, Cesc, Dimitri, Alma, Alla, Alexey, Ina, Irina, Helena, Nastya, Agi, Robert, Pedro, Thais, Alfredo, Jose, Harri, Willy, Bart… Thank you all for the great moments during the coffee breaks, Friday drinks, barbecues, dinners, secret Santa… It has been a pleasure to share these funny moments with all of you!

Further, I express my appreciation to all the people I have collaborated with during this thesis project in the frame of M4CO2 project, without whom this work would not have been completed. Shuoi, Timothy, Angelica, Paul, Beatriz, Javier, Joaquín, Stefan and Rainer, you had a great contribution to this thesis.

Last, I would like to thank my friends and family. Even though they may have no idea what a membrane is, they have always showed interest in my PhD work. Their support has been essential during these years.

Gracias a mis amigas del pueblo Natalia, Marta y Aitziber. Muchas gracias por seguir haciendo de los momenticos en Legaria momentos tan especiales, por hacer que siga teniendo la misma ilusión y ganas como en la infancia de pasar los veranos y fines de semana en Legaria. Aitzi, zuri bereziki eskerrik asko, munduko musika talde hoberenak dioen bezala… Niretzako berezia zara! Mila esker kuadrilako guztiei, bereziki Delftera bixitan etorri zaretenoi, Nahikari, Zuri, Eider eta Ibon, plazer bat izan da momentu horiek zuek alboan izana. Alaitz, Alkain, Haizea eta Karla eskerrik asko urte hauetan "bide-lagun" izateagatik, kantxa barruan eta kanpoan bizitako momentu zoragarri guztiengatik eta Holandara egindako bixita ta bidai zoroengatik!!

Aita, ama eta Martin, mila esker momentu oro nire alboan egoteagatik, eskerrik asko txikitatik erakutsitako guztiagatik ta transmititu dizkidazuen bizi baloreengatik, bidai luze hau bukatzea lortu badet neurri haundi batez zuei esker izan da. Irantzu eskerrik asko Martinen txisteak aguantatzeagatik eta Ega aukeratzeagatik! :)

Mila esker guztioi bihotz-bihotzez!!

Miren

About the author

Miren Etxeberria Benavides was born on 31st of August 1985 in Donostia-San Sebastian. After graduating from high school in 2003, she started studying Chemistry at the University of the Basque Country (UPV-EHU). In 2008 she obtained her Degree in Chemistry with the specialization in Macromolecules.

In 2008, she started a two years training grant at the research institute Inasmet (now part of Tecnalia). Since 2010 she works at Tecnalia as part of the Membrane Technology and Process Intensification group. While she was working, she decided to study a master to gain more knowledge on polymeric materials and their applications. In 2013 she obtained the master degree in Applied Chemistry and Polymeric Materials at the UPV-EHU with the thesis title "Synthesis of 6FDA-6FpDA polyimide for gas separation membranes".

In 2015 she started the PhD research in the frame of the European project M4CO2 in the group of Catalysis Engineering of TU Delft under the supervision of Prof. dr. Freek Kapteijn and Prof. dr. Jorge Gascon. The PhD research was performed in close collaboration with Tecnalia within the Membrane Technology and Process Intensification group under the supervision of Dr. Oana David. The results of her PhD research on high productivity hollow fiber membranes for CO_2 capture are presented in this thesis.